Faculté des Bioingénieurs
Institut de la matière condensée et des nanosciences

Fibronectin and collagen-based biomimetic surfaces to improve cell-material interactions for biomedical applications

Thèse soutenue en vue de l'obtention du grade de docteur en sciences agronomiques et ingénierie biologique par

Sara Mauquoy

Composition du jury
Pr. Christine Dupont-Gillain (UCL/IMCN) - *Promoteur*
Pr. Eric Gaigneaux (UCL/IMCN) - *Président*
Pr. Sophie Demoustier-Champagne (UCL/IMCN)
Pr. Bernard Knoops (UCL/ISV)
Dr. Jessem Landoulsi (Université Pierre et Marie Curie - Paris VI, France)
Pr. Emmanuel Pauthe (Université Cergy-Pontoise, France)

Louvain-la-Neuve
Novembre 2016

Remerciements

Mes premiers remerciements iront à ma promotrice de thèse, le professeur Christine Dupont. Merci de m'avoir accueillie au sein de votre laboratoire dès mon mémoire et de m'avoir donné les moyens de réaliser cette thèse. Merci pour votre aide et vos précieux conseils scientifiques. Merci aussi pour votre écoute et votre compréhension dans les moments les plus difficiles. Et merci de m'avoir permis de participer à de nombreuses activités hors-doctorat qui ont été des plus enrichissantes pour moi.

Je souhaite aussi remercier les membres de mon comité d'accompagnement, les professeurs Sophie Demoustier et Denis Dufrane. Merci aux membres de mon jury, les professeurs Bernard Knoops, Emmanuel Pauthe, Sophie Demoustier et Jessem Landoulsi, pour avoir accepté de prendre le temps de juger mon travail. Merci à Eric Gaigneaux pour avoir accepté de présider ce jury. Je voudrais adresser un merci tout particulier au professeur Bernard Knoops pour m'avoir accueillie au sein de son laboratoire afin de réaliser mes expériences de culture cellulaire.

Je remercie aussi toutes les personnes qui m'ont aidée et qui ont contribué au bon déroulement de la partie culture cellulaire de cette thèse. Merci au professeur Denis Dufrane et à Patricia Palacios pour m'avoir permis d'utiliser les cellules isolées dans leur laboratoire. Patricia, je te remercie aussi pour toute l'aide que tu m'as apportée pour l'apprentissage de la culture, pour tes réponses à mes nombreuses questions et pour ta bonne humeur. Merci à Sarah Becker pour tout le temps consacré à répondre aux nombreuses questions pratiques que je me suis posées durant les expériences de culture. Merci aussi à Julie Vanacker et à Julian Leprince qui ont accueilli Cédric lors de son mémoire et qui ont permis à ce dernier de tester nos surfaces sur d'autres cellules.

Je souhaite ensuite remercier toutes les personnes qui font, ou ont fait, l'âme de ce labo durant les quelques années de ma thèse et de mon mémoire. Merci Françoise pour toute l'aide que tu m'as apportée et pour ton sourire. Profite de

ta retraite bien méritée ! Merci Rose-Anne et Yasmine pour toute l'aide logistique, pour votre bonne humeur et pour nos bavardages quotidiens. Merci à Sylvie, Michel et Pierre pour vos conseils scientifiques et pour votre soutien. Je remercie aussi tous les anciens du labo, Kévin, Pierre, Emilienne pour tous leurs conseils lors de mon mémoire. Merci aussi à Simon et Marie qui m'ont beaucoup aidée lors du début de cette thèse, merci pour vos conseils, votre aide au jour le jour et votre amitié. Merci à toutes les personnes avec qui j'ai partagé quelques mois ou années de travail durant cette thèse ; Gilles, mon collègue de bureau pendant deux ans, Nicolas, Séverine, ainsi que tous les mémorants. Je remercie plus particulièrement les trois mémorants qui ont travaillé avec moi sur ce projet et ont contribué à ce travail, Maxime, Gosia et Cédric. Thank you also Ana for the nice discussions we had during my thesis and for you kindness. I wish you a lot of success in Science and life for the future.

J'adresse aussi tous mes remerciements aux personnes qui ont fait partie de l'ACIM. J'ai adoré faire partie de l'association des chercheurs et je vous remercie tous pour les belles rencontres que cela m'a permis de faire.

Ensuite, je voudrais remercier les trois doctorants qui ont partagé l'expérience de la thèse avec moi ; Loïc, Jean-François et Aurélien. J'ai beaucoup de « mercis » à vous dire car on s'est quand même bien amusés pendant ces quelques années. Merci à tous pour vos conseils scientifiques, pour votre soutien et pour toutes les pauses de midi où on a bien rigolé. Loïc, merci pour tous les moments où tu m'as écoutée me plaindre et pour m'avoir redonné le moral dans les moments de démotivation. Jean-François, merci pour toutes les gentilles moqueries que tu as pu faire sur nous tous durant ces quelques années. Aurélien, merci de nous faire souvent rire comme ça, sans toujours le vouloir. Courage à vous trois pour votre thèse. Et Aurélien, n'oublie pas tes futurs goûters d'anniversaire !

Finalement je souhaiterais remercier tous mes proches. D'abord mes amis, et particulièrement les anciens AGRO. Merci, vous êtes super ! Ensuite je souhaiterais remercier toute ma belle-famille pour tous les bons moments

passés ensemble. Je remercie sincèrement mes parents et ma petite sœur. Merci pour le soutien inconditionnel que vous m'avez apporté et qui m'a permis d'arriver au bout de ce travail. Et pour finir je remercie Nicolas, mon mari, pour tout. Merci de m'avoir supportée les plus mauvais jours, merci pour tes blagues et merci pour toutes les belles choses qui nous sont arrivées durant ces quatre années.

Foreword

This dissertation is composed of four parts:

- **Part I:** General introduction that will present the context of the research, the aim and the strategy.
- **Part II:** Detailed presentation of the results obtained in this thesis, divided in three chapters:
  - Chapter 1: Preliminary studies: PS substrate preparation and characterization, and parameters of LbL assembly
  - Chapter 2: Combination of collagen and fibronectin to design biomimetic interfaces: do these proteins form layer-by-layer assemblies?
  - Chapter 3: Adipose-derived stem cell response to biointerfaces based on collagen and fibronectin
- **Part III:** Presentation of the main conclusions of the work as well as the future prospects
- **Part IV:** Appendices
  - *Appendix 1:* Silanization of polystyrene with methacryloxy-propyltrimethoxy-silane with a view to improve polymer adhesion
  - *Appendix 2:* Study of dental stem cell behavior on the designed interfaces
  - *Appendix 3:* Preliminary results about demineralized bone matrix analysis

The author also contributed to the following paper:

- Mauquoy, S., E. Zuyderhoff, J. Landoulsi, D. Kalaskar, S. Demoustier-Champagne & C. Dupont-Gillain (2014) Biointerfaces Designed Through Directed Collagen Assembly. Journal of Bionanoscience, 8, 407-418.
- Mauquoy, S. & C. Dupont-Gillain (2016) Combination of collagen and fibronectin to design biomimetic interfaces: Do these proteins form layer-by-layer assemblies? Colloids and Surfaces B: Biointerfaces, 147, 54-64.

The author participated to the following international scientific events:

- Presentation of a poster at the European Science Foundation research conference on Biological surfaces and interfaces organized from the 30th of June to the 4th of July 2013 in Sant Feliu de Guixols (Spain).

- Oral presentation at the 26th conference of the European Society for Biomaterials organized from the 31th of Augustus to the 3rd of September 2014 in Liverpool (UK).

- Oral presentation at the 8th conference of the Scandinavian Society for biomaterials organized from 6th to 8th of May 2015 in Sigulda (Latvia).

- Presentation of a poster at the NANOinBIO conference organized from the 31st of May to the 5th of June in Le Gosier (Guadeloupe, France).

Abstract

The lack of donors for tissue or organ grafts has led to the development of several strategies in the last decades, based first on the use of biomaterials, then on tissue engineering. For both approaches, a key challenge is the control of cell-material interactions, which can be addressed by modifying the physical and/or chemical properties of material surfaces. A biomimetic way to modify interfaces is the adsorption of molecules from the extracellular matrix. In this work, two proteins, collagen and fibronectin, were chosen as building blocks to create well-organized biointerfaces to improve interactions with stem cells.

To design biomimetic surfaces, layer-by-layer (LbL) deposition was compared to simultaneous adsorption of both proteins. The influence of the buffer composition, of a polyethyleneimine (PEI) anchoring layer and of collagen denaturation on LbL assembly was examined.

The results showed that true LbL building was not obtained by assembly of collagen and fibronectin. However, multilayers were built and results showed that a PEI anchoring layer allowed thicker films to be obtained, and that Hepes buffer allowed obtaining the most regular assembly. Moreover, comparison with simultaneous adsorption revealed interesting features. Films obtained by simultaneous adsorption were of the same thickness, or even thicker than those prepared by LbL, and they presented a different morphology, with more collagen fibrils, a lower contact angle and lower water content. Adipose derived mesenchymal stem cells were cultured on films obtained by both deposition methods, in Hepes, with or without PEI anchoring layer. All the protein films supported cell adhesion and proliferation better than pure polystyrene. The main influence observed on cells was the one of the PEI anchoring layer, which decreased proliferation rate but improved cell osteogenic differentiation.

Biointerfaces were thus designed based on collagen and fibronectin, two major proteins of the extracellular matrices. Mesenchymal stem cell behavior was influenced by the organization and nature of biomolecules present in these biointerfaces, which may open the way to new strategies for tissue engineering applications.

List of abbreviations

AFM	Atomic force microscopy
ALP	Alkaline phosphatase
AMSC	Adipose-derived mesenchymal stem cell
BCA	Bicinchoninic acid assay
BMP-2	Bone morphogenetic protein
BSA	Bovine serum albumin
Col	Collagen
d-Col	Denatured collagen
n-Col	Native collagen
DBM	Demineralized bone matrix
DPSC	Dental papilla stem cell
ECM	Extracellular matrix
EDC	1-ethyl-3-(3-dimethylaminopropyl)carbodiimide
ELISA	Enzyme-linked immunosorbent assay
F_{ad}	Adsorption force
FACS	Fluorescent-activated cell sorting
FAK	Focal adhesion kinase
Fn	Fibronectin
GAG	Glycosaminoglycan
Hepes	4-(2-hydroxyethyl)-1-piperazineethanesulfonic acid
HESC	Human embryonic stem cell
iep	Isoelectric point
IGF-I	Insulin-like growth factor
LbL	Layer-by-Layer
MAPK	Mitogen Activated Protein Kinase
MOPTMS	Methacryloxypropyltrimethoxy silane
MSC	Mesenchymal stem cell

MTS	(3-(4,5-dimethylthiazol-2-yl)-5-(3-carboxymethoxyphenyl)-2-(4-sulfophenyl)-2H-tetrazolium
NHS	N-hydroxysuccinimide
ODMS	Octadecyldimethylchlorosilane
PBS	Phosphate Saline Buffer
PDGF	Platelet-derived growth factor
PDMS	Poly(dimethylsiloxane)
PEI	Poly(ethyleneimine)
PLL	Poly(L-lysine)
PMMA	Poly(methylmethacrylate)
pNP	p-nitrophenol
pNPP	p-nitrophenyl phosphate
PS	Polystyrene
PSS	Poly(styrene sulfonate)
QCM-D	Quartz crystal microbalance with dissipation monitoring
RGD	L-arginine, glycine, L-aspartic acid
rpm	Rotation per minute
SCAP	Stem cell from apical papilla
SEM	Scanning electron microscopy
TCPS	Tissue culture polystyrene
TGF-β1	Transforming growth factor
VEGF	Vascular endothelial growth factor
XPS	X-ray photoelectron spectroscopy
Θ	Water contact angle
ΔD	Shift of dissipation
Δf	Shift of frequency

Table of contents

Part I: Introduction 17

1. Context of research 19
   1.1. Biomaterials and tissue engineering 19
   1.2. Extracellular matrix and integrins 23
      1.2.1. Extracellular matrix 23
      1.2.2. Signal transmission between cells and ECM: Integrins 31
   1.3. Cell-material interactions 34
      1.3.1. Influence of chemical properties 34
      1.3.2. Influence of mechanical properties 38
      1.3.3. Influence of topography 40
      1.3.4. Summary and role of integrins 42
   1.4. Layer-by-Layer method to create complex assemblies of proteins 44
      1.4.1. Principles of layer-by-layer deposition 44
      1.4.2. Layer-by-layer assembly of proteins 46
      1.4.3. Layer-by-layer based on collagen or fibronectin 47
2. Aim of the thesis 51
3. Research strategy 52
   3.1. Preparation of polystyrene substrates 53
      3.1.1. Silanization to improve adhesion 53
      3.1.2. Spin-coating 54
   3.2. Protein coating 55
      3.2.1. Deposition method 55
      3.2.2. Collagen denaturation 56
      3.2.3. Polyethyleneimine anchoring layer 57
      3.2.4. Influence of the buffer 57
   3.3. Surface characterization 59
      3.3.1. Quartz crystal microbalance with dissipation monitoring 59
      3.3.2. Ellipsometry 61
      3.3.3. Atomic force microscopy 62
      3.3.4. Contact angle 63
      3.3.5. X-Ray photoelectron spectroscopy 65

3.4. Cell culture 66
3.4.1. Stem cells generality 66
3.4.2. Adipose-derived mesenchymal stem cells 68
3.4.3. Study of AMSC behavior 70

Part II: Results 83

Chapter 1: Preliminary studies: PS substrate preparation and characterization, and parameters of LbL assembly 85
1. Introduction 86
2. Methods of characterization 86
3. Preparation and characterization of the polystyrene substrates 88
3.1. Protocol optimization with a long-chain alkylchlorosilane 89
3.2. Final silanization protocol 93
4. Development of the proteins LbL deposition protocols 94
4.1. Influence of the order of the layers 95
4.2. Influence of protein concentration 96
4.3. Influence of protein denaturation and of the addition of an anchoring layer 98
4.4. QCM flow and adsorption time 100
4.5. Buffer choice 103
4.6. Temperature effect 105
4.7. Summary of the conditions for LbL assembly 108
5. Characterization of collagen layers 109
5.1. Materials and method 109
5.2. Results and discussion 110
6. Conclusions 114

Chapter 2: Combination of collagen and fibronectin to design biomimetic interfaces: do these proteins form layer-by-layer assemblies? 117
1. Introduction 118
2. Materials and method 122
3. Results 126
3.1. In situ monitoring of assembly with QCM-D 126
3.2. Ex situ measurement of dry thickness and water contact angle 130
3.3. Immunodetection of Fn 133

3.4. Film morphology depending on last deposited layer and on construction method 135
4. Discussion 137
4.1. Amount of water contained in the films 137
4.2. Effect of collagen denaturation and of an anchoring layer on assembly 139
4.3. Effect of the buffer on assembly 140
4.4. True LbL assembly or step-by-step saturation of the interface? 141
4.5. Comparison of simultaneous adsorption and LbL assembly 142
5. Conclusion 143

Chapter 3: Adipose-derived stem cell response to biointerfaces based on collagen and fibronectin 149
1. Introduction 150
2. Materials and method 153
2.1. Preparation of biointerfaces by layer-by-layer method or simultaneous adsorption 153
2.2. Film characterization 155
2.3. Cell culture 156
3. Results and discussion 160
3.1. Film characterization 160
3.1.1. In situ monitoring of assembly by QCM-D and stability study 160
3.1.2. Measurement of dry thickness and water contact angle 161
3.1.3. Film morphology 163
3.1.4. Impact of the anchoring layer and of the deposition method 164
3.2. Study of cell behavior 164
3.2.1. Fluorescent imaging of AMSC: Adhesion and proliferation 164
3.2.2. Measurement of AMSC metabolic activity by Alamar blue assay 166
3.2.3. Effect of PEI addition at different time of culture 169
3.2.4. PEI cytotoxicity analysis 170
3.2.5. Osteogenic differentiation study 172
3.2.6. Summary of the impact of the PEI anchoring layer and of the protein deposition method on cell behavior 177
4. Conclusion 178

Part III: Conclusions and future prospects 185

1. Main achievements 187
   1.1. Elaboration of biomimetic films containing fibronectin and collagen ... 187
   1.2. Influence of the films on AMSC behavior 190
2. Future prospects 191
   2.1. Strategies for improvement of LbL deposition 191
   2.2. Study of other cell types behavior 194
   2.3. Inclusion of specific signals in the films 195
   2.4. Future applications 196

Part IV: Appendices 201

Appendix 1: Silanization of polystyrene with methacryloxypropyltrimethoxy-silane with a view to improve polymer adhesion 203

1. Initial silanization protocol with MOPTMS 203
2. Protocol optimization with MOPTMS 204
3. Conclusion 207

Appendix 2: Study of dental stem cell behavior on the designed interfaces 209

1. Dental mesenchymal stem cells 209
2. Comparison of the results 210
3. Study of cell behavior 212
4. Conclusion 216

Appendix 3: Preliminary results about demineralized bone matrix analysis 217

1. Introduction 217
2. Materials and methods 218
3. Results and discussion 220
   3.1. Chemical and morphological analysis of DBM powder 220
   3.2. Chemical analysis of DBM extract 223
   3.3. Detection of specific proteins in the extract 225
4. Conclusions 227

Part I:
Introduction

1. Context of research

One of the biggest challenges of current research is to find new solutions to replace malfunctioning organs, mostly in reason of population aging. Medical advances make people live longer. Cancers, diseases and accidents can however cause serious damages to specific organs which cannot be repaired. Organs have thus to be replaced. Unfortunately, the number of organ donors is lower than the number of people waiting for a graft. And even if a graft is available, problems of rejection can occur. Two approaches can be developed to answer this problem: the use of devices based on biomaterials on the one hand, and tissue engineering, on the other hand.

The research project of this thesis aims at improving the knowledge of cell-material interactions that is useful for the design of new biomaterials and new tissue engineering applications. This work will be focused on cell interactions with a material coating made of proteins that mimic the complex architecture of the extracellular matrix. Section 1 of this introduction chapter is dedicated to a state of the art on several important topics to better understand the specific aim and the strategy of the research project, which will be respectively detailed in section 2 and 3 of this introduction chapter.

1.1. Biomaterials and tissue engineering

Even if biomaterials science constitutes a popular research field, definition of what is exactly a biomaterial is not so easy to establish. A first consensus was found in 1987 saying that [1, 2] "*A biomaterial is a nonviable material used in a medical device intended to interact with biological systems".* Later, a wider definition was proposed by Williams [2] to take into account the vast diversity of new materials that can be considered as biomaterials (drug delivery systems, gene therapy vectors, some diagnostic and imaging systems, biosensors, etc.) saying that "*A biomaterial is a substance that has been engineered to take a form which, alone or as part of a complex system, is used to direct, by control of interactions with components of living systems, the course of any therapeutic or diagnostic procedure, in human or veterinary medicine".*

Biomaterials science is a field in evolution since its first applications. In the beginning, biomaterials were just bioinert materials that were implanted in the body. With time, more sophisticated biomaterials were developed, such as bioactive materials for orthopedics and dentistry as well as resorbable materials for sutures. Now, new biomaterials are even conceived to trigger a specific response of cells in contact with them by influencing cell adhesion, proliferation, differentiation and apoptosis [3].

As shown on Fig. I.1, examples of clinical applications of biomaterials are very diverse. They include cardiovascular applications (heart valves, catheters, stents, pacemakers), dental implants, sutures, biological glues, contact lenses, orthopedic prostheses, artificial skin, drug delivery systems, biosensors, etc.[1]. Each of these different devices requires a specific design, which raises many questions:

- What are the biological/medical requirements for the biomaterial?
- Which materials are needed to obtain the desired mechanical properties (elasticity; ductility; brittleness; resistance to tension, compression, shear and fatigue; etc.) and chemical properties (promote/disadvantage protein adsorption and cell adhesion; bioactive/bioinert; bioresorbable or not; which kind of degradation products; etc.)?
- What will be the body response after implantation (inflammation, foreign body response, toxicity, immunologic response, blood response, infection, etc.)?
- How many people will be interested by this new biomaterial? Where in the world? What are the regulations and standards to apply depending on the market?
- What is the cost of the designed biomaterial?

To answer these questions and understand all the parameters included in the design/production, physicians, dentists, engineers, biologists, material engineers, polymer scientists, economists, jurists, etc. need to work together. Biomaterial design is thus a multidisciplinary field that opens many new treatment possibilities [1].

Figure I. 1: Illustration of the vast diversity of devices based on biomaterials used in clinical applications

Tissue engineering is also a more recent approach to replace malfunctioning organs. This approach is described in Fig. I.2. Cells are collected from the patient. Their proliferation is ensured using *in vitro* culture. They are then placed on a well-designed scaffold that, with specific biomolecules and signaling molecules, will specifically direct cell fate. Finally, a graft is produced that can be implanted in the patient. A precise definition was given by Williams [2]: "*Tissue engineering is the creation (or formation) of new tissue for the therapeutic reconstruction of the human body, by deliberate and controlled stimulation of selected target cells through a systematic combination of molecular and mechanical signals"*. Tissue engineering is not yet used routinely

in clinical applications. Some approaches are however already well developed. For example, skin patches can be reconstructed to treat burns. However, important research efforts are still needed to achieve the successful building of complete organs.

Figure I. 2: Principle of tissue engineering

The boundary between the biomaterial-based and tissue engineering approaches is not always clear. In tissue engineering, culture plates and scaffolds can indeed be considered as biomaterials. The cell-material interaction plays anyway an important role in both cases. Next sections of this chapter present major knowledge regarding cell-material interaction. Moreover, as cells are embedded *in vivo* in an extracellular matrix, the composition of this matrix will be described to better understand how it influences cell behavior.

> ***In summary, therapeutic approaches based on biomaterials and on tissue engineering are highly desired to solve the problem of graft availability and compatibility. The improvement of these approaches through the design of surfaces which direct cell behavior is thus a key challenge.***

1.2. Extracellular matrix and integrins

1.2.1. Extracellular matrix

In vivo, cells are embedded in an extracellular matrix (ECM). This matrix gives mechanical properties to tissues but also influences cell behavior. The general composition of the ECM and its properties will be presented in this section. Collagen and fibronectin; two important ECM biomolecules for this work, will be discussed in details.

a) Extracellular matrix components and properties

Fig. I.3 shows the general structure of the extracellular matrix. **Fibrous proteins** such as collagen, fibronectin, elastin and fibrillin constitute a major class of ECM components [4]. These fibers form a network that gives strength and resilience to the ECM [4, 5]. **Collagen** is one of the major fibrous proteins and is the one that gives strength to the tissues. **Fibronectin** is "the adhesion protein" of the ECM and allows to transmit signals from the outside to the inside of the cell and conversely. These two proteins will be presented in more detail thereafter. **Elastic fibers** are mainly composed of elastin and give resilience to the tissues. Elastin forms fibrils by cross-linking after secretion by the cells. This protein is structured in hydrophobic segments and alanine and lysine rich segments. The first are responsible for the elasticity and the second for the cross-linking between molecules. Elastic fibers are also composed of fibrillin microfibrils that cover elastin fibrils. These microfibrils act as a guide for elastin deposition [5].

Between the fibrils of the fibrous network, **glycosaminoglycans and proteoglycans** form a well hydrated gel. Glycosaminoglycans are polysaccharides with two repeating units. They are composed of N-acetylated and O- or N-sulfated sugars and of uronic acids (sugar monomers oxidized on the last carbon to produce COOH function). These polysaccharides are thus hydrophilic and negatively charged. They are often linked to a core protein to give proteoglycans. Thanks to their high negative charge, these molecules

attract a high number of Na^+ ions and are thus swelled with water due to osmotic pressure. Moreover, they interact specifically with signaling molecules such as growth factors and thus regulate the activity and availability of these molecules [4, 5].

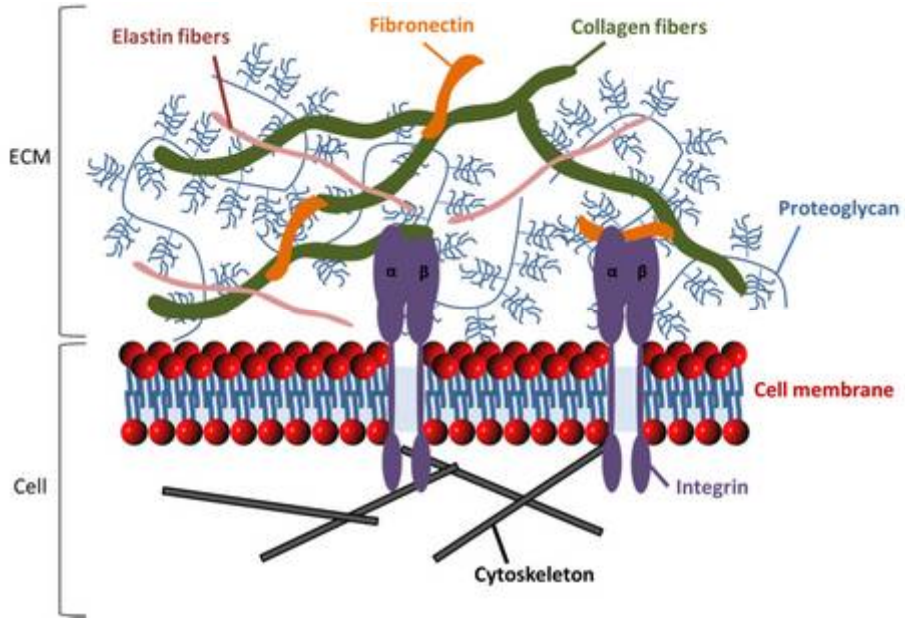

Figure I. 3: Schematic representation of the extracellular matrix (ECM) and its different components, in contact with a cell (inspired from [6])

b) Collagen

Collagen is the structural protein of tissues and is the protein present in the highest amount in the human body. At least 20 different types of collagen exist, that can form fibrils or not [7]. This work will be focused on type I collagen, the structure of which will be described in details hereunder. Type I collagen (Col) is a protein of 300 nm in length and 1.5 nm in diameter. Col is composed of two α1 and one α2 polypeptide chains, each forming a left-handed α-helix. Each chain has a primary structure rich in repeated Glycine-X-Y triplets where X and Y are often proline and hydroxyproline respectively. The three chains are assembled together in a triple helix structure. This structure is favored owing to the glycine residues at every third position. Glycines, that are indeed very small

residues, are positioned in the middle of the triple helix and thus allow the close packing of the helix. Triple helical structure is stabilized by hydrogen bonding between hydroxyproline residues [7, 8].

As shown on Fig. I.4, collagen molecules **synthesis** begins with the synthesis of procollagen that contains non-helical propeptides at each end of the molecule. These non-helical parts increase the molecule solubility to allow transport in the cell. After synthesis, post-translational modifications happen. Some proline and lysine residues are hydroxylated to obtain hydroxyproline and hydroxylysine. Hydroxyprolines are responsible for the stability of the triple helix as explained before. Hydroxylysines offer glycosylation sites. The two propeptides contribute to the formation of the triple helical structure and prevent collagen fibrillation inside the cells. After formation of the triple helical structure and secretion of procollagen by the cells, propeptides are cleaved. Collagen fibrils formation can then be initiated [7, 8].

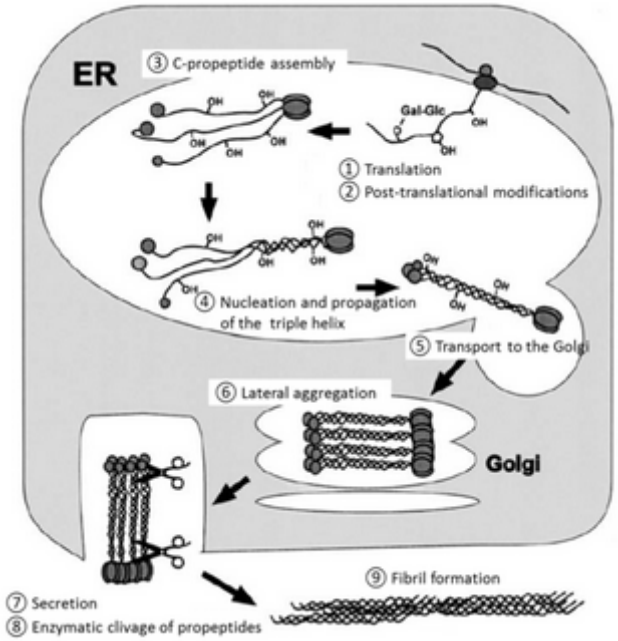

Figure I. 4: Schematic summary of collagen synthesis by the cells (adapted from [9])

Collagen **fibrillation** is the Col triple helix parallel self-assembly to form microfibrils. Due to the well-ordered character of the microfibrils, they present a D-banding pattern of 67 nm that can be observed on a negatively stained electron micrograph (see Fig. I.5) [10]. Col molecules are cross-linked in the microfibrils by lysyl oxidase enzyme [7]. Microfibrils assemble thereafter into fibrils and these fibrils into fibers that give strength to tissues.

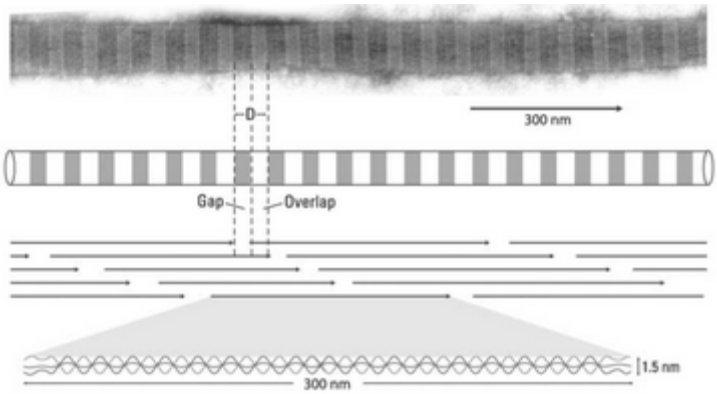

Figure I. 5: Negatively stained electron micrograph of a collagen fibril and schematic representation of the D-banding pattern [10]

Col also transmits signals to cells. As it will be explained in the section 1.2.2, the signal transmission between ECM molecules and cells is based on the recognition of ECM molecules by cell membrane-bound integrins. The main amino acids sequence recognized by integrins on Col molecule is Gxx'GEx'' where x is a hydrophobic residue and x' and x'' are in general hydroxyproline and R, respectively. RGD sequences and DGEA sequences are also known to play a role in integrin recognition [11].

Col molecules can be extracted from tissues for several applications and for *in vitro* studies. Different methods of extraction exist such as (i) cold extraction at neutral pH, (ii) extraction in acidic solution and (iii) extraction with proteases. The third method will lead to the cleavage of telopeptides (ie non-helical terminations of the polypeptide chains of collagen). Since telopeptides are involved in Col self-assembly, this will alter the fibrillation properties of Col [8].

Depending on the extraction method, the Col properties can change, which makes this molecule challenging to study.

Collagen fibrillation in solution has been extensively studied *in vitro*, with a view to unravel the involved mechanism. Fibrillation seems to be initiated by linear aggregation in trimers, followed by lateral aggregation of five trimers [12]. Many parameters affect Col fibrillation including temperature, pH, ionic strength, Col concentration and presence of specific ions [13-17]. For example, increasing temperature, or decreasing ionic strength at a constant temperature of 25°C, increases fibrillation rate but decreases fibril width [14]. Increasing Col concentration also increases fibrillation rate [14, 15]. Effect of pH depends on the conditions used. For instance, Wood shows an increased fibrillation rate by decreasing the pH from 7-8 to 6 [14] while Li shows that increasing pH increases fibrillation rate until pH 9.2 [13]. Nevertheless, Col is known to be soluble at very acidic pH such as 2.5 [17] and can be stored without fibrillation at pH 4 at 4°C. The effect of some of these different parameters, such as pH and ionic strength, shows that Col fibrillation is influenced by electrostatic interactions. As hypothesized by Li et al. [13], Col fibrillation could be favored when repulsive charges are minimized, as shown by the higher fibrillation rate at pH values close to the iep.

Col fibrillation at interfaces is also interesting to consider. Fibrils formed upon adsorption are generally smaller than fibrils produced in solution. Fibrillation on the interface increases with adsorption time and Col concentration [18]. If the concentration in solution increases, there are more molecules available for self-assembly. Moreover, longer adsorption times favor fibrillation because the molecules have more possibilities to reorganize into fibrils. Interestingly, fibrillation is enhanced on more hydrophobic surfaces, as proved by a higher fibrillation on polystyrene (PS) substates compared to oxidized PS (PSox) [18, 19]. Even if the affinity between Col molecules and hydrophobic PS is higher than the affinity between Col and PSox, the mobility of Col molecules is higher on hydrophobic PS [20]. The higher mobility promotes fibril formation because it allows adsorbed Col molecules to reorganize, thereby getting closer to each other to self-assemble. This property of differential fibrillation on hydrophobic/

hydrophilic surfaces was used by Zuyderhoff et al. [21] to design nano-organized collagen layers. Col adsorption was performed on surfaces featuring domains of two different polymers, one more hydrophobic and one more hydrophilic. This produced interfaces that presented different Col organizations. The results of these experiments will be presented in section 1.3.1. Other experiments related to Col fibrillation showed that Col thermal denaturation at 90°C prevents fibrillation at interfaces [22]. This is attributed to the fact that denaturation disturbs the tertiary helical structure of Col molecules that is needed for fibrillation. The Col source also highly influences the fibrillation pattern obtained after adsorption [18].

Finally, **the isoelectric point** (iep) is also an important parameter to take into account. The theoretical value of Col iep is computed to be 9.6, based on the primary structure of the protein. The negative and positive charges on Col molecules result from deprotonation or protonation of amino acid residues with acidic or basic functions, respectively. Negative charges are found on aspartic acid and glutamic acid, which represent 7.4 % of the total amino acid residues. Positive charges are found on arginine, lysine and histidine, which represent 8.8 % of the total amino acid residues. Computed iep values of proteins do not take into account the structure of the protein molecule and the intramolecular interactions. In the case of Col, a highly anisotropic molecule, with a very specific structure, experimental measurements of iep may deliver very different values from the theoretical approximation.

Col iep was measured experimentally using different approaches. Röβler et al. have measured an iep of 6.0 ± 0.2 by microelectrophoresis [23]. The drawback of this measurement comes from the use of an approximation, which considers the molecule as a sphere with a mean charge. This is clearly not the case of the Col molecule, a filament about 300 nm in length. Hattori et al. have measured an iep of 9.3 with a method based on pH equilibrium reached in a mixture of denatured Col solution in water, anion exchange resin and cation exchange resin [24]. Li et al. have measured an iep of 9.2, that is shifted to 7.4 in presence of 10 mM Na_2HPO_4 [13]. The determination was performed by electrophoretic mobility measurement, from which zeta potential and iep are

deduced thanks to a model based on several approximations such as a homogeneous charge and sphericity. To conclude, experimental determination of iep for Col molecules is complex. It strongly depends on the approach and on approximations made to obtain the iep value from experimental data. The link between the computed iep value and experimental date is also difficult to establish.

c) Fibronectin

Fibronectin (Fn) is a glycoprotein of the extracellular matrix composed of two identical subunits of 220 kDa linked together by disulfide bonds at the C-teminal end [25]. Each subunit has a length of 61 nm and a diameter of 2 nm [26]. Fn has an experimental iep of 5.2 ± 0.2 [27]. The theoretical iep of bovine Fn is computed at 5.3. The negative charges on Fn molecules come from aspartic acid and glutamic acid which represent 11 % of the total amino acid residues. The positive charges are attributed to arginine, lysine and histidine, which represent 10.4 % of the total amino acid residues. In contrast with Col, there is a good agreement between computed and experimental values of the iep. This can be related to the much more compact shape of Fn compared to Col.

Fn is composed of different domains that interact with specific ECM molecules, such as collagen, fibrin and heparin, or with cells. The amino acid sequence of Fn is composed of three different repeating units: Fn type I, type II or type III as shown on Fig. I.6 [28]. Several of these motifs taken together compose the recognition domains of Fn [5, 28] .

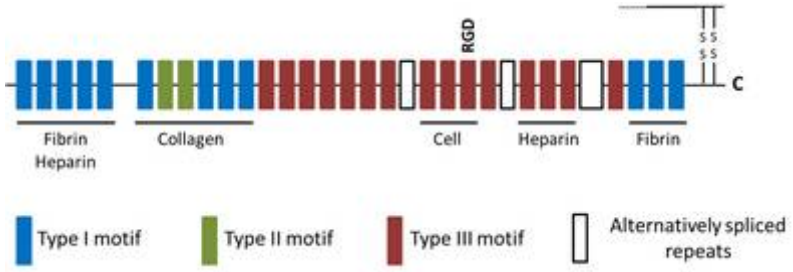

Figure I. 6: Schematic structure of fibronectin, inspired of [28, 29]

Fn has domains that interact with cells through recognition by integrins, which are cell membrane-bound receptors (see section 1.2.2). In particular, the RGD amino acids sequence is well-known to allow this interaction. Other sequences are also known to trigger this interaction. PHRSN is an amino acids sequence that works in synergy with RGD [29, 30]. This peptide does not promote adhesion alone, but it greatly increases the adhesion on RGD sequences. Other sequences, such as LDV and REDV sequences, present on alternatively spliced region of Fn, are also recognized by integrins [29, 31]. These interactions will be explained in more details thereafter.

Fn has also different interaction sites with ECM molecules and thus with collagen. The interaction between Fn and Col is well-known *in vitro*. It was studied by Gold and Pearlstein [32] by adding labelled Fn on surfaces made of different Col types, gelatinized by exposure to NH_3, and air-dried. They have shown that Fn interacts with many Col types and that interaction happens at pH from 2.6 to 10.6 and ionic strength from 0.15 to 4.0 M NaCl. Some studies have shown that interaction between denatured Col and Fn is stronger and more versatile than with native Col [33-35]. It is probably due to the structure of native collagen that masks some interaction sites with Fn. Denaturation allows the exposure of these sites and improves interaction [35].

Fn can also interact with itself. This assembly happens spontaneously when Fn is in contact with cells. Indeed, cryptic sites need to be released to induce interaction between Fn molecules and thus cause fibrillation. The cryptic sites can be exposed when Fn interact with cell integrins because this recognition induces change in Fn conformation. *In vitro*, it is possible to induce Fn fibrillation by addition of denaturing, oxidizing or reducing agent, by application of a mechanical force or by adsorption of Fn on a surface that induces Fn unfolding [36].

After this description of the different components of the ECM, the next section will describe how cells interact with the ECM and how this matrix can influence cell behavior.

1.2.2. Signal transmission between cells and ECM: Integrins

Integrins are transmembrane proteins of the cells. They are composed of two subunits, subunits α and β, having a short intracellular portion and a long extracellular part as shown on Fig. I.7. With the diversity of possible combination between existing α and β subunits, at least 22 different integrins exist [37].

Integrins have two conformations: active and inactive conformation (Fig. I.7). The inactive integrin is less spread than the active form. They switch from one to the other depending on extra- or intracellular signals. It gives to cells the properties to attach to and detach from the matrix. The switch is based on allosteric regulation. The binding of a ligand induce conformational change in integrins. If an extracellular ligand binds the integrin, conformation change will release an intracellular binding site for talin, which triggers a reaction path inside the cells (outside-in signaling). At the opposite, some molecules inside the cells are able to activate talin to induce its integrin binding. Integrins are thus activated and have a higher affinity to extracellular matrix (inside-out signaling) [5, 37]. Integrin activation allows to make a link between ECM molecules and actin filaments inside the cells and thus to transmit signals from ECM to the cells.

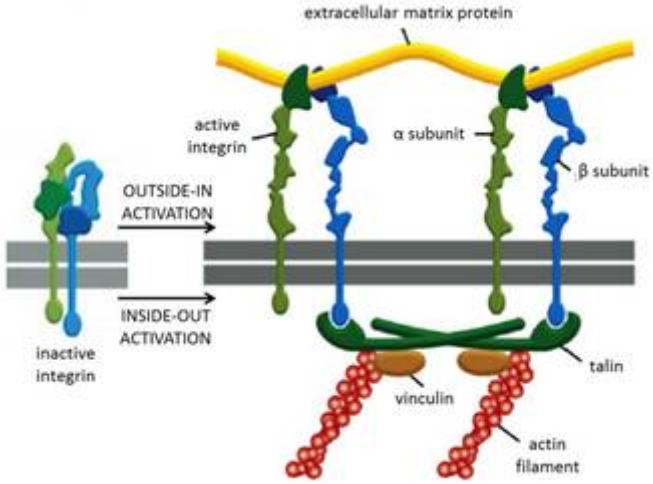

Figure I. 7: Schematic representation of integrin structure and of activation mechanisms [5]

After the integrin ligation, clustering can take place because integrins are mobile in the cell membrane. Focal adhesion points are thus formed, and many intracellular proteins such as vinculin, paxillin, tensin and talin are associated to the clustered integrins (see Fig. I.7). Focal adhesion points are mainly localized at the end of stress fibers because actin filaments of cytoskeleton are linked and polymerized thanks to them.

As shown in Fig. I.8, the formation of the focal adhesion points activates intracellular pathways that will influence cell behavior. More specifically, it triggers phosphorylation of intracellular proteins and can thus regulate many cell functions.

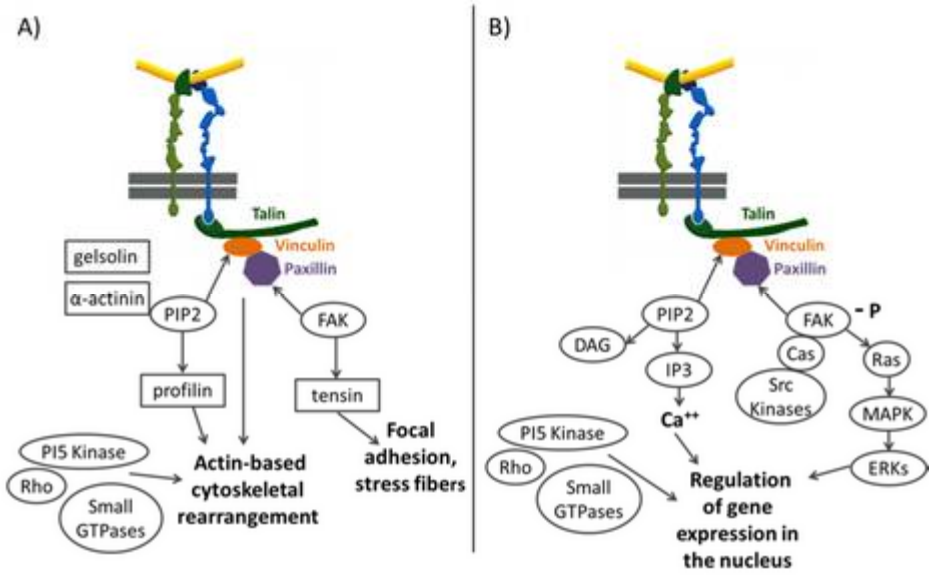

Figure I. 8: Reaction pathways after integrin ligation that conduct to cytoskeleton rearrangement (A) and to modification of gene expression in the nucleus (B). Gelsolin and profilin are actin-binding proteins that regulate actin filaments building; PIP2 is a phospolipid of cell membranes; Ras and Rho are GTPases; IP3 (=triphosphoinositol) and DAG (= diacylglycerol) are molecules implied in signal transduction; ERK = extracellular regulated kinase; CAS = Crk associated substrate; FAK = Focal adhesion kinase; MAPK = mitogen-activated protein kinase (adapted from [5, 37])

Focal adhesion kinase (FAK) is a tyrosine kinase that is phosphorylated with integrins clustering. The activity of FAK will activate other kinases and GTPases. These reaction cascades will recruit molecules implied in actin filament assembly and structuration and will thus influence cytoskeleton and create stress fibers (Fig. I.8.A). These phosphorylations will also activate mitogen-activated protein kinase (MAPK) and other molecules that will finally transmit signals to the nucleus to regulate gene expression and thus modulate cell behavior, metabolism and activity [4, 5, 37] (Fig. I.8.B). The anchorage to ECM, or surfaces decorated with ECM compounds, by integrins is thus essential for growth, proliferation and survival of many cells.

Thanks to this 1.2 section on extracellular matrix components and on the interactions between cells and their environment, we know more about the complex mechanisms that are involved in cell adhesion to ECM. The next section of this chapter will focus on cell interactions with synthetic materials. These interactions are mainly based on mechanisms involving recognition by cell integrins. The properties of interfaces can be tuned to influence this recognition and then modify cell behavior.

> ***In summary, the extracellular matrix possesses a very complex organization. It is made of different biomolecules organized together to give signals to the cells. Collagen and fibronectin are two key ECM proteins. Collagen self-assembles into fibrils, giving very important structural properties to the ECM. Fibronectin delivers cues to cells, playing a very important role for cell behavior and fate. Biomimetic layers based on these two proteins are expected to bring advances for the control of cell-material interactions, with potential applications in biomaterials science and tissue engineering.***

1.3. Cell-material interactions

When a biomaterial is introduced in the body, the first outcome will be protein adsorption on the material. Cells of the body will then interact with these proteins. Chemical properties of a material are thus interesting to optimize with a view to direct this protein adsorption. Mechanical and topographical properties are also important to tailor cell response to the material. For tissue engineering approach, some *in vitro* steps require the use of materials with good surface properties for cells, such as culture plates or flasks and scaffolds. Designing these surfaces with interesting properties for cell adhesion, proliferation and differentiation is thus promising. Understanding cell-material interactions is thus a key for the success of these new strategies. This section will describe in details different approaches used to control this interaction.

1.3.1. Influence of chemical properties

The surface properties of a material have a strong influence on protein adsorption. It is thus possible to modify the material surface properties to influence protein adsorption and thereby influence cell behavior. Another possibility is to modify the surface of a material to add signals which directly influence cell behavior.

a) Chemical properties and protein adsorption

Chemical modification of an interface can influence cell adhesion depending on how proteins adsorb to this interface. Indeed, adsorbed proteins will translate the surface physico-chemical properties to the cells that will be in contact with the surface. It is for example well known that polystyrene plates need to undergo an oxidizing treatment to become tissue-culture polystyrene and be adhesive. It is not because cells directly prefer oxidized polystyrene but it is because proteins adsorbed from serum on oxidized polystyrene are more favorable to cell adhesion. Many studies indeed show that cell adhesion is better on more hydrophilic substrates. As summarized in Fig. I.9 [38], on hydrophobic surfaces with a contact angle higher than 80°, many non-adhesive proteins (ie which cannot interact with integrins) can adsorb and this prevents

adsorption of adhesive proteins. Moreover, if adhesive proteins adsorb, interaction with hydrophobic surfaces may leads to denaturation [38]. These adhesive proteins are thus not anymore in the appropriate conformation to be recognized by integrins. Cell adhesion is improved on more hydrophilic surfaces but when surfaces are too hydrophilic, with a contact angle lower than 45°, adhesion will depend on other surface properties such as material rigidity.

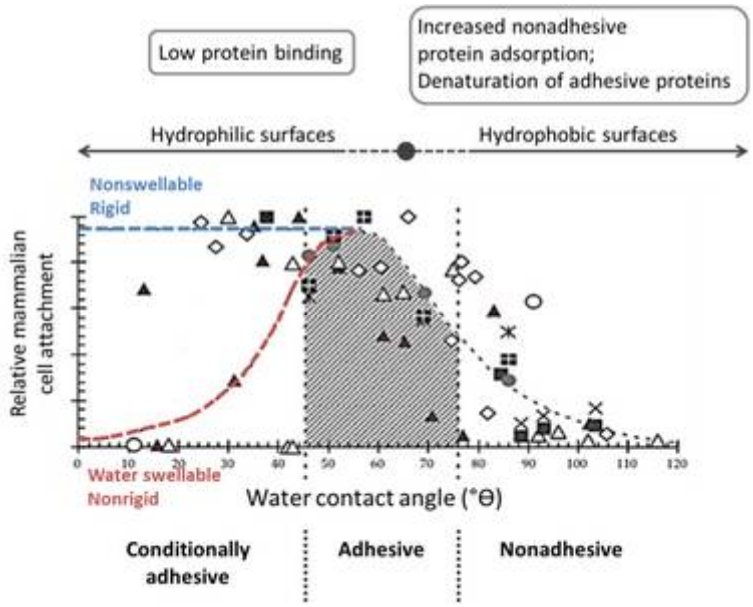

Figure I. 9: Experimental cell adhesion in function of surface hydrophobicity (adapted from [38])

The work of Zuyderhoff et al. (Fig. I.10) [39] is a good illustration of the influence of surface chemistry on protein adsorption and thus on cell behavior. A first part of this work shows that adsorbed collagen presents a different morphology on poly(methylmethacrylate) (PMMA) hydrophilic surfaces (Θ=70°) compared to polystyrene (PS) hydrophobic surfaces (Θ=90°), with a more fibrillar structure on PS. The creation of surfaces with a lateral heterogeneity composed of these two polymers allows to generate a vast diversity of collagen organization on interfaces [21]. A second part of the work focuses on cell behavior on the collagen layers. Cell morphology changes depending on the

surface chemistry. As observed in Fig. I.10, cells present an elongated shape when PS fraction is higher and are more spread with a round shape when PS fraction tends to zero and surfaces are more hydrophilic. It can thus be concluded that protein conformation at the interface will highly influence cell behavior and that this conformation is directed by surface chemistry.

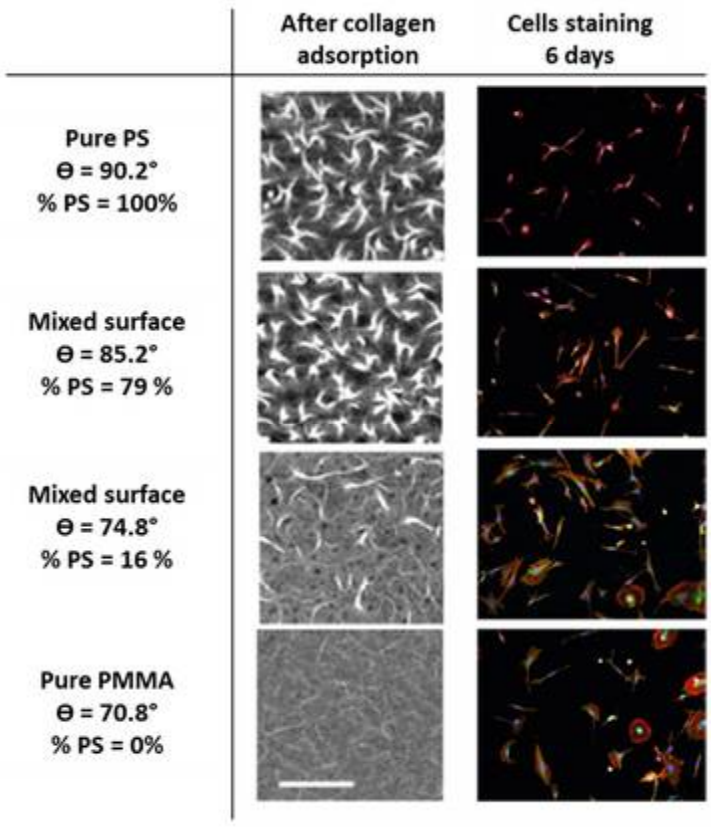

Figure I. 10: Topography images (2.5 x 2.5 µm², Z= 30 nm) obtained by atomic force microscopy of different collagen organization on surfaces with different chemistry (left). Cell images (660 x 870 µm²)after fluorescent staining of MC3T3 (right) (adapted from [39]).

The work of Lin et al. [40] also gives a good example of how surface chemistry influences protein adsorption. In this work, self-assembled monolayers with terminal –OH, -CH_3 and –NH_2 are built. Measurement of adsorption force (F_{ad}) of Fn on these different substrates was performed. This F_{ad} was determined by measuring resistance to shear stress of Fn-coated microsphere injected on the self-assembled monolayers. It shows that $F_{ad}OH << F_{ad}CH_3 < F_{ad}NH_2$. However, even if less Fn is adsorbed on –OH surfaces, cell binding domains of Fn are more exposed on this substrate probably due to a better protein conformation. Cell behavior study on these interfaces then reveals very interesting conclusions. After 2 h, cell adhesion is better on –OH surfaces. Early adhesion is thus linked to accessibility of Fn adhesion site. But after 12 h, adhesion is better for –NH_2 surfaces. At this point, adhesion is thus linked to Fn adsorption force. Actually, Fn adsorbed on –OH surfaces is probably not enough bound to the substrate to support cell traction, unlike -NH_2 surfaces. This study demonstrates that, in addition to protein conformation, adsorption force of a protein can also direct cell behavior.

b) Adhesive pattern to influence cell behavior

Many studies deal with the creation of patterns of adsorbed biomolecules to influence cell behavior. There are different possibilities to create patterns on surfaces. These methods will not be detailed in this section; they include lithographic methods such as microcontact printing, dip-pen lithography, diblock copolymer micelle lithography, etc.[41].

Chen et al. [42] have studied cell behavior as a function of the area of adhesive islands. They have proved that if the size of the adhesive area increases from 75 to 3000 μm^2, cell apoptosis decreases greatly and DNA synthesis increases. Cells need to be well spread to live. Cell behavior on subcellular adhesive spots (30 or 75 μm^2) was also studied. Each spot alone was too small to promote cell adhesion. However, if a pattern of these spots was designed, with each spot separated by 6 µm and 10 µm, for 30 or 75 μm^2 respectively, cell adhesion was improved. Cells can indeed spread across the area without adhesive molecules.

Patterns of multiple subcellular spots were compared to one adhesive island with the same total adhesive area. It was shown that cell growth is improved on patterns of multiple subcellular spots because a higher projected area was developed.

A lot of interest goes to the patterning of RGD sequences. Patterns of gold nanodots can be obtained with specific size and spacing [41] by diblock copolymer micelle lithography. Gold nanodots can then be functionalized by RGD adhesive sequences and the substrate between the nanodots with nonadhesive poly(ethylene oxide). The nanodots size is designed to be the anchoring point of only one integrin. The spacing of the nanodots is shown to be an important parameter to control cell spreading. Actually, a 58 nm spacing gives a good cell spreading unlike a 73 nm spacing for which cells are not well spread. The low spreading of cells on 73 nm-spaced nanodots is due to the limitation of integrins clustering which causes less vinculin clustering and less actin fibers formation.

Next part of this section will now describe the influence of mechanical properties on cell behavior.

1.3.2. Influence of mechanical properties

Mechanical properties are important to govern cell behavior. In the body, mechanical properties vary depending of the tissues [43] and can be characterized by an elastic modulus as shown on Fig. I.11. It can thus be easily understood that material stiffness will influence cell behavior.

Material elasticity influences cell differentiation. Substrates that mimic the stiffness of a specific tissue can guide the differentiation in a cell type specific to this tissue. Engler et al [44] showed that mesenchymal stem cells can undergo neurogenic differentiation on substrates from 0.1 to 1 kPa, myogenic differentiation on substrates from 8 to 17 kPa and osteogenic differentiation on substrates from 25 to 40 kPa.

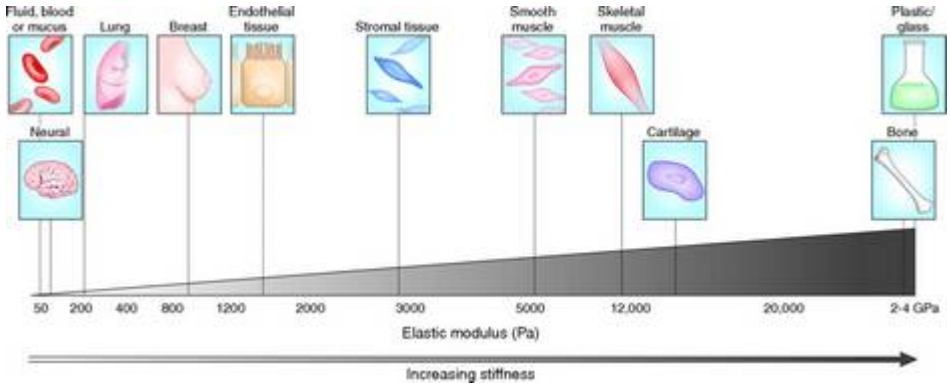

Figure I. 11: Elastic modulus of tissues (from [43])

An interesting work focuses on the creation of a stiffness gradient to study on the same sample the impact of elasticity on cells. Almodóvar et al. [45] have designed layer-by-layer films composed of poly-L-lysine and hyaluronan. Stiffness gradient from 600 kPa to 200 kPa was obtained by the creation of a cross-linking gradient in a microfluidic channel of 45 mm in length. Results obtained with MC3T3 cells have shown that there is higher number of cells and that the cells are more spread on stiffer parts of the channel. Cells are thus clearly influenced by mechanical properties of the layer-by-layer film.

Degand et al. [46] also studied cell reaction to mechanical properties of their substrate. Surfaces were designed to present mechanical heterogeneities. As presented in Fig. I.12, the design of these surfaces is based on colloidal lithography of silica particles. On the top of the particles, a layer of poly(dimethylsiloxane) (PDMS) is then spin-coated. Thanks to this elastomer layer, homogeneous chemistry is obtained on all samples. Moreover, a mechanical heterogeneity is produced, with stiffer parts above colloids, and softer parts around them. Culture of MC3T3 on such substrates has shown that cells are influenced by this mechanical heterogeneity. Proliferation is indeed higher and cell focal adhesion points are more developed on films with colloids. A more detailed analysis was undertaken to compare different cell types: MC3T3 preosteoblasts, C2C12 myoblasts and gingival fibroblasts [47]. It was shown that these cells do not have the same response to different material stiffness. However, the adhesion and the proliferation rates were higher

(MC3T3 preosteoblasts and C2C12 myoblasts) or at least equal (gingival fibroblasts) when cells were grown on mechanically heterogeneous substrates compare to all homogeneous ones. Mechanically heterogeneous substrates are thus more universal to use with different cell types. It is hypothesized that cells can choose the areas with the best mechanical properties for their growth on surfaces which are heterogeneous at the subcellular scale.

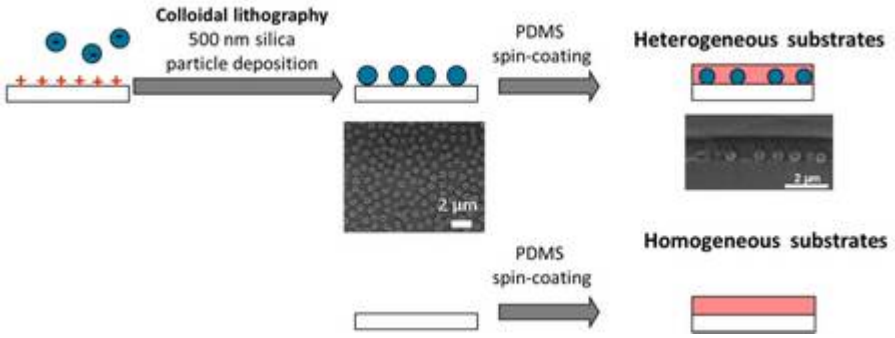

Figure I. 12: Design of surfaces with heterogeneous stiffness for cell culture (adapted from [46])

1.3.3. Influence of topography

The influence of surface topography on cell behavior is also an important parameter to consider. Different types of structures, such as grooves, pillars, pits, etc., can be obtained by photolithography, electron-beam lithography, colloidal lithography or even polymer demixing [48]. These methods allow organized surface patterns to be obtained. Less organized roughness, obtained by acid etching, grit blasting, anodization etc., are also of interest to influence cell behavior [49, 50]. It is well known that roughness of dental implants is an important parameter to improve osteointegration [49]. For example, it is shown that a surface with a rough microtopography increases the secretion of factors that improve osteoblast differentiation and decrease osteoclast formation [50]. Improvement of surface treatment to obtain different kinds of micro- and nano-structures is thus always interesting to consider.

It is not easy to generalize the effect of topography on cells. However, for a specific pattern, there is always an effect of structure size, with adhesion properties that can be better or worse depending on the size of the pattern [48]. One example, the effect of micro-grooved topography, will be developed to illustrate this effect.

Myoblasts behavior was studied on surfaces with grooves having a width in the range of 5 to 75 µm by Charest et al. [51]. Cells were aligned to the grooves and were elongated in the direction parallel to the grooves. Alignment was the best for grooves widths of 5, 10 and 25 µm, with a maximum at 10 µm (Fig. I.13). However, myogenic differentiation was not influenced by the topography.

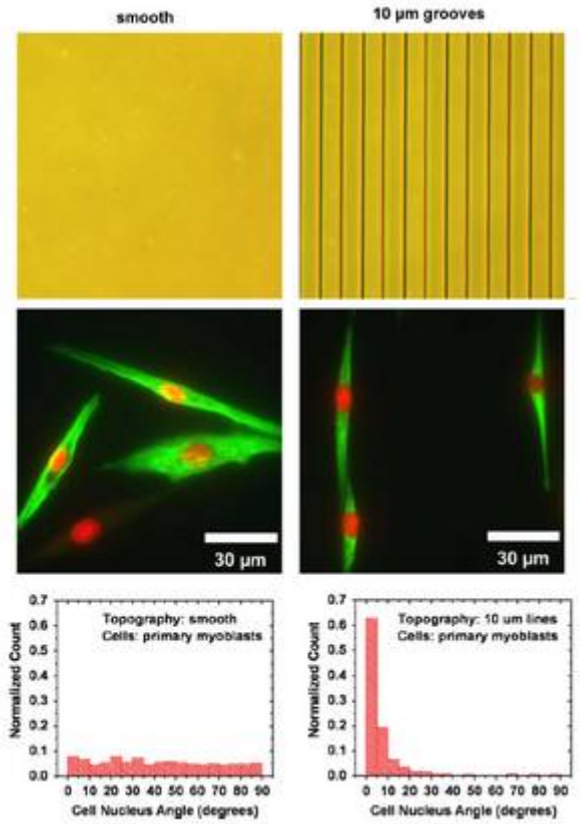

Figure I. 13: Cell alignment on a surface with 10 µm grooves (right), as compared to a smooth control surface (left) [51]

Fibroblasts behavior was also studied on microgrooved surfaces by Dalby et al. [52]. On 12.5 µm-wide grooves, fibroblasts were aligned parallel to the grooves and their nuclei followed the same alignment. As proved by cDNA microarrays, this alignment changed the gene expression and is thus shown to influence cell behavior. Another example developed by Lee et al. [53] shows that grooved surfaces can direct differentiation of human embryonic stem cells (HESC). They have proved that HESC cultured on a ridge/grooved pattern (350 nm in width, 500 nm in height) were elongated in the direction of the pattern. Moreover, neural differentiation was induced on this nanoscale ridge/grooved pattern without addition of biochemical cues. A possible explanation to this behavior is that the cell alignment creates an elongation of the cytoskeleton. This elongation creates a tensional force to the nuclei that influences gene expression [53].

1.3.4. Summary and role of integrins

As shown in the different examples described above, cells are influenced by many physico-chemical characteristics of their substate. However, the mechanisms that trigger cell behavior are almost always the same. They are mainly based on interactions of adhesive proteins with integrins and on the reaction cascade that follows and that involves different focal adhesion proteins [54].

As far as **surface chemistry** is concerned, it is easy to understand that providing sequences that directly interact with cell integrins, or designing patterns of these sequences on an interface, will influence behavior. Moreover, modifying the chemical properties of an interface to influence protein adsorption will modify the way proteins present their adhesion signals and will thus change their interaction with integrins.

It is more complex to understand how mechanical properties and topography influence cell behavior. **Mechanical properties** influence the traction force on cytoskeleton that influences different signaling cascades of the cell. These traction forces can also change the folding of adhesion proteins adsorbed on the surface and thus change their interaction with cells [54]. Three mechanisms

of mechanostranduction can indeed be highlighted. First, when a force is applied on an integrin, the binding activity of this integrin will increase due to conformational changes. This happens a few subseconds after application of tension. Then, a few seconds after tension, integrin-actin connection is strengthened and stabilized by tension due to recruitment of cytoskeletal proteins. Finally, a few minutes after tension, force applied on cells will lead to the conversion of unoccupied low affinity integrins to high affinity integrins [55]. These mechanisms will thus modify integrin response to the material and will influence the signaling pathway explained in section 1.2.2. **Topography** is known to change nucleus shape, which in turn can modify gene expression of the cells [52] and influence their behavior. Influence of topography can, in some cases, be due to differential adsorption of proteins on the interface depending on the topography [54]. This differential adsorption could influence the exposure of signal sequences at the subcellular scale, and thus influence their recognition by integrins. Topography at the cellular scale (µm) may also create limitation in cell expansion in given directions [51]. Changing the cell shape could thereafter change focal adhesion organization and thus change cell behavior.

Finally, the contribution of surface chemical composition, topography and mechanical properties on cell behavior are very difficult to separate. Most of the time, the influence on cells comes from a combination of these properties. For example, surface chemical modification by addition of signal molecules at the interface can also influence surface topography and mechanical properties, even if it is not the first aim of the modification.

> ***In summary, many parameters may be tuned in a view to improve cell-material interaction. Most of the involved mechanisms are based on signal sequence recognition by integrins. Modification of the surface chemistry with two ECM molecules, collagen and fibronectin, could influence different properties of the substrate. Controlling their organization at interfaces is thus of major interest.***

1.4. Layer-by-Layer method to create complex assemblies of proteins

As explained above, materials that mimic ECM signals are promising to improve cell-material interactions. Coating surfaces with ECM proteins is thus of major interest. Combining signals from the main ECM proteins on the same interface can be a key to create materials that mimic better the complexity of the ECM. Moreover, creation of interfaces with a 3D architecture is more close to the real cell environment. Layer-by-layer method, described in details thereafter, is a method that could be used to create complex architectures. It has already been used to assemble proteins and even ECM proteins like collagen and fibronectin. This section will summarize major studies on these assemblies.

1.4.1. Principles of layer-by-layer deposition

Layer-by-layer (LbL) method (Fig. I.14) is a versatile method to combine properties of different polyelectrolytes within multilayered films. Developed by Decher in 1992 [56], the method is based on the alternate dipping of the substrate in polycation and polyanion solutions. A charged substrate is dipped in polyions solution of the opposite charge, which results in polyions adsorption through electrostatic attraction. More than one charge equivalent is however adsorbed on the surface. This overcompensation reverses the global surface charge which gives the opportunity to adsorb a second polyion of opposite charge. Cycles are thus possible and give multilayer structures. This overcompensation is also an interesting feature because it allows the self-limitation of adsorption for each layer, which is necessary to obtain monolayers [57].

Strong polyelectrolytes, as well as weak polyelectrolytes, can be used to build LbL based on electrostatic interactions. Two modes of growth of the multilayers exist: linear and exponential. **Linear growth** is observed when the same amount of polyelectrolyte is adsorbed at new deposition cycle at each layer. It is mainly the case for strong polyelectrolytes. **Exponential growth**, often observed when polysaccharides or polypeptides are used, is characterized by a thickness that increases faster than the number of layers. A higher amount of molecules is adsorbed at each new deposition cycle. The explanation of

exponential growth comes from diffusion of at least one polyelectrolyte in the film. If polyelectrolyte A is mobile into the film, it will diffuse inside it when the film is in contact with polyelectrolyte A solution. Then, when the film will be dipped into polyelectrolyte B solution, polyelectrolyte A will diffuse towards the surface of the film and will create complexes with polyelectrolyte B. These complexes are at the origin of the additional increment of mass at each deposition cycle because the amount of mobile polyelectrolyte A chains available for complexation increases with the film thickness [58, 59].

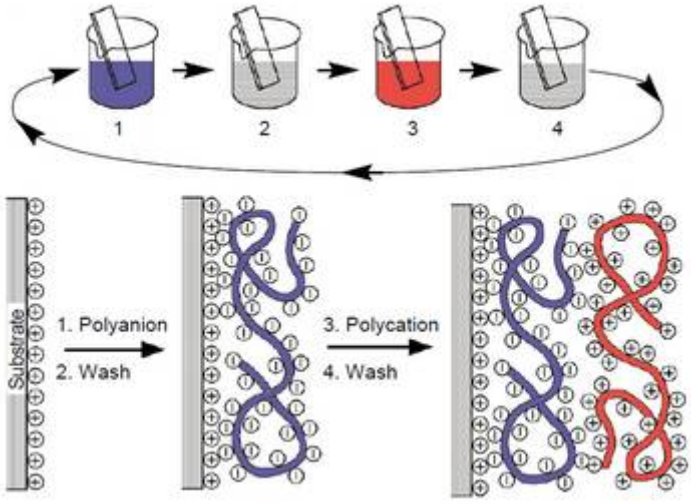

Figure I. 14: Layer-by-layer deposition method (adapted from [57])

LbL assemblies were initially built based on electrostatic interactions between charged entities (polyelectrolytes, charged particles), with charge reversal at each adsorption step. The electrostatic interaction, and thus charge reversal, was often described as being the driving factor of assembly. However, it is more likely a gain of entropy which is the driving factor. This gain is due to the release of small counter ions during the assembly [58]. The charge reversal could just be very advantageous because it prevents charge repulsion when charged polyelectrolytes reach the surface to deposit on the previously built LBL film. Moreover, charge reversal is not observed for each kind of LbL

building [58] and sometimes, molecules with very low charge density can be involved in sustainable assemblies [59]. Other interactions can indeed be govern LbL building, such as donor/acceptor interaction, hydrogen bonding, specific recognition, host-guest interaction, hydrophobic interaction, etc. [59, 60]. This method is thus very versatile and can be applied to different kinds of materials with different shapes. Moreover, the diversity of molecules that can be used to build the layers is high. This includes polymers (linear or branched), colloids, biomacromolecules and small molecules. Finally, the parameters governing the assembly, including concentration, adsorption time, ionic strength, solvent and temperature, can be tuned to obtain films with the desired properties [60].

1.4.2. Layer-by-layer assembly of proteins

As LbL is a versatile method, it can theoretically be applied to proteins. However, proteins have particular properties that make assembly difficult to carry out. First, proteins are weak polyelectolytes, their global charge thus changes with pH. Moreover, proteins are polyampholytes which means that even if the global charge is well defined, domains of the protein can locally bear opposite charges. Accessible charges thus depend on protein structure and charges can be very heterogeneously distributed on the molecule. Finally, the isoelectric point of some proteins is difficult to predict. It is particularly the case for proteins with an anisotropic structure. This isoelectric point indeed depends on the structure of the protein, the nature of surrounding ions and experimental conditions. All these characteristics of proteins make that electrostatic interactions between two proteins are difficult to predict and control. Moreover, proteins generally adsorb in monolayers, even when deposited from mixed proteins solution. Performing LbL assembly based on two proteins is thus unnatural and very challenging.

Despite these difficulties, LbL assembly including proteins has already been reported. Lvov et al. [61] studied the assembly of different proteins with well-known polyelectrolytes. For example, glucose oxidase was combined with poly(ethyleneimine); hemoglobin with poly(ethyleneimine) or

poly(styrenesulfonate) depending on the pH; myoglobine with poly(styrene sulfonate); etc. Many other combinations are also possible and, most of the time, proteins are combined with strong and/or synthetic polyelectrolytes [62]. For the build-up of these assemblies containing a polypeptide, exponential growth is often observed [58]. We will now focus on LbL films based on collagen or fibronectin.

1.4.3. Layer-by-layer based on collagen or fibronectin

Many authors studied the assembly of a given polyelectrolyte with collagen. In our group, the assembly of collagen, native or denatured, with a synthetic polyelectrolyte such as poly(styrene sulfonate) was studied and construction of multilayers was proved [63]. Collagen was also combined to natural polyelectrolytes such as alginate [64, 65], heparin [66-70], chondroitin sulfate [70] and hyaluronic acid [71-73]. In most of the cases, Col is used as a polycation and assembly is performed around pH 4.

Li et al. [64] studied the formation of **Col/alginate** multilayers with and without a poly(ethyleneimine) (PEI) anchoring layer. The PEI layer was reported to slightly increase the film thickness. The films had a morphology with fibrils and were stable in air, in MilliQ water and in buffer at pH 4. Films were however not stable in presence of HPO_4^{2-} ions and at high pH. Cross-linking with EDC (1-ethyl-3-(3-dimethylaminopropyl)carbodiimide hydrochloride) and NHS (N-Hydroxysuccinimide) during 24h improved film stability. Chaubaroux et al. [65] also studied this assembly with an anchoring layer of PEI. They also obtained films with fibrils. In this case, films were crosslinked with genipin to increase stability in physiological conditions. In both studies, films seemed to favor cell adhesion and proliferation.

Films made of Col and **heparin** were also well proposed for cardiovascular applications. The aim of this type of films is to create surfaces with good properties for endothelialization, which explains the use of collagen, but that prevent coagulation, which justifies the use of heparin. Lin et al. [67] studied the assembly on a PEI anchoring layer with quartz crystal microbalance. Results showed that the assembly is sustainable and that films are stable in

physiological conditions. Such LbL coating improves antithrombogenic properties of stainless steel samples by increasing the time for clot formation, as observed by increasing plasma recalcification time with the number of layers (Fig. I.15), and decreasing platelet adhesion. Moreover, the films promote endothelial cell adhesion and proliferation, with a maximum reached after 5 bilayers deposition (Fig. I.15). These properties were also observed for LbL coatings are deposited on stents, which is very promising for cardiovascular disease treatment. The same conclusions were obtained on titanium surfaces with endothelial progenitor cells [69]. When the morphology of the LbL films is studied by AFM, fibrillar structures attributed to collagen, are observed [70].

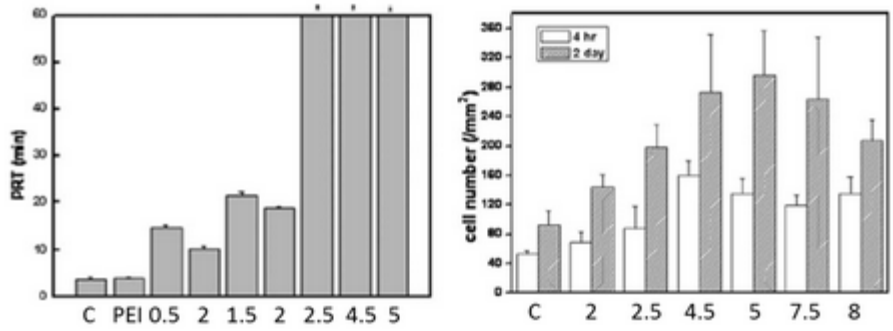

Figure I. 15: Plasma recalcification time (PRT) in min (left) and endothelial cell numbers on Col/Heparin coating (right). PRT time is a measurement of time for clot formation. Control is stainless steel, represented as C on the graphs. PEI sample is just stainless steel coated with a layer of PEI. Other samples are PEI/(Heparin/Col)$_n$ with n represented on the x axis of the graphs [67].

Multilayer films made of collagen and **hyaluronic acid** were also studied to improve cells-material interactions. Johansson et al. [71] studied their assembly by ellipsometry and showed that multilayers are obtained. A dry thickness around 40 nm was measured after 8 bilayers adsorption. Assembly is stable at pH 4, the pH value used for film preparation, but not at pH 7. Films thus need to be crosslinked with EDC/NHS to be used in biological applications. Film roughness increases with the number of layers and collagen fibrils can be observed by atomic force microscopy. This assembly was also studied on a PEI anchoring layer by Zhang et al. [72]. They prove that the charge of the surface is negative after hyaluronic acid adsorption and positive after Col adsorption, as

shown on Fig. I.16. They obtained very thick films of 270 nm after 5 bilayer adsorption and of around 15 µm after 120 bilayers (Fig. I.16). Finally, cell behavior was well studied on these assemblies by Li et al. [73]. They obtained films with a thickness closer to the thickness measured by Johansson by working without PEI. Film degradation was studied in PBS, showing that after 1 day, 25 % of the 4.5 bilayers film is degraded. Despite this degradation, they showed that proliferation and differentiation of preosteoblastic cells is enhanced with the coating compare to virgin titanium surfaces. This type of assembly is thus also interesting to improve cell response.

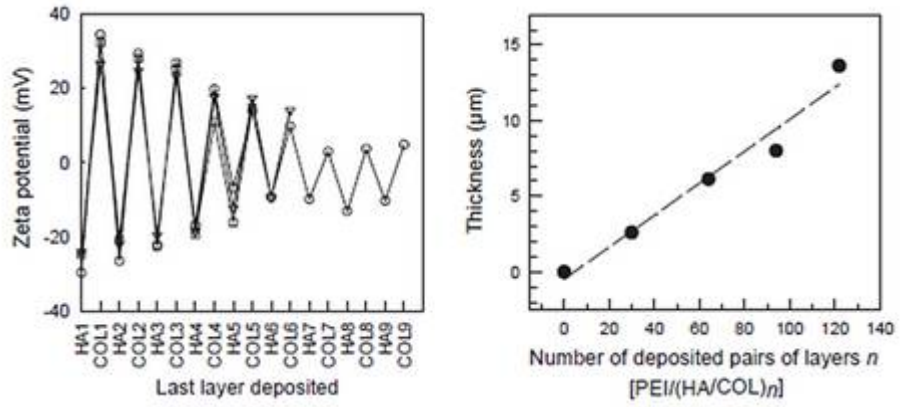

Figure I. 16: Zeta potential measurement (left) and thickness measurement by confocal microscopy section (right) of a PEI/(hyaluronic acid/CoI)$_n$ film building [72].

Fibronectin can also be included in multilayer films. Films of Fn and synthetic polyelectrolytes were prepared in many studies. Fn can be used as an anionic polyelectrolyte at pH 7.4 and thus be combined with poly-L-lysine [74] or poly-D-lysine [75, 76]. Fn can also be combined with natural polyelectrolytes. Films with heparin were studied by Nishiguchi et al. [77]. Assembly was monitored using quartz crystal microbalance and gives a thickness of 26 nm after 5 bilayers. In this work, assemblies were prepared directly on cells to improve cell aggregation and produce *in vitro* 3D-tissue construction. Another study showed that these Fn/Heparin films elaborated on titanium surfaces show anticoagulation properties [78].

Films made of Fn and gelatin, a product obtain from collagen hydrolysis, were also well developed [79-84]. Assembly was monitored by quartz crystal microbalance or by measuring the fluorescence intensity during construction with fluorescent-labeled Fn. These films can be used for different purposes in tissue engineering applications such as the creation of 3D cell assemblies. The protein film can be deposited on a substrate to immobilize a first cell layer and thereafter be deposited again on this cell layer to immobilize a second layer of the same, or of a different, cell type [79]. The film can also be built directly around cells, to protect them from physical stress [82], or to form 3D tissues by cell accumulation technique [83, 84].

Finally, a few papers report the assembly of Fn with Col. Attempts were made to use type IV Col [85] as well as type I Col [86] to construct multilayers. In both studies, the protein layers give interesting properties regarding cell behavior, but assemblies were not characterized in enough details to prove that a LbL construction was achieved with these two proteins.

In summary, layer-by-layer assembly is a promising technique to create complex multilayers based on collagen and fibronectin, and to control the organization of these to proteins at interfaces. The separate use of each of these proteins in layer-by-layer assemblies was shown as promising to improve cell-material interactions for biomedical applications. However, combining these two proteins within the same layer-by-layer assembly was not performed before, is very challenging, and will be investigated in this thesis.

2. Aim of the thesis

Cell-material interactions constitute a key to improve biomaterials and tissue engineering approaches. These interactions depend on many parameters, including chemistry, topography and mechanical properties of the material surface. However, despite the diversity of signals that influence cell behavior, cell-material interactions are ultimately governed by the way integrins at the cell surface interact with the extracellular environment.

In this work, we will focus on modifying interfaces by mimicking the complex organization of the extracellular matrix. The model surface chosen for this study is a polystyrene substrate. Polystyrene is indeed the plastic mainly used for cell culture *in vitro*, which is one of the steps of the tissue engineering approach. Improvement of the properties of these substrates, by improvement of cell adhesion, cell proliferation and differentiation could clearly reduce the time needed for this step and thus improve clinical applications of tissue engineering. On this substrate, we have decided to investigate the deposition of collagen and fibronectin, the two main proteins of the extracellular matrix. Deposition in multilayers of these two proteins, to create thicker layers and more complex architectures, is one of the challenges of this work. Even if it is theoretically possible, this kind of assembly was never reported in details in literature. Moreover, this kind of coating could also be useful for other biomedical applications on other materials than polystyrene.

To summarize, the aim will be to adsorb collagen and fibronectin with different methods and conditions, with a view to tailor biointerfaces with a well-controlled supramolecular organization, and finally to study how cells react to this organization. The strategy followed to design the interfaces will be described in details in the next section. Methods for surface characterization and for study of cell response to the obtained biointerfaces will be presented as well.

3. Research strategy

This section will summarize the main strategic choices that were made throughout the thesis. Some of these decisions were made even before the beginning of the thesis; others were made after a long development of the protocols. In this section, we will focus on a description of the strategic choices. The protocol developments that have sometimes helped to make these choices will be described in chapter 1 of the second part of the thesis.

The research strategy is divided in several parts described on Fig.I.17: (1) The polystyrene substrate was prepared, then (2) different deposition methods of Fn and Col, with different experimental conditions, were tested and the more interesting conditions were selected for (3) a detailed characterization of the properties of the film (thickness, morphology, wettability,…). Finally, (4) stem cell culture experiments were performed to determine how the films influence their behavior.

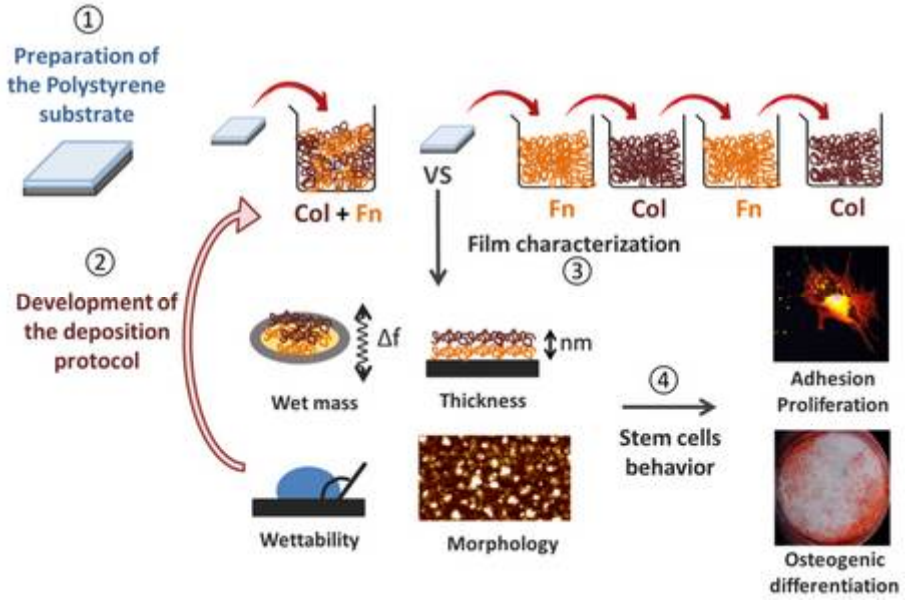

Figure I. 17: Research strategy

3.1. Preparation of polystyrene substrates

Polystyrene (PS) surfaces were chosen as substrate to elaborate biointerfaces. This polymer is the most used as a substrate for *in vitro* cell culture, which is one important step of tissue engineering approach. Many culture flasks and multi-well plates are indeed made of PS. To characterize protein adsorption and to perform some cell culture experiments, it is not always possible to work directly on commercial PS plates. Indeed, characterization techniques are often design to work on small, flat and thin samples. Moreover, specific substrates are sometimes needed for some techniques, such as silicon for ellipsometry and gold covered quartz crystal for quartz crystal microbalance. A well-known technique to obtain PS films on a substrate is spin-coating. However, a major issue appears when PS spin-coated silicon wafers or glass coverslips are immersed for a long time in aqueous medium: the polymer film tends to detach. To improve adhesion between silicon or glass and the polymer, silanization with a well-selected silane can be performed before spin-coating.

3.1.1. Silanization to improve adhesion

Silanization of a surface is based on the reaction between silanol (Si-OH) functions present on the surface of silicon or glass and the Si-Cl or Si-O-R function of a silane molecule. If reaction parameters are well controlled, this method can give well-organized and uniform self-assembled monolayers [87]. These monolayers are very often used to design surfaces with a well-defined chemistry, based on the nature of the terminal function of the selected silane. This method can also be used to improve adhesion of PS films on silica surface as performed by Baujard-Lamotte et al. [88] in a view to study Fn adsorption. In the present work, silanization is used to make silicon/glass surface more hydrophobic. Reaction is performed in a glove box to be in anhydrous conditions and prevent hydrolysis of the silane.

A monochlorosilane, octadecyldimethylchlorosilane (Fig. I.18) was chosen. The choice of this silane will be described in details in chapter 1, section 3.

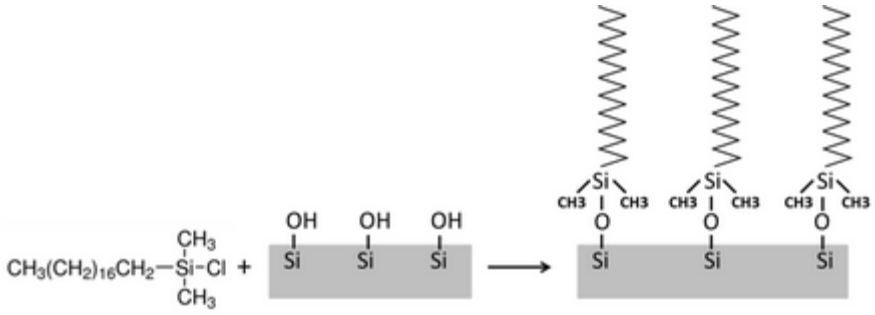

Figure I. 18: Silanization procedure

3.1.2. Spin-coating

Spin-coating is a coating technique used with a view to obtain thin and smooth polymer films, which is very important for morphological characterization and thickness measurements of deposited layers (Fig. I.19). A few drops of polymer solution are deposited on a substrate placed on a rotor. This rotor turns at a defined speed to obtain a thin film of polymer solution. Evaporation of the solvent is then very fast and a homogeneous thin polymer film is finally obtained.

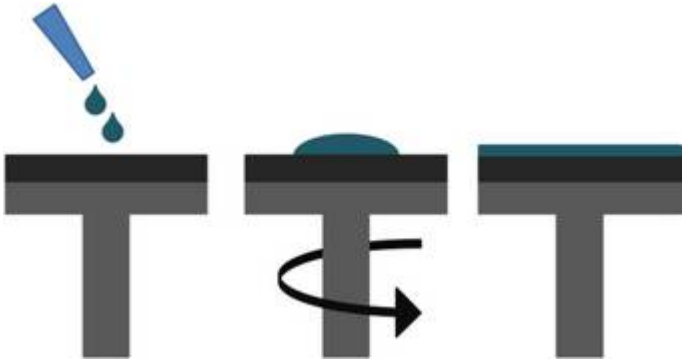

Figure I. 19: Schematic representation of spin-coating procedure

Thickness (h) of the film can be modeled by the empirical equation (I) with k a constant, w the speed of the rotor in rotation per minutes, c the polymer solution concentration and M_n the number average molar mass of the polymer. This equation is empirical but a k value around 23 ($nm.min^{-1/2}.g^{-5/4}.L.mol^{1/4}$) can be determined if units of h are nm, unit of w are rpm, unit of c are g/L and unit of Mn are $g.mol^{-1}$.

$$h = k\,.\,k^{\,k\,\frac{k}{k}}.\,k\,.\,k\,\frac{\frac{k}{k}}{k} \quad \text{(I) [89]}$$

The polymer film thickness thus decreases if the speed of the rotor increases. Thickness is directly proportional to the polymer concentration used. It also depends on the length of polymer chains, characterized by M_n, with the thickness that increases with the fourth root of the molecular mass of the polymer increases.

3.2. Protein coating

One of the aims of this work is to assemble Col and Fn into a complex architecture to mimic the ECM. A well-known method to design organized biointerfaces is the layer-by-layer method described in the 1.4 section of the introduction. However, as explained before, LbL is not so easy to apply to proteins. Moreover, LbL assemblies just based on two proteins were almost never described in literature. In this work, different conditions, including Col denaturation, the addition of an anchoring layer and the use of different buffers will be tested to assess the feasibility of a LbL assembly. This section reports the different parameters used in details.

3.2.1. Deposition method

LbL deposition method (Fig. I.20) will be used to assemble Fn and Col on substrates. LbL deposition will be compared to simultaneous adsorption of Fn and Col (Fig. I.20), obtained by adsorption of mixed solutions of the two proteins on the substrates. The aim of this comparison is to observe if the deposition method has an influence on the adsorbed amount, properties and

protein organization of the films. All the parameters for the LbL deposition method will be determined in the first chapter on the second part of this work.

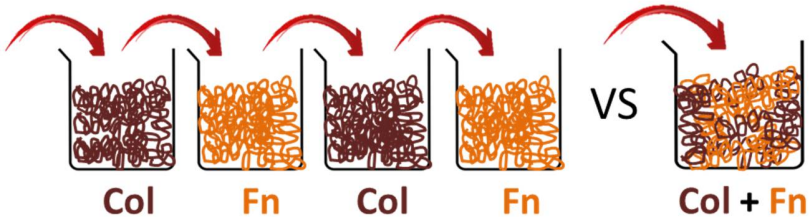

Figure I. 20: Adsorption by layer-by-layer deposition method is compared to simultaneous adsorption

3.2.2. Collagen denaturation

Col denaturation (Fig. I.21) is an interesting parameter to modify for the build-up of the assemblies. As explained in the state of the art, it prevents Col fibrillation. In absence of Col fibrillation, more homogeneous layers are expected to form, that could facilitate further assembly. Moreover, Col-Fn interaction is proved to be better with denatured Col because some interaction sites are not masked by the triple helical conformation. Upon heating of collagen, inter- and intra- helix hydrogen bounds are indeed broken. The three chains of the helix will thus be separated and will take a coiled conformation. Col chains can then form spherical aggregates [90].

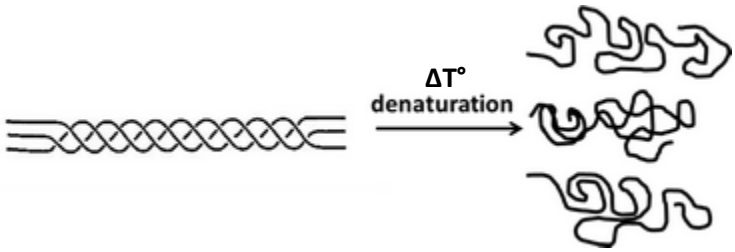

Figure I. 21: Collagen denaturation

3.2.3. Polyethyleneimine anchoring layer

The use of an anchoring layer was tested to improve protein deposition. Branched poly(ethyleneimine) (PEI) was chosen because it is known to improve LbL assembly. Indeed, PEI allows thicker films to be obtained for the same number of deposited layers. One explanation could be that PEI forms a uniform and homogeneous layer on which LbL assembly can grow [91, 92]. However, one disadvantage of the use of PEI in the applications of this work is that PEI could be cytotoxic [93]. It is mainly the case if PEI is free in solution because it can disrupt the negatively-charged membranes of the cells [94]. This effect will be discussed in chapter 3 of the second part of this work. We hope that even if PEI can be cytotoxic, the fact that it is adsorbed and buried under layers of proteins can reduce or suppress its cytotoxicity.

The structure of the PEI used in this work is presented in Fig. I.22. The iep of branched PEI was not experimentally determined. However, it is composed of primary, secondary and tertiary amine, with a pKa between 9 and 11. It can thus be assumed that the iep of PEI is > 9-10.

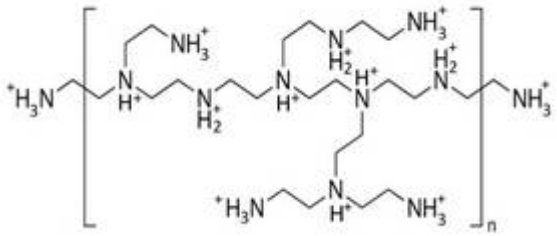

Figure I. 22: Poly(ethyleneimine) (inspired of [95])

3.2.4. Influence of the buffer

Three different buffers, with a close ionic strength, will be tested for the assembly. The first one is phosphate buffer saline (PBS) at pH 7.4. This buffer was chosen because it is widely used to mimic physiological conditions. It will be compared to Hepes buffer (Fig. I.23), also at pH 7.4. The aim of this

comparison is to test the effect of surrounding ions on the assembly. It is indeed known that the phosphates ions of PBS can influence Col properties. For example, isoelectric point of Col is shifted from 9.2 to 7.4 in presence of phosphate ions [13]. The use of Hepes buffer, also widely used in biological applications, and which does not contain phosphate ions, is thus interesting. A third buffer, acetate buffer at pH 5.4, will also be tested. This buffer is extensively used in LbL building and has a different pH than the two other buffers. The signs of the global electrical charges of each type of molecule which used in assemblies are summarized in Table I.1.

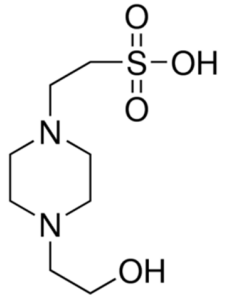

Figure I. 23: HEPES [95]

Table I. 1: Sign of electrical charges of the different molecules involved in the assembly, depending on the buffer (ND = Not defined).

	PBS (pH 7.4)	**Hepes** (pH 7.4)	**Acetate** (pH 5.4)
PEI (iep > 9-10)	+	+	+
Fn (iep ≈ 5.2)	-	-	≈ 0
Col			
•theoretical iep ≈ 9.4	+	+	+
•iep measured by Rossler ≈ 6 [23]	-	-	+
•iep measured by Li with HPO_4^{2-} ≈ 7.5 [13]	≈ 0	ND	ND
•iep measured by Li without HPO_4^{2-} ≈ 9.2 [13]	ND	+	+

3.3. Surface characterization

Five characterization techniques were mainly used to study the designed interfaces. They will be described briefly here, emphasizing on the main information they give.

3.3.1. Quartz crystal microbalance with dissipation monitoring

Quartz crystal microbalance with dissipation monitoring (QCM-D) is used to monitor the adsorption of proteins *in-situ* as schematized in Fig. I.24. The device measures the resonant frequency (f_0) of a quartz crystal based sensor. The adsorption of proteins on the electrode covering the crystal modifies this resonant frequency. If the deposited layer is thin, homogeneous and rigid, the shift of frequency (Δf) can be directly related to the adsorbed mass (Δm) using the Sauerbrey equation (II):

$$\Delta k = -\frac{k}{k} . \Delta k \qquad k\,kdn \quad k = \frac{k_k . k_k}{k_k} \qquad \text{(II) [96]}$$

where **n** is the harmonic number, $\mathbf{t_q}$ the thickness of the crystal and $\boldsymbol{\rho_q}$ the crystal volumetric mass density. The Sauerbrey equation is not always applicable because adsorbed protein layers are not always rigid, homogeneous and thin. They are often swollen with water and thus highly viscoelastic. To offset this problem, QCM-D is also able to measure the dissipation (ΔD) to assess the viscoelasticity of the film by measuring how oscillations decrease after an excitation at the resonant frequency. The shorter the decay, the softer the adsorbed layer is. This measurement of ΔD combined with the measurement of Δf gives relevant information about the properties of the film adsorbed on the crystal. Vicoelastic models can be used to estimate the adsorbed mass. However, the use of such models is not trivial, particularly with complex systems made of layers with different properties, because of the necessary approximations, and the results are thus an evaluation of the real adsorbed mass. It should also be noted that water coupled to the adsorbed layer is included in the deduced Δm, which is then called a “wet mass”.

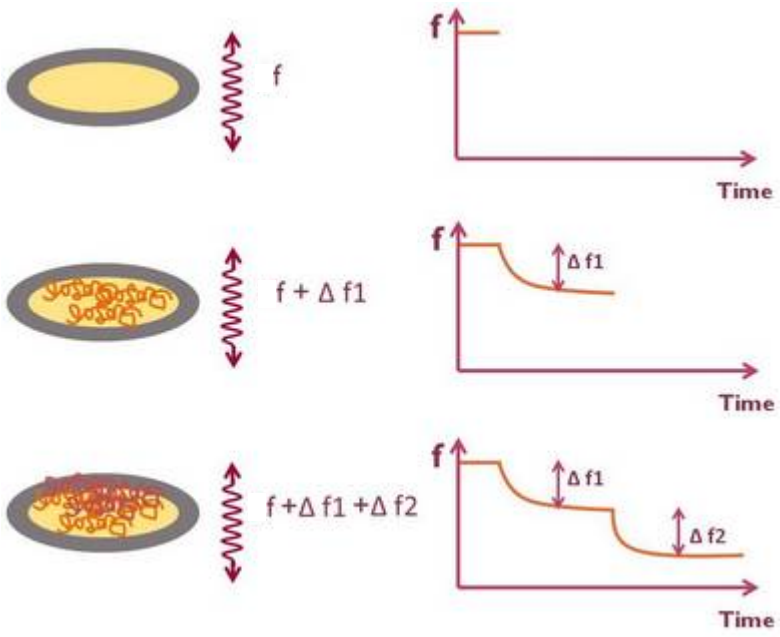

Figure I. 24: Principle of QCM-D. The shift of frequency (Δf) measured after each adsorption step can be related to the adsorbed mass

The main advantage of QCM-D monitoring is that *in situ* measurements are possible. The frequency shift can be measured at each moment of the assembly. It is thus possible to have information on the kinetic of adsorption and on the influence of the rinsing steps. The main disadvantage of this technique is that, as explained before, data treatment is not trivial. It can thus be difficult to extract the exact mass or thickness of the deposited film. It is especially the case when Col is used. Col has indeed a very anisotropic structure, which is 300 nm in length and 1.5 nm in diameter. After deposition, parts of adsorbed Col molecules can stay free in solution and interact with water molecules. Besides, Col can form fibrils. Adsorbed Col layers are thus very difficult to model. Moreover, the wet mass is measured, and not the amount of deposited protein. This technique thus needs to be combined with another one, like ellipsometry, to determine the dry thickness and water content of the films.

3.3.2. Ellipsometry

Ellipsometry measurements allow the dry thickness of thin films to be determined. As illustrated in Fig. I.25, this optical technique is based on polarized light that is reflected on the interface. The polarization changes with the properties of the sample. An amplitude ratio (Ψ) and a phase difference (Δ) can be then measured and can used for modeling of the optical properties and thickness. Ellispometry is generally used to measure thickness of film from sub-nanometers to a few microns.

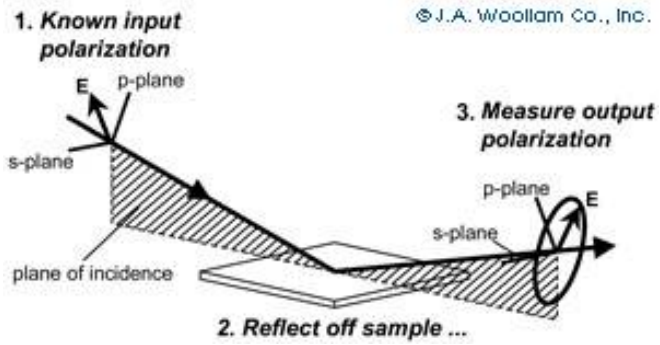

Figure I. 25: Linearly polarized light is directed to the surface and reflected to an analyzer. The polarization change is measured and gives information about the optical properties of the film [97].

In this thesis, two kinds of ellipsometer were used. The first is a multi-wavelength ellipsometer. With this ellipsometer, it is possible to determine different parameters of the films, such as thickness and refractive index, at the same time, thanks to complex models. The second ellipsometer measures Ψ and Δ at only one wavelength. It allows faster measurements for each sample but refractive index need to be known to compute the thickness. In this work, thanks to measurements with the multi-wavelength ellipsometer, we determined the refractive index of the layer and this value was further used when mono-wavelength ellipsometer was used.

The main advantage of ellipsometry is the fast measurement of a very interesting parameter to follow LbL assembly, ie the dry thickness. The main

drawback is that assumptions need to be performed to use the model. Indeed, with both ellipsometers, assumption of a homogeneous and smooth layer is always done. We also consider PS layer and protein layer as a continuous film, having the same properties. We know that these assumptions are not completely met. However, we use the same assumptions of homogeneous and continuous film for all the measurements so that the values can be compared. Moreover, even if the films are not smooth, we probably still measure an average thickness, which is also interesting to know. If needed, the information can be supplemented by analysis with atomic force microscopy to determine the morphology and roughness of the layer.

3.3.3. Atomic force microscopy

Atomic force microscopy (AFM) gives topographical images of the surface with a very high resolution (vertical resolution under 1 nm, lateral resolution of a few nm). Information related to surface chemistry, viscoelasticity and hardness can also be retrieved but will not be used in this thesis and are thus not described here. During the measurement, a tip mounted on a cantilever scans the surface of the sample. A laser is directed to the back of the cantilever and is reflected towards a photodiode to measure the deflection of the cantilever (Fig. I.26). The deflection is related to the properties, and in particular the morphology, of the interface.

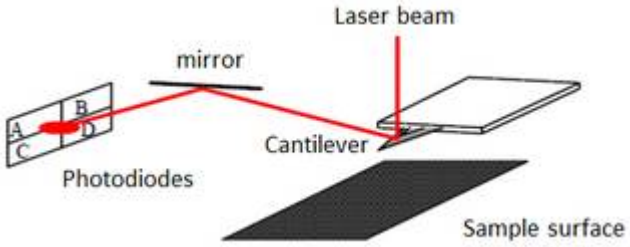

Figure I. 26: Principle of AFM [98]

Two main different imaging modes exist in AFM, the contact mode and the tapping mode. In the contact mode, the sample height is adjusted using a

feedback loop to keep deflection of the cantilever constant while scanning the sample surface. The main disadvantage of the contact mode is that it could damage very soft samples. To overcome this problem, a resonant mode can be used such as tapping mode. In tapping mode, the cantilever oscillates while scanning the interface. The amplitude of the oscillation depends on the distance between the tip and the surface. Here, the height of the sample is thus adjusted to keep the amplitude constant. The adjustments of sample height give information about the topography of the surface. Images of the morphology of the interface can thus be obtained with a very good resolution.

In this thesis, thin layers of proteins will be analyzed. Tapping mode will thus be chosen to avoid damaging the samples. The use of AFM will allow images of the sample morphology to be obtained. It can thus first be used to evaluate the quality of the PS coating. It can also be used to observe Col fibrillation on the surfaces, or holes in the protein layers. To summarize, it will help us to understand better the organization of the proteins on the interfaces.

3.3.4. Contact angle

Contact angle (Θ) measurement is a fast and easy method to determine the wettability of an interface, which is linked to its chemical composition. The method consists in the deposition of a water drop on the surface. The angle between the drop and the flat surface is then measured. The angle is high if the water does not spread. The surface is thus hydrophobic. If the water spreads on the surface, the angle is low and the surface is hydrophilic.

The contact angle is indeed determined by the equilibrium of the forces at the interfaces between liquid, vapor and solid. The Young equation can be derived from this equilibrium, as described in Fig. I.27. The Wenzel equation (Fig. I.27) may further be used to take surface roughness into account. If roughness increases, f, the ratio between the real surface in contact with the liquid and its projection, increases. If Θ > 90°, Θ* will increase; if Θ < 90°, Θ* will decrease with Θ the contact angle of a corresponding smooth surface with the same chemistry as the rough surface, which has a contact angle Θ*. Increase the roughness of a hydrophilic surface will thus turns it in more hydrophilic surface

and increase the roughness of a hydrophobic surface will thus turns it in more hydrophobic surface. Finally, Cassie-Baxter equation (Fig. I.27) describes the contact angle Θ* on heterogeneous surfaces with mixed composition [99]. Θ* can be computed thanks to the contact angle of each kind of domains composing the surface and their respective area. However, some deviations from the Cassie law are observed in real experiments. It is known that advancing contact angle is more influenced by hydrophobic zones of the sample while receding contact angle is more influenced by hydrophilic zones. Static contact angle can be compared to advancing contact angle. It will thus be always more hydrophobic than the one predicted by the Cassie law.

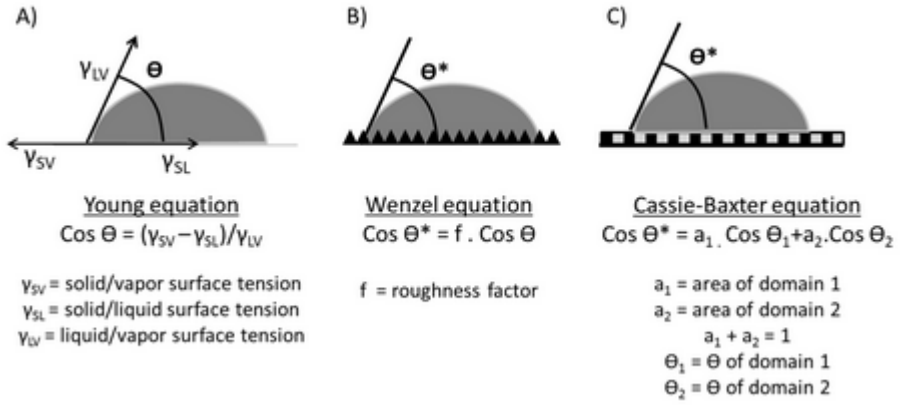

Figure I. 27 : Contact angle measurement and description of the different laws that govern its value, inspired and adapted from [99].

The major advantages of water contact angle measurements are that it gives macroscopic information about the samples and that it is a very rapid and easy characterization technique. However, its major drawback is the difficulty to exactly interpret the change in the wettability of the samples. It needs to be combined with other techniques, like AFM, to characterize the roughness of the sample or even to detect the presence of two phases in the samples. This comparison can help to better understand the change of wettability and to determine their causes.

3.3.5. X-Ray photoelectron spectroscopy

X-Ray photoelectron spectroscopy (XPS) is used to determine the chemical composition of interfaces. This technique is based on the photoelectric effect. If an atom is irradiated by X-Ray photons, it expels electrons. The measurement of the kinetic energy of the expelled electrons allows their binding energy to be calculated. This binding energy is specific of the atom from which electrons come and depends also on the environment (neighboring atoms) and the oxidation state of the atom. For example, the electrons of a carbon atom linked to an oxygen atom will appear at a higher binding energy than the electrons of a carbon atom linked to hydrogen. Indeed, the electrons of the carbon linked to oxygen will be attracted by oxygen that is highly electronegative. These electrons will thus be more difficult to expel due to the reduced electron density of the carbon atom and will appear as more tightly bound. XPS thus gives information about the elementary composition of a sample and the chemical functions in which atoms are involved [100].

The photoelectrons are able to leave the sample if they come from about the first ten nanometers of the surface. The electrons expelled from atoms located underneath undergo collisions preventing them to escape from the material or making them appear in the background. XPS is thus sensitive to the extreme surface layer. Precise quantification of the percentage of each atom present at the interface can be done thanks to sensibility factors, which convert the area under each peak in its atomic percentage. All the elements can be quantified even if their molar fractions are low (typically 0.1 %), excepted Hydrogen and Helium.

XPS is a characterization technique that gives a very precise quantification of the percentage of chemical elements present at the interface. It will be used for some specific analysis described in the future results.

3.4. Cell culture

Because the final aim of this work is to determine if the designed interfaces support the development of biomedical applications, cell culture is an important part of the research strategy. Cell culture can be performed with cell lines that are well-defined and commercially available. However, stem cells are more and more used in research because they are of particularly interest for new therapies and for tissue engineering applications. This section will thus focus on a description of stem cells and more especially on adipose-derived stem cells, with a view to better understand why they were chosen for this work. A description of the different methods to characterize cell behavior will also be given.

3.4.1. Stem cells generality

To be "stem cells", cells have to present two important properties that are (i) to divide for self-renewing and (ii) to be able to differentiate [101, 102]. It exists three types of stem cells that are represented in Fig. I.28:

- **Totipotent cells**: These cells are embryonic stem cells. They come from the zygote obtained after a few divisions of a fertilized egg (up to 8 cells). They are able to form a new complete embryo and even placenta. They are thus able to differentiate into all existing cell types [101, 102].
- **Pluripotent cells**: These cells are embryonic stem cells. They come from the inner cell mass of the blastocyst and are able to differentiate in all cell types of the body [101].
- **Multipotent cells**: These cells are adult stem cells. They are extracted from specific tissues of the body and are able to differentiate only in a few cell types. There are very important for replace cells that are lost or destroyed in adult organs and **tissues** [101].

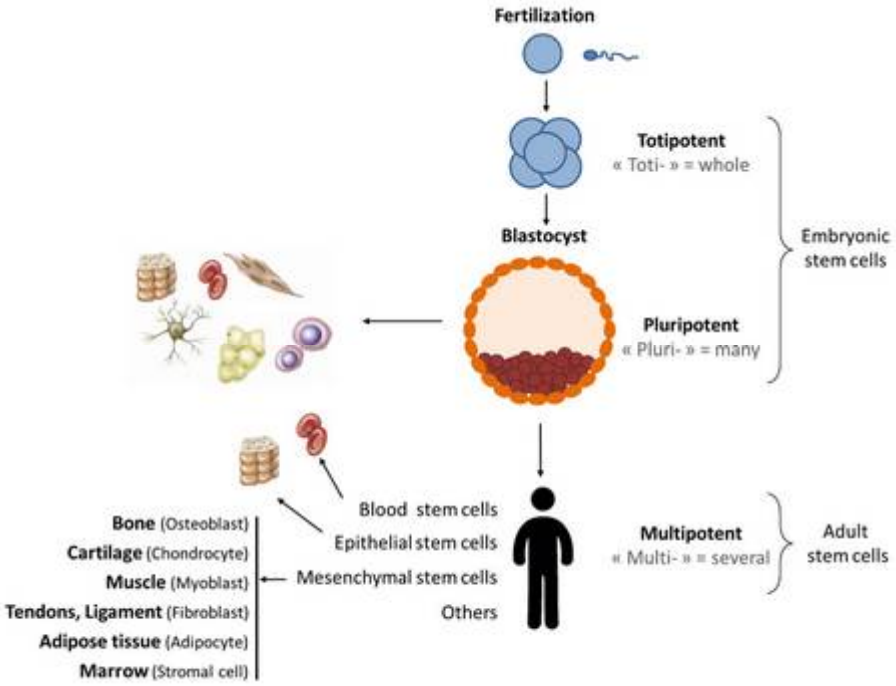

Figure I. 28: Different types of stem cells and the different cells types into tissues in which they can differentiate (inspired of [101, 103]).

Embryonic stem cells are used for very specific research purposes but they raise many ethical issues. Multipotent stem cells are thus mainly used for tissue engineering applications. One type of multipotent stem cells used is mesenchymal stem cells. They are able to differentiate into many different cell types, as shown in Fig. I.28, and especially to undergo osteogenic differentiation. They are thus of major interest for bone defect repair and bone tissue engineering [104]. Mesenchymal stem cell sources are multiple. Two cell sources are well known: bone-marrow and adipose tissue. Bone marrow mesenchymal stem cells are well studied. However, very invasive procedures are needed to collect these cells which cause donor site morbidity. The second source, adipose-tissue, attracts interest of a lot of researchers because harvesting procedures are less invasive [104]. Next section will describe these cells in more details.

3.4.2. Adipose-derived mesenchymal stem cells

Adipose-derived mesenchymal stem cells (AMSC) can be harvested from adipose tissue blocks or from lipoaspirates [104]. They can thus be easily obtained from patients [105]. Tissue blocks are minced before washing, lipoaspirates are directly washed, and both are enzymatically digested by collagenase [106] after this washing step. After digestion, tissue is filtered and centrifuged to isolate cells. Cell expansion and growth is performed *in vitro* to obtain cells that can be used for different applications [104, 106].

In addition to be easily harvested, stem cells yield is 5 times higher and a better proliferation potential is observed for AMSC compared to bone marrow mesenchymal stem cell [106]. Nevertheless, proliferation rate depends on the donor age, the type and location of adipose tissue and the culture conditions [105]. AMSC can be characterized by different surface markers and genes, as reported in Table I.2 [107], such as CD markers (cluster of differentiation). These cells can obviously differentiate into **mesodermal** cell types through adipogenic, osteogenic, chondrogenic, myogenic, cardiomyogenic, angiogenic and tenogenic differentiation [105]. They are also able to differentiate into **ectoderma**l lineages, as shown by expression of markers specific to epithelial cells and by differentiation into neural or neural precursor cells. Lastly, differentiation into **endodermal** lineages is also possible as shown by expression/production of molecules specific to hepatocytes and pancreatic cells [105].

Table I. 2: Surface markers and genes generally expressed or unexpressed by AMSC. The one in bold characters are the more commonly analyze. HLA is human leukocyte antigen; ASMA is smooth muscle cell-specific alpha actin; HLA-DR is HLA-antigen D related; MyD88 is Myeloid differentiation primary response gene 88, adapted from [107].

Positive markers and gene	Negative markers and gene
CD9	**CD11b**
CD10	**CD14**
CD13	**CD19**
CD29	CD31
CD44	**CD34**
CD49	**CD45**
CD54	**CD79α**
CD55	CD80
CD59	CD117
CD73	CD133
CD90	CD144
CD105	**HLA-DR**
CD106	**c-kit**
CD146	MyD88
CD166	STRO-1
HLA I	Lin
Fibronectin	HLA II
Endomucin	
ASMA	
Vimentin	
Collagen-1	

The osteogenic potential of AMSC is good and AMSC have thus been largely studied for bone reconstruction in animal models. Furthermore, some clinical bone reconstruction on human (calvarial defect, maxillary defect, mandibular bone defect) with AMCS seeded on different scaffold give promising results [106]. A very interesting study was performed by Schubert et al. with porcine AMSC [108, 109]. Comparison between AMSC and bone marrow stem cells was performed and confirmed that AMSC have a better *in vitro* proliferation rate. Cells were then differentiated in osteogenic medium, *in vitro*, to give osteo-

differentiated cells. These osteo-differentiated cells were tested *in vivo* with a view to improve osteogenecity of an acellular bone allograft. Osteo-differentiated AMSC are better than osteo-differentiated bone marrow stem cells to improve angiogenesis and osteogenesis [108]. In a second study by the same group, AMSC were differentiated in presence of demineralized bone matrix. It formed a kind of graft that was used to reconstruct bone defects. Results showed that promising reconstruction was obtained [109].

In this thesis, the characterization of cell reaction to the protein-based coatings is very important to better understand AMSC-material interactions.

3.4.3. Study of AMSC behavior

An important part of this thesis is to study how cells react to the designed interfaces. To perform these *in vitro* experiments, human AMSC were used. These AMSC were previously characterized by P.Palacios by fluorescent-activated cell sorting (FACS) for CD 44, CD 45, CD 73, CD 90 and CD 105. FACS were performed for different donors and give profiles positive for CD 44, CD 73, CD 90 and CD 105 and negative for CD 45. AMSC possess the best differentiation potential around passage[1] 4 and have thus to be used around this passage. However, it is impossible to use AMSC at passage 4 from the same donor for a large panel of experiments. We have thus chosen to work on frozen AMSC to avoid variations due to the donor and obtain more reliable results. AMSC extracted from a 39 years old woman were cultured, were frozen at passage 4 and were used at passage 5 for all the experiments. FACS analysis was not performed for the donor used in this work. However, observed cell behavior was the same than the one usually observed for AMSC. Moreover, FACS analyses for other donors, with the same harvesting method, were almost always characteristic of AMSC. We can thus assess that the cells used in this work are real AMSC.

[1] A “passage” is the action to detach cells from their substrate before they cover the entire surface, to suspend them in culture medium and to seed diluted cell suspension on a new surface to allow cells growth. The number of passage is used as a time unit to determine the age of the cells.

The first characteristic of cell behavior that can be studied, already after a few hours, is **cell adhesion**. Cell adhesion and spreading are indicative of good interactions between the interface and cell integrins. It also indicates that cells are healthy. In this work, cell components essential for adhesion, i.e. actin filaments and vinculin, will be stained with fluorescent dyes, as well as the nucleus. Cells will then be observed with a fluorescence microscope. A second characteristic of the cell behavior is the **proliferation rate**. In this work, metabolic activity of the cells will regularly be measured by *Alamar Blue* assay. This activity can be linked to the cell number on the interface and can thus be used to monitor the cell number as a function of time.

A third characteristic of cell behavior is **cell differentiation**. In this work, we will focus on osteogenic differentiation. During differentiation process, cells produce many different markers (osteocalcin, osteopontin, alkaline phosphatase, etc.) [110]. These markers appear at different stages of the differentiation process and different assays exist to detect them. In this work, alkaline phosphatase activity will be measured. This marker appears at the beginning of the differentiation phase. It degrades inorganic pyrophosphates to increase the concentration of phosphate ions available for mineralization [110]. During osteogenic differentiation, there is also a mineralization of the cell matrix. It is possible to color the calcium deposit with *Alizarin red*. Calcium and alizarin form a complex that is red. Stained samples can be observed macro- and microscopically, and a percentage of mineralized matrix can be computed.

Establish a link between cell behavior and interface properties is interesting to increase the general knowledge on AMSC. Even if this knowledge is not applied *in vivo* in this work, it could be used to design new scaffolds for tissue engineering in the future. This knowledge can also improve the materials used in the phase of proliferation and *in vitro* differentiation of tissue engineering approaches.

The second part of this thesis will present the different experimental results obtained during this work. **Chapter 1** will describe the protocols for silanization as well as the development performed for LbL deposition. Moreover, this first

chapter will give first results about Col adsorption on polystyrene, in specific conditions which will have been chosen. **Chapter 2** will then focus on the physico-chemical characterization of the biointerfaces built by LbL deposition method and by simultaneous adsorption. Finally, **chapter 3** will summarize the properties of the more interesting designed interfaces, which will be used for cell culture. It will also detail the behavior of cells on these assemblies and will aim at establishing a link between this behavior and physico-chemical properties of the designed biointerfaces.

References

1. Ratner, B.D., *Biomaterial Science: An Interdisciplinary Endeavor*, in *Biomaterials Science: An Introduction to Materials in Medicine*, B.D. Ratner, et al., Editors. 1996, Academic Press: San Diego. p. 1-8.
2. Williams, D.F., *On the nature of biomaterials.* Biomaterials, 2009. **30**(30): p. 5897-5909.
3. Hench, L.L. and J.M. Polak, *Third-generation biomedical materials.* Science, 2002. **295**(5557): p. 1014+1016-1017.
4. von der Mark, K. and J. Park, *Engineering biocompatible implant surfaces: Part II: Cellular recognition of biomaterial surfaces: Lessons from cell–matrix interactions.* Progress in Materials Science, 2013. **58**(3): p. 327-381.
5. Alberts, B., et al., *Molecular Biology of The Cell*. 5th ed. 2008, New-York: Garland Sciences.
6. Campbell, N. and J. Reece, *Biologie*. 7th ed. 2007, Paris: Pearson Education France.
7. Beckman, M.J., K.J. Shields, and R.F. Diegelmann, *Collagen*, in *Encyclopedia of biomaterials and biomedical engineering*, G.E. Wnek and G.L. Bowlin, Editors. 2004, Marcel Dekker: New-York p. 324-334.
8. Piez, K.A., *Collagen*, in *Encyclopedia of polymer sciences and engineering*, J. Kroschwitz, Editor. 1985, Willey: New-York. p. 699-727.
9. Koide, T. and K. Nagata, *Collagen Biosynthesis*, in *Collagen: Primer in Structure, Processing and Assembly*, J. Brinckmann, H. Notbohm, and P.K. Müller, Editors. 2005, Springer: Berlin. p. 85-114.
10. Birk, D.E. and P. Bruckner, *Collagen Suprastructures*, in *Collagen: Primer in Structure, Processing and Assembly*, J. Brinckmann, H. Notbohm, and P.K. Müller, Editors. 2005, Springer: Berlin. p. 185-205.
11. Hamaia, S. and R.W. Farndale, *Integrin recognition motifs in the human collagens*, in *Advances in Experimental Medicine and Biology*2014. p. 127-142.
12. Silver, F.H., *Type I collagen fibrillogenesis in vitro. Additional evidence for the assembly mechanism.* Journal of Biological Chemistry, 1981. **256**(10): p. 4973-4977.
13. Li, Y., et al., *pH effects on collagen fibrillogenesis in vitro: Electrostatic interactions and phosphate binding.* Materials Science and Engineering C, 2009. **29**(5): p. 1643-1649.

14. Wood, G.C. and M.K. Keech, *The formation of fibrils from collagen solutions. 1. The effect of experimental conditions: kinetic and electron-microscope studies.* The Biochemical journal, 1960. **75**: p. 588-598.
15. Gross, J. and D. Kirk, *The heat precipitation of collagen from neutral salt solutions:Some Rate-regulating factors.* Journal of biological chemistry, 1958. **233**(2): p. 355-360.
16. Harris, J.R. and A. Reiber, *Influence of saline and pH on collagen type I fibrillogenesis in vitro: Fibril polymorphism and colloidal gold labelling.* Micron, 2007. **38**(5): p. 513-521.
17. Harris, J.R., A. Soliakov, and R.J. Lewis, *In vitro fibrillogenesis of collagen type I in varying ionic and pH conditions.* Micron, 2013. **49**: p. 60-68.
18. Gurdak, E., P.G. Rouxhet, and C.C. Dupont-Gillain, *Factors and mechanisms determining the formation of fibrillar collagen structures in adsorbed phases.* Colloids and Surfaces B: Biointerfaces, 2006. **52**(1): p. 76-88.
19. Dupont-Gillain, C.C., I. Jacquemart, and P.G. Rouxhet, *Influence of the aggregation state in solution on the supramolecular organization of adsorbed type I collagen layers.* Colloids and Surfaces B: Biointerfaces, 2005. **43**(3-4): p. 179-186.
20. Gurdak, E., et al., *Resolution of the vertical and horizontal heterogeneity of adsorbed collagen layers by combination of QCM-D and AFM.* Langmuir, 2005. **21**(23): p. 10684-10692.
21. Zuyderhoff, E.M. and C.C. Dupont-Gillain, *Nano-organized collagen layers obtained by adsorption on phase-separated polymer thin films.* Langmuir, 2012. **28**(4): p. 2007-2014.
22. Gurdak, E., et al., *Influence of collagen denaturation on the nanoscale organization of adsorbed layers.* Journal of Colloid and Interface Science, 2006. **302**(2): p. 475-484.
23. Rößler, S., et al., *Investigation of the adsorption of tropocollagen type I on titanium and Ti6Al4V.* Journal of Adhesion Science and Technology, 2000. **14**(3): p. 453-465.
24. Hattori, S., et al., *Alkali-treated collagen retained the triple helical conformation and the ligand activity for the cell adhesion via alpha2beta1 integrin.* J Biochem, 1999. **125**(4): p. 676-84.
25. Hynes, R.O. and K.M. Yamada, *Fibronectins: Multifunctional modular glycoproteins.* Journal of Cell Biology, 1982. **95**(2 I): p. 369-377.

26. Engel, J., et al., *Shapes, domain organizations and flexibility of laminin and fibronectin, two multifunctional proteins of the extracellular matrix.* Journal of Molecular Biology, 1981. **150**(1): p. 97-120.
27. Tooney, N.M., et al., *Solution and surface effects on plasma fibronectin structure.* Journal of Cell Biology, 1983. **97**(6): p. 1686-1692.
28. Aumailley, M. and B. Gayraud, *Structure and biological activity of the extracellular matrix.* Journal of Molecular Medicine, 1998. **76**(3-4): p. 253-265.
29. Pankov, R. and K.M. Yamada, *Fibronectin at a glance.* Journal of Cell Science, 2002. **115**(20): p. 3861-3863.
30. Redick, S.D., et al., *Defining Fibronectin's Cell Adhesion Synergy Site by Site-Directed Mutagenesis.* The Journal of Cell Biology, 2000. **149**(2): p. 521-527.
31. Akiyama, S.K., K. Olden, and K.M. Yamada, *Fibronectin and integrins in invasion and metastasis.* Cancer and Metastasis Reviews, 1995. **14**(3): p. 173-189.
32. Gold, L.I. and E. Pearlstein, *Fibronectin-collagen binding and requirement during cellular adhesion.* Biochemical Journal, 1980. **186**(2): p. 551-559.
33. Engvall, E., M.L. Bell, and E. Ruoslahti, *Affinity chromatography of collagen on collagen-binding fragments of fibronectin.* Collagen and Related Research, 1981. **1**(6): p. 505-516.
34. Engvall, E., E. Ruoslahti, and E.J. Miller, *Affinity of fibronectin to collagens of different genetic types and to fibrinogen.* Journal of Experimental Medicine, 1978. **147**(6): p. 1584-1595.
35. Ingham, K.C., R. Landwehr, and J. Engel, *Interaction of fibronectin with C1q and collagen.* European Journal of Biochemistry, 1985. **148**(2): p. 219-224.
36. Cantini, M., P. Rico, and M. Salmerón-Sánchez, *Fibronectin Fibrillogenesis at the Cell-Material Interface*. 2012. p. 189-212.
37. Giliberti, D.C., K.K. White, and K.C. Dee, *Control of cell-biomaterial interactions*, in *Polymeric Biomaterials*, S. Dumitriu, Editor. 2002, Marcel Dekker: New-York. p. 361-375
38. Harbers, G.M. and D.W. Grainger, *Cell-material interactions: Fundamental design issues for tissue engineering and clinical considerations*, in *An introduction to biomaterials*

S.A. Guelcher and J.O. Hollinger, Editors. 2006, Taylor and Francis group: USA. p. 15-45.
39. Zuyderhoff, E.M., *Heterogeneous surfaces with organized collagen layers for the control of cell behavior*, 2012, Université catholique de Louvain: Louvain-la-Neuve.
40. Lin, M., et al., *Adsorption Force of Fibronectin on Various Surface Chemistries and Its Vital Role in Osteoblast Adhesion.* Biomacromolecules, 2015. **16**(3): p. 973-984.
41. Spatz, J.P., *Cell-Nanostructure interactions*, in *Nanobiotechnology*, C. Niemeyer and C. Mirkin, Editors. 2004, Wiley-VCH: Weinheim.
42. Chen, C.S., et al., *Geometric control of cell life and death.* Science, 1997. **276**(5317): p. 1425-1428.
43. Cox, T.R. and J.T. Erler, *Remodeling and homeostasis of the extracellular matrix: implications for fibrotic diseases and cancer.* Disease Models and Mechanisms, 2011. **4**(2): p. 165-178.
44. Engler, A.J., et al., *Matrix Elasticity Directs Stem Cell Lineage Specification.* Cell, 2006. **126**(4): p. 677-689.
45. Almodóvar, J., et al., *Gradients of physical and biochemical cues on polyelectrolyte multilayer films generated via microfluidics.* Lab on a Chip - Miniaturisation for Chemistry and Biology, 2013. **13**(8): p. 1562-1570.
46. Degand, S., B. Knoops, and C.C. Dupont-Gillain, *Design and characterization of surfaces presenting mechanical nanoheterogeneities for a better control of cell-material interactions.* Colloids and Surfaces A: Physicochemical and Engineering Aspects, 2014. **442**: p. 164-172.
47. Degand, S., *Design of surfaces with mechanical nanoheterogeneities for a better control of cell-material interactions*, 2013, Université catholique de Louvain: Louvain-la-Neuve.
48. Kearns, V.R., R.J. McMurray, and M.J. Dalby, *Biomaterial topography to control cellular response: technologies, cell behaviour and biomedical applications*, in *Surface modification of biomaterials: Methods, analysis and applications*, R. Williams, Editor. 2011, Woodhead Publishing Cambridge. p. 169-201.
49. Sammons, R.L., *Modifying biomaterial surfaces to optimise interactions with bone*, in *Surface modification of biomaterials: Methods, analysis and applications*, R. Williams, Editor. 2011, Woodhead Publishing Cambridge. p. 365-400.

50. Lossdörfer, S., et al., *Microrough implant surface topographies increase osteogenesis by reducing osteoclast formation and activity.* Journal of Biomedical Materials Research - Part A, 2004. **70**(3): p. 361-369.
51. Charest, J.L., A.J. García, and W.P. King, *Myoblast alignment and differentiation on cell culture substrates with microscale topography and model chemistries.* Biomaterials, 2007. **28**(13): p. 2202-2210.
52. Dalby, M.J., et al., *Nucleus alignment and cell signaling in fibroblasts: Response to a micro-grooved topography.* Experimental Cell Research, 2003. **284**(2): p. 274-282.
53. Lee, M.R., et al., *Direct differentiation of human embryonic stem cells into selective neurons on nanoscale ridge/groove pattern arrays.* Biomaterials, 2010. **31**(15): p. 4360-4366.
54. Janson, I.A. and A.J. Putnam, *Extracellular matrix elasticity and topography: Material-based cues that affect cell function via conserved mechanisms.* Journal of Biomedical Materials Research - Part A, 2014.
55. Ross, T.D., et al., *Integrins in mechanotransduction.* Current Opinion in Cell Biology, 2013. **25**(5): p. 613-618.
56. Decher, G., J.D. Hong, and J. Schmitt, *Buildup of ultrathin multilayer films by a self-assembly process: III. Consecutively alternating adsorption of anionic and cationic polyelectrolytes on charged surfaces.* Thin Solid Films, 1992. **210-211**(Part 2): p. 831-835.
57. Decher, G., *Fuzzy nanoassemblies: Toward layered polymeric multicomposites.* Science, 1997. **277**(5330): p. 1232-1237.
58. V. Klitzing, R., *Internal structure of polyelectrolyte multilayer assemblies.* Physical Chemistry Chemical Physics, 2006. **8**(43): p. 5012-5033.
59. Borges, J. and J.F. Mano, *Molecular interactions driving the layer-by-layer assembly of multilayers.* Chemical Reviews, 2014. **114**(18): p. 8883-8942.
60. Decher, G., *Polyelectrolyte multilayers, an overview*, in *Multilayer thin films: Sequential assembly of nanocomposite materials*, G. Decher and J.B. Schlenoff, Editors. 2003, Wiley: Weinheim. p. 1-46.
61. Lvov, Y., et al., *Assembly of multicomponent protein films by means of electrostatic layer-by-layer adsorption.* Journal of the American Chemical Society, 1995. **117**(22): p. 6117-6123.
62. Lvov, Y., *Electrostatic layer-by-layer assembly of proteins and polyions*, in *Protein architecture: Interfacing molecular assemblies and*

immobilization biotechnology, Y. Lvov and H. Möhwald, Editors. 2000, Marcel Dekker: New-York. p. 125-167.

63. Landoulsi, J., S. Demoustier-Champagne, and C. Dupont-Gillain, *Self-assembled multilayers based on native or denatured collagen: Mechanism and synthesis of size-controlled nanotubes.* Soft Matter, 2011. **7**(7): p. 3337-3347.
64. Li, W., et al., *Natural Polyelectrolyte Self-Assembled Multilayers Based on Collagen and Alginate: Stability and Cytocompatibility.* Biomacromolecules, 2013. **14**(8): p. 2647-2656.
65. Chaubaroux, C., et al., *Collagen-based fibrillar multilayer films cross-linked by a natural agent.* Biomacromolecules, 2012. **13**(7): p. 2128-2135.
66. Lu, S., et al., *Synthetic ePTFE Grafts Coated with an Anti-CD133 Antibody-Functionalized Heparin/Collagen Multilayer with Rapid in vivo Endothelialization Properties.* ACS Applied Materials & Interfaces, 2013.
67. Lin, Q., et al., *Heparin/collagen multilayer as a thromboresistant and endothelial favorable coating for intravascular stent.* Journal of Biomedical Materials Research - Part A, 2011. **96**(1): p. 132-141.
68. Chou, C.C., H.J. Zeng, and C.H. Yeh, *Blood compatibility and adhesion of collagen/heparin multilayers coated on two titanium surfaces by a layer-by-layer technique.* Thin Solid Films, 2013.
69. Chen, J., et al., *Collagen/heparin coating on titanium surface improves the biocompatibility of titanium applied as a blood-contacting biomaterial.* Journal of Biomedical Materials Research - Part A, 2010. **95**(2): p. 341-349.
70. Mhanna, R.F., J. VörÖs, and M. Zenobi-Wong, *Layer-by-layer films made from extracellular matrix macromolecules on silicone substrates.* Biomacromolecules, 2011. **12**(3): p. 609-616.
71. Johansson, J.Å., et al., *Build-up of collagen and hyaluronic acid polyelectrolyte multilayers.* Biomacromolecules, 2005. **6**(3): p. 1353-1359.
72. Zhang, J., et al., *Natural polyelectrolyte films based on layer-by layer deposition of collagen and hyaluronic acid.* Biomaterials, 2005. **26**(16): p. 3353-3361.
73. Li, X., et al., *The responses of preosteoblasts to collagen/hyaluronic acid polyelectrolyte multilayer coating on titanium.* Polymers for Advanced Technologies, 2012. **23**(4): p. 756-764.

74. Soumetz, F.C., L. Pastorino, and C. Ruggiero, *Human osteoblast-like cells response to nanofunctionalized surfaces for tissue engineering.* Journal of Biomedical Materials Research - Part B Applied Biomaterials, 2008. **84**(1): p. 249-255.
75. Ai, H., et al. *Coating bio-nanofilm on PDMS through layer-by-layer self-assembly*. in *Annual International Conference of the IEEE Engineering in Medicine and Biology - Proceedings*. 2002.
76. Ai, H., et al., *Biocompatibility of layer-by-layer self-assembled nanofilm on silicone rubber for neurons.* Journal of Neuroscience Methods, 2003. **128**(1-2): p. 1-8.
77. Nishiguchi, A., M. Matsusaki, and M. Akashi, *Cell-cell crosslinking by bio-molecular recognition of heparin-based layer-by-layer nanofilms.* Macromolecular Bioscience, 2015. **15**(3): p. 312-317.
78. Li, G., P. Yang, and N. Huang. *Layer-by-layer construction of the heparin/fibronectin coatings on titanium surface:Stability and functionality*. in *Physics Procedia*. 2011.
79. Matsusaki, M., et al., *Fabrication of cellular multilayers with nanometer-sized extracellular matrix films.* Angewandte Chemie - International Edition, 2007. **46**(25): p. 4689-4692.
80. Uchida, N., et al., *Nanometer-sized extracellular matrix coating on polymer-based scaffold for tissue engineering applications.* Journal of Biomedical Materials Research - Part A, 2015.
81. Kadowaki, K., M. Matsusaki, and M. Akashi, *Control of cell surface and functions by layer-by-layer nanofilms.* Langmuir, 2010. **26**(8): p. 5670-5678.
82. Matsuzawa, A., M. Matsusaki, and M. Akashi, *Effectiveness of nanometer-sized extracellular matrix layer-by-layer assembled films for a cell membrane coating protecting cells from physical stress.* Langmuir, 2013. **29**(24): p. 7362-7368.
83. Matsusaki, M., et al., *Layer-by-layer assembly through weak interactions and their biomedical applications.* Advanced Materials, 2012. **24**(4): p. 454-474.
84. Matsuzawa, A., M. Matsusaki, and M. Akashi, *Construction of three-dimensional liver tissue models by cell accumulation technique and maintaining their metabolic functions for long-term culture without medium change.* Journal of Biomedical Materials Research - Part A, 2014.

85. Mehta, G., et al., *Polyelectrolyte-clay-protein layer films on microfluidic PDMS bioreactor surfaces for primary murine bone marrow culture**.* Advanced Functional Materials, 2007. **17**(15): p. 2701-2709.
86. Omorphos, N.P., L. Kahn, and D.M. Kalaskar, *Design of extracellular protein based particles for intra and extra-cellular targeting.* Colloids and Surfaces B: Biointerfaces, 2015. **136**: p. 440-448.
87. Wang, M., et al., *Self-assembled silane monolayers: Fabrication with nanoscale uniformity.* Langmuir, 2005. **21**(5): p. 1848-1857.
88. Baujard-Lamotte, L., et al., *Kinetics of conformational changes of fibronectin adsorbed onto model surfaces.* Colloids and Surfaces B: Biointerfaces, 2008. **63**(1): p. 129-137.
89. Vanden Eynde, X., Polymer surfaces studied by ToF-SIMS: Molecular weight effect and quantification, Université catholique de Louvain, 1999.
90. Mu, C., et al., *Temperature induced denaturation of collagen in acidic solution.* Biopolymers, 2007. **86**(4): p. 282-287.
91. Elzbieciak-Wodka, M. and P. Warszyński, *Effect of deposition conditions on thickness and permeability of the multilayer films formed from natural polyelectrolytes.* Electrochimica Acta, 2013. **104**: p. 348-357.
92. Kolasińska, M., R. Krastev, and P. Warszyński, *Characteristics of polyelectrolyte multilayers: Effect of PEI anchoring layer and posttreatment after deposition.* Journal of Colloid and Interface Science, 2007. **305**(1): p. 46-56.
93. Brunot, C., et al., *Cytotoxicity of polyethyleneimine (PEI), precursor base layer of polyelectrolyte multilayer films.* Biomaterials, 2007. **28**(4): p. 632-640.
94. Ahn, H.H., et al., *Polyethyleneimine-mediated gene delivery into human adipose derived stem cells.* Biomaterials, 2008. **29**(15): p. 2415-2422.
95. Sigma-Aldrich. *https://www.sigmaaldrich.com*.
96. Dixon, M.C., *Quartz crystal microbalance with dissipation monitoring: enabling real-time characterization of biological materials and their interactions.* Journal of biomolecular techniques, 2008. **19**: p. 151-158.
97. J. A. Wollam Co. : Ellipsometry solutions. *Ellipsometry tutorial, http://www.jawoollam.com/*. consulted in February 2014.
98. Biophyresearch, *La microscopie à force atomique, http://www.biophyresearch.com/afm.htm*. Consulted in mars 2012.
99. Whyman, G., E. Bormashenko, and T. Stein, *The rigorous derivation of Young, Cassie-Baxter and Wenzel equations and the analysis of the*

contact angle hysteresis phenomenon. Chemical Physics Letters, 2008. **450**(4-6): p. 355-359.

100. Genet, M.J., C.C. Dupont-Gilain, and P.G. Rouxhet, *XPS analysis of biosystems and biomaterials*, in *Medical Applications of Colloids*. 2008, Springer: New York. p. 177-307.
101. International Society for Stem Cell Research, *Stem cell facts, http://www.closerlookatstemcells.org/docs/default-source/patient-resources/stem-cell-facts.pdf?sfvrsn=4*. consulted in January 2016.
102. Fortier, L.A., *Stem Cells: Classifications, Controversies, and Clinical Applications.* Veterinary Surgery, 2005. **34**(5): p. 415-423.
103. DiMarino, A.M., A.I. Caplan, and T.L. Bonfield, *Mesenchymal Stem Cells in Tissue Repair.* Frontiers in Immunology, 2013. **4**.
104. Ma, J., et al., *Concise review: Cell-based strategies in bone tissue engineering and regenerative medicine.* Stem Cells Translational Medicine, 2014. **3**(1): p. 98-107.
105. Mizuno, H., M. Tobita, and A.C. Uysal, *Concise review: Adipose-derived stem cells as a novel tool for future regenerative medicine.* Stem Cells, 2012. **30**(5): p. 804-810.
106. Barba, M., et al., *Adipose-Derived Mesenchymal Cells for Bone Regereneration: State of the Art.* BioMed Research International, 2013. **2013**: p. 11.
107. Schäffler, A. and C. Büchler, *Concise review: Adipose tissue-derived stromal cells - Basic and clinical implications for novel cell-based therapies.* Stem Cells, 2007. **25**(4): p. 818-827.
108. Schubert, T., et al., *The enhanced performance of bone allografts using osteogenic-differentiated adipose-derived mesenchymal stem cells.* Biomaterials, 2011. **32**(34): p. 8880-8891.
109. Schubert, T., et al., *Critical size bone defect reconstruction by an autologous 3D osteogenic-like tissue derived from differentiated adipose MSCs.* Biomaterials, 2013. **34**(18): p. 4428-4438.
110. Marie, P., *Différenciation, fonction et contrôle de l'ostéoblaste.* Medecine sciences, 2001. **17**(12): p. 1252-1259.

Part II:

Results

Chapter 1: Preliminary studies: PS substrate preparation and characterization, and parameters of LbL assembly

Abstract:

Before studying the layer-by-layer (LbL) assembly of Fn and Col in details, development of the preparation protocol of the substrates and of the assembly protocol was needed. The first aim of this chapter was thus to improve the protocol to prepare polystyrene substrates by spin-coating on glass. The results have demonstrated that the use of octadecyldimethylchlorosilane is a good solution to avoid polystyrene film detachment. The second aim of this chapter was to develop the LbL deposition protocol. Several parameters were shown to play a role in LbL building such as the adsorption time, the use of an anchoring layer, the denaturation of proteins, the nature of the buffer, etc. Finally, the selected parameters were applied to collagen adsorption. Collagen is well adsorbed on PS substrates and forms fibrils in its native form. All the results obtained in this chapter will serve as a basis for the detailed study performed in chapter 2.

1. Introduction

This first chapter aims at introducing and explaining in details the path that was followed to develop different steps of the future protocols. It will also help to better understand some aspects of the work strategy. Moreover, it will give some preliminary results that could be helpful to better understand further work. It will thus be different from the two following chapters that will be more focused on the main achievements of the thesis.

Materials and methods section will describe the general procedures and the main techniques used to obtain the results of the chapter. More details about each specific protocol will be given in the following sections, depending on the experiment that will be made.

The first results that will be discussed concern the development of the silanization protocol (section 3). This silanization step is needed to obtain more hydrophobic glass substrates before spin-coating and thus to avoid polymer film detachment from glass. First experiments will be performed with the silanization and spin-coating protocol used by Zuyderhoff et al. [1, 2], and this protocol will be further improved.

As explained in the introduction part of this thesis (section 1.4.2), combination of two proteins in LbL assembly is not easy to achieve. The fourth section of this chapter will thus describe all the steps and tests that were performed to develop the deposition protocol and to define the conditions that will be used in the following chapters for LbL assembly. Finally, the last section (section 5) will present results of collagen adsorption alone in the specific conditions selected for LbL assembly.

2. Methods of characterization

Water contact angle analysis: Static contact angles are measured using the sessile drop method with a CDD camera and an image analysis processor (Electronisch Ontwerpbureau De Boer, The Netherlands). A 0.3 µL drop of ultrapure water is deposited on the surface and the angle value is read after 5

s. On each sample, at least 5 measurements are performed on different locations.

XPS analysis: The analyses were performed on a SSX 100/206 photoelectron spectrometer from Surface Science Instruments (USA) equipped with a monochromatized microfocused Al X-ray source (powered at 20 mA and 10 kV). The pressure in the analysis chamber was around 10^{-6} Pa. The analyzed area was approximately 1.4 mm^2 and the pass energy was set at 150 eV. The C-(C,H) component of the C 1s peak of carbon was fixed to 284.8 eV to set the binding energy scale. Data treatment was performed with the CasaXPS program (Casa Software Ltd, UK), some spectra were decomposed with the least squares fitting routine provided by the software with a Gaussian/Lorentzian (85/15) product function and after subtraction of a nonlinear baseline. Molar fractions were calculated using peak areas normalized on the basis of acquisition parameters and sensitivity factors provided by the manufacturer.

AFM analysis: AFM topographic images are recorded on dried samples on a Nanoscope V multimode microscope (Digital instuments, Santa Barbara, USA) in moderate to light tapping mode, using AFM tips with a spring constant of 20 to 80 $N.m^{-1}$ and resonant frequency in air from 358 to 382 Hz (Veeco, Camarillo, Canada). Image sizes were 10 x 5 μm^2. Images are treated with the Nanoscope analysis software and submitted to 3rd order flattening.

QCM-D analysis: The assembly is performed on gold-covered quartz crystals spin-coated with polystyrene. QCM-D crystals are AT-cut 5 MHz crystals coated with 100 nm Au from Q-Sense (Gothenburg, Sweden) or Fil-tech (Boston, USA). Crystals are washed by 3 x 5 min sonication in toluene to remove the PS film used in a precedent experiment and are submitted during 15 min to UV/O_3 (UVO cleaner, Jelight Company, USA) before spin-coating. The crystals are spin-coated with a WS-400B-6NPP/Lite spin-coater (Laurell technologies corporation, North Wales, USA) during 20 s at 2000 rpm with PS 0.5 % w/w in toluene followed by a 30 min treatment at 80°C to evacuate the solvent.

Measurements are performed in a Q-Sense E4 system (Gothenburg, Sweden). Resonance frequencies of the crystal are obtained under buffer for the different overtones and the shifts of frequency (Δf) and of dissipation (ΔD) are

then measured as a function of time and deposition steps. Temperature was fixed at 25°C. Results for the 5th overtone are presented in this thesis.

Ellipsometry analysis: For each sample, the thickness of the PS layer is measured before protein deposition and subtracted to the total thickness measured after protein deposition. A spectroscopic ellipsometer (Uvisel, Horiba-Jobin-Yvon, France) was used to make measurements from 1.5 to 5 eV with an incidence angle around 70°. Data are fitted with the DeltapPsi 2 software. A layer of SiO_2 of 1.55 nm was considered and a Cauchy absorbent model was applied on 2 eV – 4 eV data to determine the PS or protein film thickness. Three measurements are performed on each sample before and after protein deposition. A single-wavelength ellipsometer (Horiba-Jobin-Yvon) was also used. To fit the data, the refractive index was considered constant before and after deposition and fixed at n=1.6. Five measurements are performed on each sample before and after protein deposition. No significant differences were observed between measurements performed on different ellipsometers.

3. Preparation and characterization of the polystyrene substrates

In this work, protein adsorption is performed on PS substrates to mimic the surface of culture plates. These substrates need to be prepared by spin-coating of polymer to obtain smooth polymer films, on which it is easier to make protein films characterization. For this purpose, PS solution is spin-coated on thin 12 mm in diameter glass coverslips or pieces of silicon wafer. However, a well-known problem appears when polymer films are deposited on a hydrophilic substrate: the polymeric film detaches from the support. This detachment comes from accumulation of water in the polymer-glass interface. This accumulation decreases the contact area between glass and polymer, leading to a decrease of adhesion force between them [3]. In the work of Zuyderhoff et al. [2], this problem was already raised. To solve it,

methacryloxypropyltrimethoxy silane (MOPTMS, see Fig. II.1.1) was used as a coupling agent to increase adhesion.

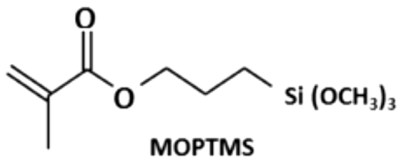

Figure II.1. 1: MOPTMS structure

However, the structure of this silane may not be the best to achieve a satisfactory glass-PS adhesion. It is indeed more efficient to have a long aliphatic chain on the silane to obtain a regular and hydrophobic layer. Given its previous use for that purpose, we used MOPTMS as a compatibilizing agent in several preliminary experiments described in Appendix 1. We concluded however that MOPTMS is not the best choice to hydrophobize the glass surface.

3.1. Protocol optimization with a long-chain alkylchlorosilane

As MOPTMS is not the best choice to perform silanization, another silane was chosen. A chlorosilane terminated with a long aliphatic chain was tested for the silanization step. This strategy was already adopted by Baujard-Lamotte et al. [4] which used the grafting of octadecyltrichlorosilane on glass before spin-coating a PS layer in a view to study Fn adsorption. However, to avoid cross-reaction between the Cl groups of the different chlorosilane molecules, monochlorosilane, with only one Cl reactive group, was used in the present work. It avoids the creation of silane aggregates on the surface, which is an advantage compared to the use of MOPTMS. Octadecyldimethylchlorosilane (ODMS, see Fig. II.1.2) was thus chosen. Another advantage of this silane, compared to MOPTMS, is that the ODMS chain pointing outwards from the substrate is more hydrophobic. Grafting could thus give more hydrophobic surfaces. Finally, this ODMS silane possesses a long aliphatic chain. These chains can align under the action of van der Walls forces and this alignment allows a better self-assembly, resulting in a more regular silane layer. To avoid

chemical reaction with water, the silanization process was performed under an atmosphere with very low humidity level. Two techniques were tested: liquid phase silanization and gas phase silanization.

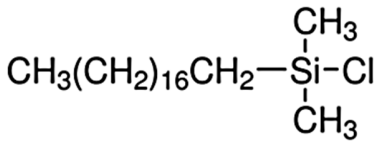

Figure II.1. 2: ODMS structure

Method: Liquid phase silanization was performed in a glove box. ODMS was diluted in anhydrous toluene, supplemented with a few drops of triethylamine. Piranha-cleaned glass or silicon surfaces were immersed overnight in this solution. They were then rinsed in toluene and dried under N_2 flow. Gas phase silanisation was performed in a schlenk, in anhydrous conditions, with a rack designed to silanize 10 surfaces at the same time. A few drops of pure silane were deposited and were evaporated at 80°C, close to the substrates to be modified. Surfaces were then rinsed with toluene to remove excess of silane.

Results and discussion: As shown in Fig. II.1.3, both techniques allow the creation of hydrophobic glass or silicon ($\Theta \geq 60°$). Since silanization in gaz phase does not allow preparation of a high number of surfaces at the same time, liquid phase silanization was favored.

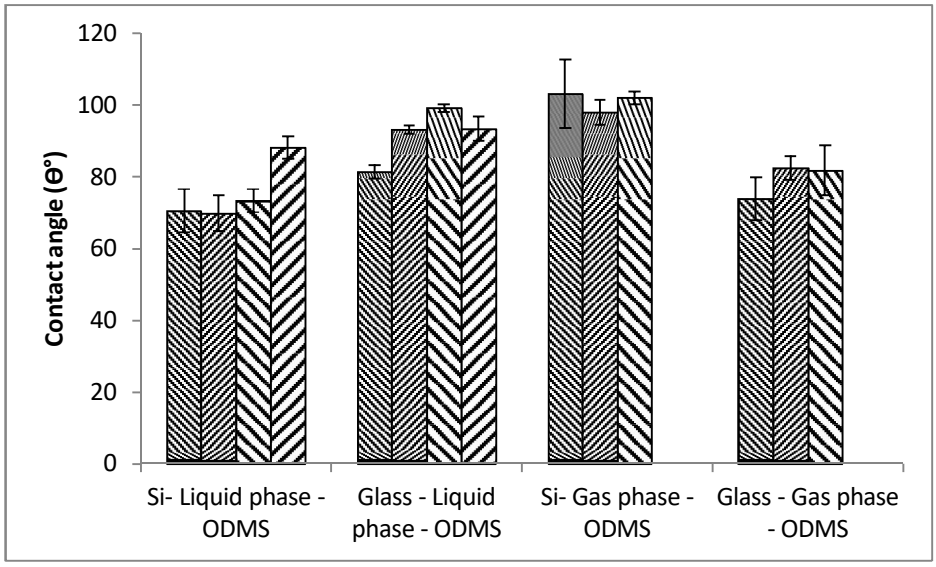

Figure II. 1. 3: Contact angle measurements after silanisation of glass and silicon with ODMS, in liquid or gas phase. Error bar represent confidence interval at 95%. Results for three or four surfaces are shown in the figure.

It is now important to determine if adhesion of PS film is really improved with ODMS silanisation in liquid phase. Here, silanized surfaces, with or without PS film on them, have both contact angles around 90°. It is thus impossible to check film adhesion with contact angle measurements. XPS was thus used to determine if Si is detected after immersion and handling of spin-coated surfaces in PBS. If Si is detected, detachment of the film took place. Results are presented in Table II.1.1. They clearly prove that the use of ODMS improves film adhesion compared to MOPTMS.

Table II. 1. 1: Results of film adhesion experiment of PS films on glass and silicon. Handling and pipetting tests are made on different surfaces. The scorings in the table indicate number of spots where Si is detected by XPS measurement on 3 spots. The ODMS silanized surface, 3 days, pipetting, C (marked with a *) was scratched deliberately to check if Si is well detected. Green color highlights best conditions, orange, the intermediate one, and red, the worst one.

Silane	Immersion time	Pipetting or Handling	Surface	Spot with Si detection (on 3 spots)
ODMS	3 h	Handling	A	1
			B	0
			C	0
	3 days	Handling	A	1
			B	0
			C	0
		Pipetting	A	0
			B	0
			C*	2*
MOPTMS	3 h	Handling	A	2
			B	3
			C	2
	3 days	Handling	A	1
			B	3
			C	1
		Pipetting	A	2
			B	2
			C	0

Finally, film morphology needs to be characterized to be sure that there are not too many aggregates on the surfaces. AFM pictures will not be presented here, but they have shown the presence of aggregates on the surfaces. A last optimization was thus needed. As explained by Wang et al. [5], sonication can decrease the number of aggregates and allows obtaining a more homogeneous silane layer. A sonication step will thus be added to define the final protocol.

3.2. Final silanization protocol

Method: Liquid phase silanization was thus chosen as the final protocol. As described just above, silanization was performed in a glove box. ODMS was diluted in anhydrous toluene, supplemented with a few drops of triethylamine. Glass or silicon surfaces were immersed overnight in this solution. They were then rinsed by immersion one time simply in toluene, one time in toluene with sonication during 2 min and then one time simply in toluene. After these three rinsing steps, they were taken with tweezers, dipped in toluene and gently agitated and then dried under N_2 flow. Freshly silanized samples were spin-coated with a PS solution of 20 g/l, at 5000 rpm during 40 s and were stored in a desiccator until their use.

Results and discussion: Morphology of the surfaces was characterized after silanization with this last protocol, before and after spin-coating with PS (Fig. II.1.4). After silanization, some aggregates are always observed on the surfaces but they are very small after PS spin-coating. One surface was sacrificed after each silanization batch to check the contact angle. The measurements are not very reproducible but always show an increased hydrophobicity of the surfaces.

With this silanization process, we are probably not in the best conditions to obtain a well-organized silane monolayer, as shown by aggregates detection and non-reproducibility of the contact angle. However, we did not observe polymer film detachment anymore, and surfaces are smooth enough to be used in further experiments.

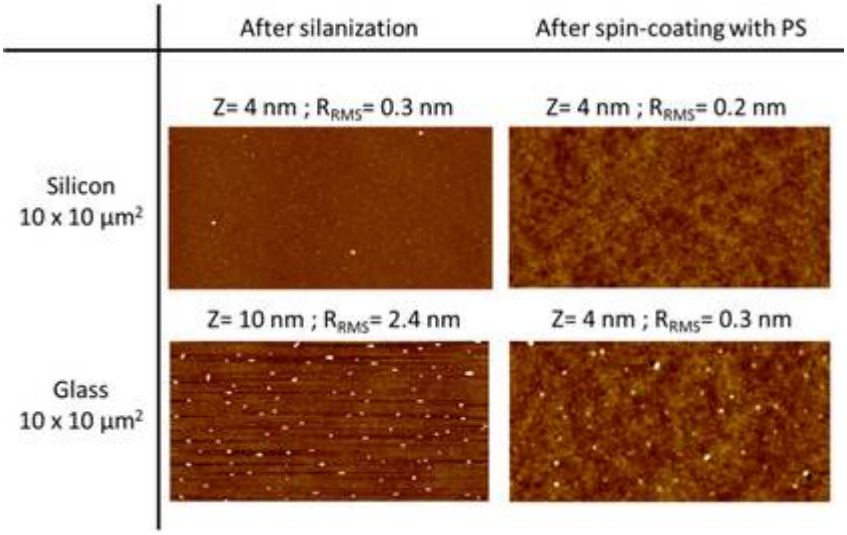

Figure II. 1. 4: AFM imaging in tapping mode of silicon (top) and glass (bottom) after silanization (left), and after silanization followed by spin-coating with polystyrene (right).

4. Development of the proteins LbL deposition protocols

One of the deposition methods used in this thesis is the layer-by-layer deposition. Numbers of parameters can be adjusted and modified for LbL assemblies building, including order of the layer, temperature, concentration, QCM flow, time of adsorption, ionic strength, pH etc. Some choices are thus needed to begin experimental investigations. In this section, different parameters of the first applied protocol are challenged, to progressively improve the deposition and define a robust protocol for the rest of the work. The aim is to obtain a protocol allowing a regular assembly to be achieved, (i) with a defined films growth after each layer addition, (ii) resulting in thick films and (iii) resulting in films containing both Fn and Col in significant amount. Most of the time, experiments are performed by QCM-D that allows *in situ* monitoring of protein adsorption.

Initial protocol: QCM-D monitoring of the protein film building was performed at 25°C. QCM crystal were spin-coated with PS. Flow was first fixed at 10 µl/ml. Protein solutions were prepared in the cold room and are then stored at 4° C until use. Before use, solutions were warmed up at room temperature during

about 15 min and degassed. Fn and n-Col solution concentration was fixed at 25 µg/ml and solutions were prepared in PBS. Each adsorption step was performed during 30 min. The QCM-D data were treated to extract the Δf and ΔD values of the 5th overtone.

For temperature effect study, films were built outside the QCM device on PS spin-coated substrates and were observed by AFM.

4.1. Influence of the order of the layers

One of the first parameters that need to be selected is the choice of the first protein layer. This first section will thus analyze the results obtained with Fn as the first layer, or n-Col as the first layer.

Method: The deposition of 3 bilayers was monitored by QCM-D. Experimental parameters are the same as described in the initial protocol description and are summarized in Table II.1.2.

Table II. 1. 2: Experimental parameters for order of layers selection

Concentration	n-Col = 25 µg/ml Fn = 25 µg/ml	Buffer	PBS
Pump Flow	10 µl/min	Adsorption time	30 min

Results and discussion: The results for the films $(Fn/n\text{-}Col)_3$ and $(n\text{-}Col/Fn)_3$ are presented in Fig. II.1.5. Even if the films are a little bit thicker when n-Col is used as the first layer, the reproducibility of the results is very poor. It is probably due to the higher heterogeneity generally observed upon n-Col adsorption. Indeed, n-Col adsorption is less reproducible than Fn adsorption because n-Col is a complex protein, which can self-assemble, and which is very much affected by small experimental variations. The following layers are probably influenced by the higher heterogeneity of the first layer. With so large standard deviation values observed during the assembly, it will be difficult to interpret the future data. It was thus decided to continue all the experiments with Fn as the first layer.

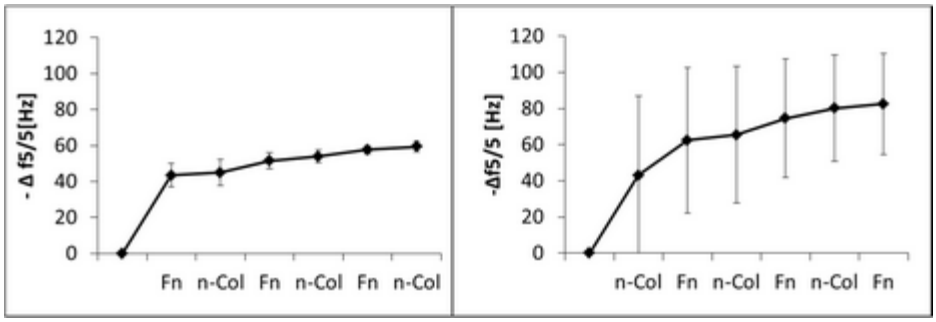

Figure II. 1. 5: Comparison of the results obtained by QCM-D monitoring of LbL assembly with Fn as the first layer (left) or n-Col as the first layer (right). Error bars are standard deviation (n = 4 when Fn is the first layer; n = 3 when Col is the first layer)

4.2. Influence of protein concentration

Method: QCM-D monitoring of the protein film building was performed as explained in the initial protocol. In this initial protocol, the protein concentration was fixed at 25 µg/ml. In this section, this concentration will be compared with the use of a concentration of 100 µg/ml for both proteins. Even if 25 µg/ml was already enough to cover the surface, adsorption could be faster with a higher concentration. Moreover, if concentration is higher, the faster coverage of the substrate by protein molecules prevents further protein reorganization at the interface and its denaturation. The resulting protein layer may be organized quite differently. A concentration of 100 µg/ml is thus interesting to study. Experimental parameters are summarized in Table II.1.3.

Table II. 1. 3: Experimental parameters for protein concentration study

Concentration of n-Col and Fn	25 µg/ml or 100 µg/ml	Buffer	PBS
Pump Flow	10 µl/min	Adsorption time	30 min

Results and discussion: In the beginning, the protein concentration was fixed at 25 µg/ml. However, as shown on the black curve of Fig. II.1.6, the results were not satisfactory. They were not enough characteristic of an LbL building. After the first adsorption step, there is no more adsorption of a large amount of protein. Behavior is far from classical LbL profile and is more close to the

behavior expected for a saturation of the interface. After a few tests, we decided to check if the concentration of 25 µg/ml was not too low for obtaining good results. A test was thus performed with a concentration of 100 µg/ml for Fn and n-Col. Results are shown in Fig. II.1.6 (grey curve) and reveal that concentration has not a big influence on the assembly. It is probably because 25 µg/ml was already enough to have a high adsorption level. We know from Lhoest et al. [6] that adsorption isotherm plateau is only reached at 50 µg/ml but 25 µg/ml is not so far from this plateau. It should be noted that, whether with 100 µg/ml or 25 µg/ml, the adsorption plateau is not reached after 30 min of adsorption (not shown). However, whatever the concentration, almost the same amount of Fn is adsorbed.

After this experiment, we decided that there is no need to increase protein concentration. However, concentration of n-Col will be increased to 100 µg/ml in some cases. As increasing concentration does not allow to obtain better results, it was thus necessary to find other parameters to optimize the building, as explained in the next paragraphs. Depending of the experiments, n-Col concentration can be 25 µg/ml or 100 µg/ml.

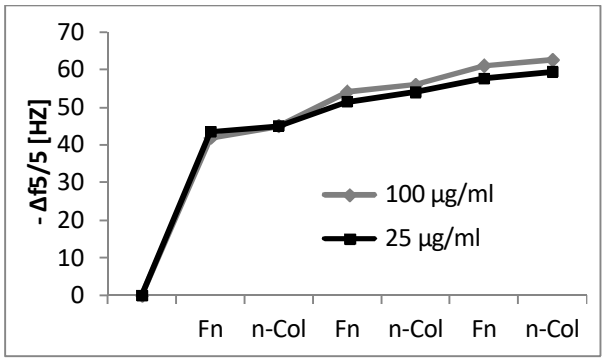

Figure II.1. 6: Influence of protein concentration on the $(Fn/n\text{-}Col)_3$ assembly by layer-by-layer method. Fn and n-Col concentration were fixed either at 25 µg/ml for both proteins or at 100 µg/ml for both proteins.

4.3. Influence of protein denaturation and of the addition of an anchoring layer

It is well known that denatured collagen (d-Col) interacts better with Fn than native one [7]. The reason is probably that some interaction sites are masked in the triple helical conformation of n-Col. Moreover, films combining Fn with gelatin, close to d-Col, were already built by Matsusaki et al. [8]. It is thus interesting to test LbL assemblies with denatured proteins with the hope to improve specific interaction between them, and thus to improve LbL building.

A second interesting parameter to test is the addition of an anchoring layer to see if it improves or not the LbL building. In literature, anchoring layer of polyethyleneimine (PEI) are often used to build regular and thick LbL films [9, 10]. This polyelectrolyte was thus chosen as the first layer in some experiments.

Method: Denaturation of Fn and Col was performed by heating protein solutions, diluted down to their final concentration, at 90°C during 1h in a thermostatic bath. They were then stored at 4°C until their use. The conditions of QCM-D experiment are reminded in Table II.1.4. PEI solution was prepared in NaCl 0.05 M for this experiment at a concentration of 1 mg/ml. PEI was adsorbed first during 30 min.

Table II. 1. 4: Experimental parameters for denaturation of protein and anchoring layer testing

Concentration	n-Col = 100 µg/ml Fn = 25 µg/ml	Buffer	PBS
Pump Flow	10 µl/min	Adsorption time	30 min

Results and discussion: The influence of Col denaturation is presented in Fig. II.1.7. Results obtained for $(Fn/n\text{-}Col)_3$ are compared to the results obtained for $(Fn/d\text{-}Col)_3$. The use of d-Col seems to improve the film building by giving thicker films and more regular growth. The use of Fn denaturation was also tested (results not shown). Assemblies did not work with this denaturation. Denatured Fn was thus never used in further experiments. The use of the PEI anchoring layer was also tested and the results are presented in Fig. II.1.8. $(Fn/n\text{-}Col)_3$ are compared to $PEI/(Fn/n\text{-}Col)_3$ films and this comparison shows

that the anchoring layer increases the adsorbed mass on the crystal. As the $(Fn/d\text{-}Col)_3$ and $PEI/(Fn/n\text{-}Col)_3$ films give protein multilayers which are very promising to obtain the desired LbL assemblies, these films will be part of the future films studied in details in this thesis.

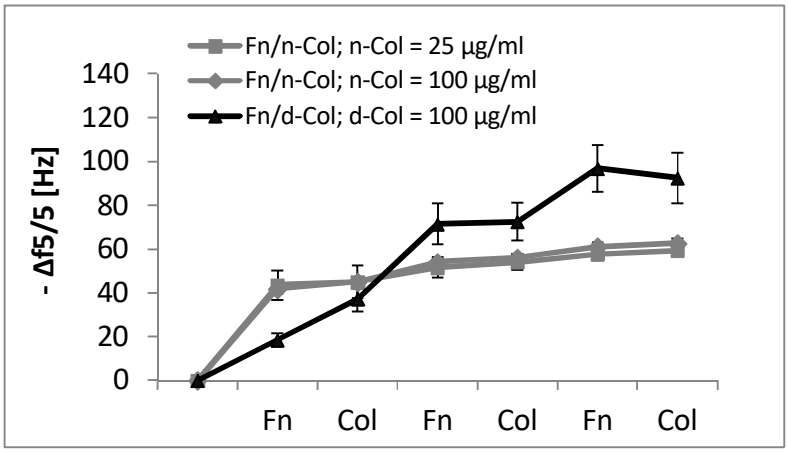

Figure II.1. 7: Comparison of the results obtained by QCM-D monitoring of LbL assembly with n-Col or d-Col. Error bars are standard deviation (n = 4 for n-Col 25 µg/ml and d-Col 100 µg/ml; n = 2 for n-Col 100 µg/ml)

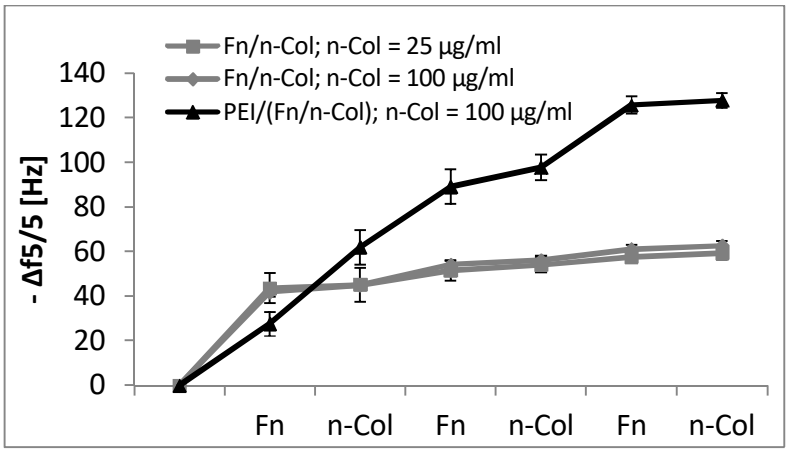

Figure II.1. 8: Comparison of the results obtained by QCM-D monitoring of LbL assembly with n-Col on a PEI anchoring layer of PEI. For the films with PEI, the baseline is artificially put at 0 Hz after PEI adsorption. Error bars are standard deviation (n = 4 for n-Col 25 µg/ml without PEI and n-Col 100 µg/ml with PEI; n = 2 for n-Col 100 µg/ml without PEI).

4.4. QCM flow and adsorption time

Until now, a flow of 10 µl/min was used for the experiments, with an adsorption time of 30 min. With an idea to reduce total experiment time, we have decided to test buildings with a higher flow and a shorter adsorption time. It allows to use the same total amount of proteins and to build the layers faster. Moreover, the use a higher flow normally allows a faster stabilization during the rinsing steps. Increasing this flow could thus be beneficial.

Method: The QCM-D flow was increased to 30 µl/min and the adsorption time was decreased to 10 min. The parameters are reminded in Table II.1.5. Experiments were realized for three different types of films, with d-Col and with the anchoring layer. On the contrary to the first test with PEI anchoring layer, PEI was this time dissolved in the buffer used for the assembly, ie PBS.

Table II. 1. 5: Experimental parameters for impact of QCM-D flow and adsorption time testing

Concentration	n-Col = 100 µg/ml Fn = 25 µg/ml	Buffer	PBS
Pump Flow	30 µl/min	Adsorption time	10 min

Results and discussion: The results for the three different types of films are presented in Fig. II.1.9. It shows that the same order of values is obtained whatever the flow/time combination used. It was thus decided to continue some experiments with this higher flow to see if good LbL assembly can be built. Moreover, thanks to the reduction of adsorption time, it was easier to build film with 6 bilayers.

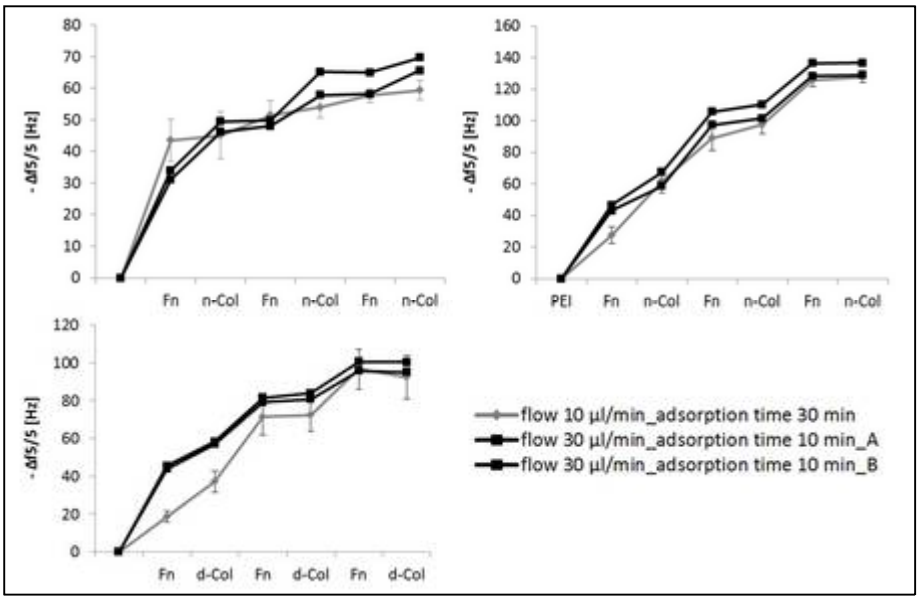

Figure II. 1. 9: Comparison of the results obtained by QCM-D monitoring of LbL assemblies without a PEI anchoring layer and with n-Col or d-Col (left), and with PEI and n-Col (right). Grey symbols and curve are obtained with a flow of 10 µl/min and adsorption during 30 min. Error bars are standard deviation (n = 4 for each). For the $(Fn/n\text{-}Col)_3$ films, results are obtained with n-Col concentration of 25 µg/ml. All the other results are for Col concentration of 100 µg/ml. Black symbols represent the results obtained with a flow of 30 µl/min and adsorption time of 10 min. Two repetitions are presented on each graph.

Films built in PBS, with n-Col and d-Col, with or without an anchoring layer, were studied more systematically. A part of these results were already presented in Mauquoy et al. [11]. Fig. II.1.10 is extracted from this paper and gives information about building of the three types of film. In this graph, Δf and ΔD are presented in function of time, which gives more information about kinetic behavior. Moreover, dissipation results will also be discussed in this section.

As already described before, the results obtained with a PEI anchoring layer or with d-Col are better than for the films combining Fn and n-Col. Analysis of dissipation monitoring shows that n-Col dissipates more than Fn. ΔD increases at each addition of n-Col and decreases after Fn adsorption. It is probably due to n-Col conformation. It is a long, anisotropic molecule, which probably

extends in solution and creates highly hydrated films. With (Fn/d-Col) films, dissipation is almost the same for each d-Col and Fn adsorption steps and is low. Col denaturation changes molecules properties and gives a less extended molecule that produces less hydrated films.

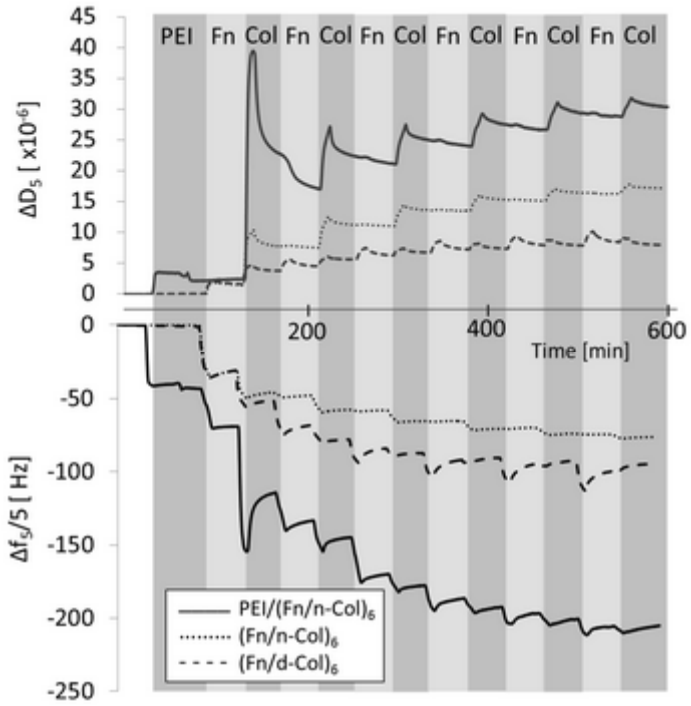

Figure II. 1. 10: QCM monitoring of the construction of $(Fn/Col)_6$ films. The assembly is performed in phosphate buffered saline (PBS) on gold-covered quartz crystals spin-coated with polystyrene. C_{PEI} = 1 mg/ml; C_{Col} = 100 µg/ml; C_{Fn} = 25 µg/ml; flow = 30 µl/min; T = 25°C. After each adsorption step, rinsing is performed using PBS. Plain line: a first layer of PEI was used and n-Col was assembled; dotted line: n-Col was used; broken line: d-Col was used [11].

With these results, some questions need always to be solved. First, it is clear that adsorption plateau is not reached at each adsorption step. We thus need to test longer adsorption time, even with the increased flow, to be more close to the adsorption plateau. After this experiment, an adsorption time of 1h was thus chosen. The results obtained with this adsorption time will be discussed in the next chapter, chapter 2. Moreover, with these results, we are not sure to

have a true LbL building or a step-by-step saturation of the interfaces. It will thus be interesting to compare the results with the one obtained for simultaneous adsorption of Fn and Col. It will also be discussed in the next chapter.

4.5. Buffer choice

Buffer selection was made in parallel to the different optimization proposed above. Even if Fn and n-Col have theoretically opposite charges in PBS, the results of (Fn/n-Col) building were not satisfactory in this buffer. It could be because they do not have opposite charges experimentally. We thus want to check if other pH or ionic strength will not be in favor of a better interaction between Col and Fn. All the experiments of this buffer selection are not performed on the same moment of protocol development. They are thus not performed in exactly the same experimental conditions. For example, some experiments are made with the Col concentration of 25 µg/ml and others with 100 µg/ml, some with a QCM flow of 10 µl/min and others with a flow of 30 µl/min. This section will summarize the different tests that were performed. We will not go into many details in the results because a major part of the tested buffers give worst results than in PBS.

Method: Different buffers were tested to change some properties of the buffer used to solubilize proteins.

- Modification of ionic strength: PBS was used and its concentration was changed. It was diluted 10, 20 and 100 times to test if decreasing ionic strength allows better assemblies to be obtained.
- Modification of pH: To change the pH, we have used citrate/phosphate buffer. Two salt solutions, one of citric acid and one of sodium hydrogen phosphate were prepared. Depending on the proportion of each of these solutions used to prepare the buffer, the pH changes from 5.2 to 6.8.
- One buffer for each protein: Fn was diluted in acetate buffer (made with sodium acetate and acetic acid), with a pH of 4.65, and n-Col in PBS. With these conditions, it was sure than in solution, proteins have opposite charges.

Results and discussion: The influence of ionic strength was first studied. It was shown by Ingham [7] that interaction between Fn and n-Col is better in medium with a low ionic strength. PBS diluted 10 and 100 time were thus compared to undiluted PBS. Some troubles were observed with these two new buffers. Measurements of pH showed that dilution 100 times of the buffer was too strong to keep the buffering properties of PBS, pH was thus not stable. With PBS diluted 10 times, a rapid fibrillation of n-Col was observed. These two buffers are thus not interesting to use. With PBS diluted 20 times, rapid fibrillation of n-Col also takes place.

The test performed with citrate-phosphate buffer, at different pH, has given smaller or equal Δf measurements than with PBS. These different buffers were thus not the solution to improve LbL building. It can depend on the chosen pH but also on the ions present in the buffer. Indeed, phosphate ions are present in PBS as well as in citrate-phosphate buffer and can influence the interaction between Fn and n-Col. They are already shown as influencing electrostatic interaction between Col molecules during fibrillation [12] because they adsorb on Col molecules and change its iep. It was moreover shown in this paper that iep changes from 9.2 to around 7.4 in presence of 10 mM Na_2HPO_4. It will thus be interesting to test buffer which are composed of other ions than phosphates.

Finally, the test of the assembly with each proteins in a different buffer was also not promising. Even if Fn is adsorbed in acetate buffer, the adsorbed Fn layer is in contact with PBS when the next n-Col layer is added. The interaction between both proteins is thus again the same than in PBS.

With all these results and literature, we found out that a buffer without phosphate and with a low ionic strength would be interesting. However, the problem of the use of very low ionic strength is that pH is more difficult to control and to measure. After all these experiments, we decided to continue working in PBS as a reference, because it is a buffer often used for biological applications. We decided to compare it to a buffer without phosphate, at the same pH, *ie* Hepes buffer, also widely used for biological applications. It allows

working in physiological condition, close to the one that needs to be used in cell culture. Finally, we have decided to use acetate buffer, at pH 5.4, to see how it influences protein assembly. This buffer has a different pH and is often used in LbL assembly studies. The results obtained for LbL assemblies with these two new buffers will be presented in the next chapter.

4.6. Temperature effect

Another parameter that can be studied is temperature. This parameter was not tested by QCM-D, for which it was fixed at 25°C for all experiments. However, when films were built outside QCM device, for characterization by AFM, contact angle or ellipsometry, films can be easily prepared at other temperatures. The first that was chosen was 37°C to be more close to the physiological condition. Films built at this temperature were compared to films built at room temperature.

Method: Films were prepared on spin-coated polystyrene. PEI, n-Col, d-Col and Fn were adsorbed during 30 min. After each step of adsorption, three rinsing with PBS were performed during 1 min. The temperature was fixed at 37°C. At the end of the construction, the films were rinsed 7 times with water, dried under a nitrogen flow and stored in a desiccator before analysis. Films with n-Col or d-Col, with or without an anchoring layer, were built with 6 bilayers and were analyzed by AFM.

Results and discussion: AFM pictures after adsorption at 37°C are presented in Fig. II.1.11. For 50 µm pictures, results clearly show n-Col fibrillation. These fibrils are very big and are probably due to fibrillation in solution, before adsorption. Results for d-Col at 50 µm are not presented because surfaces are completely smooth. For 10 µm picture, results show that films built with d-Col are very smooth compare to film with n-Col. With n-Col, fibrillation happens that gives rougher surfaces. Smaller fibrils than the one observed on 50 µm picture can be observed, probably due to fibrillation in the adsorbed state. Films with PEI are the roughest.

The results obtained at 37°C thus show quite big fibrils that can be negative for the building of LbL layer. If n-Col is involved in fibrils formation, fewer molecules will be available to interact with Fn. As it is well known that fibrillation is favored at higher temperature [13], we decide that the next experiments will be performed at room temperature.

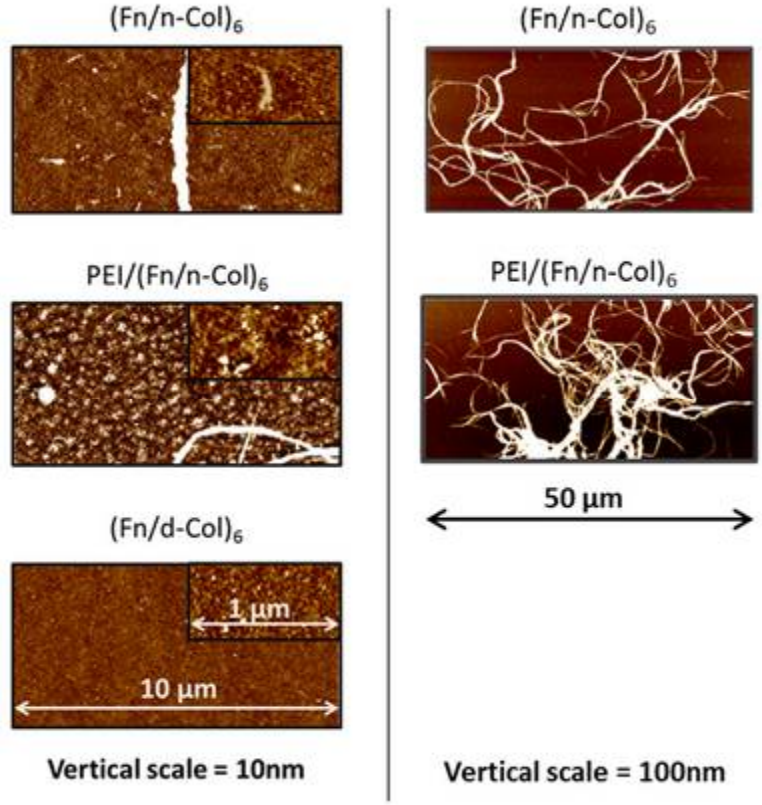

Figure II. 1. 11: AFM topographic images acquired in tapping mode in air. Films were prepared on silicon spin-coated with polystyrene. PEI is adsorbed during 30 min at a concentration of 1 mg/ml; n-Col and d-Col are adsorbed during 30 min at a concentration of 100 µg/ml and Fn during 30 min at a concentration of 25 µg/ml. After each step of adsorption, three rinsing with PBS are performed during 1 min. The temperature is fixed at 37°C. At the end of the construction, the films are rinsed 7 times with water and dried under a nitrogen flow [11].

The AFM images of Fig. II.1.12 show the morphology of the films built at room temperature. At room temperature, big fibrils are not often observed. Small fibrils are observed on the $(Fn/n\text{-}Col)_6$ sample. The fibrils are probably formed in the adsorbed phase. However, some images of the same film do not present these small fibrils. Even if some big fibrils, coming from fibrillation in solution, are sometimes observed at room temperature, they are much rare than at 37°C. Room temperature will thus be chosen for future experiments.

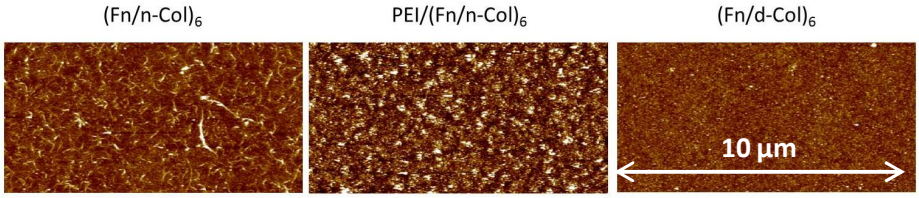

Figure II. 1. 12: AFM topographic images acquired in tapping mode in air (Z scale = 10 nm). Films were prepared on silicon spin-coated with polystyrene. Each adsorption step is performed during 30 min with concentrations C_{PEI} = 1 mg/ml; C_{Col} = 100 µg/ml; C_{Fn} = 25 µg/ml, T= 20°C. After each step of adsorption, three rinsing are performed with PBS during 1 min. Assembly was performed at room temperature. At the end of the construction, the films are rinsed 7 times with water and dried under a nitrogen flow.

4.7. Summary of the conditions for LbL assembly

After all these preliminary experiments, some parameters (Table II.1.6) were chosen for the next LbL building, which will be presented in the chapter 2. In the next section (section 5) of this first chapter, some experiments will be already performed with these parameters.

Table II. 1. 6: Summary of the parameters that will be used for the next experiments and that were chosen based on the preliminary data presented above.

Parameter	Effects	Selection
Protein concentration	• Increasing concentration does not improve assembly	25 µg/ml Fn 100 µg/ml Col
Order of the layers	• Fn as the first layer gives more **reproducible** films	Fn as the first layer
Protein denaturation	• **Collagen** denaturation: ✓ • **Fibronectin** denaturation: ✗	Collagen denaturation
Anchoring layer	• Addition of an anchoring layer gives **thicker** assembly	Polyethyleneimine (PEI)
QCM flow	• Not too fast to avoid high consumption of Fn	30 µl/ml
Adsorption time	• Too **long**: Difficult to implement • Too **short**: Far from the adsorption plateau	1h
Buffer	• Modification of **protein charge** • Modification of **surrounding ions** nature	Hepes (pH 7.4) PBS (pH 7.4) Acetate (pH 5.4)
Temperature	• Too **high temperature** causes collagen fibrillation in solution	20-25° C

5. Characterization of collagen layers

The last part of this chapter will be focused on the characterization of surfaces with adsorbed collagen, in the different conditions chosen after the protocol development of the previous section (section 4). This adsorption of Col directly on PS or on PEI-coated PS will not be analyzed in the future chapters. However, the characterization of these samples can be useful to better understand future results. It will thus be detailed here. On the contrary, adsorption of Fn on the substrates with or without PEI will be the first step of each future LbL assembly. This first layer will thus be analyzed in details in the future chapters and will not be presented here.

As explained previously, three interesting buffers will be tested for LbL building. Col adsorption was thus studied in these different conditions, in its native and denatured state. Moreover, as some films built with n-Col are built on an anchoring layer of PEI, n-Col adsorption on this layer was also studied. The Col layers properties were studied by QCM-D, water contact angle measurements, ellipsometry and AFM, as it will be the case in next chapter for films with Fn.

5.1. Materials and method

Col adsorption was performed with a concentration of 100 µg/ml Col in the buffers. For n-Col adsorption, the solution was prepared into the cold room and then stored at 4° C until its use. For d-Col adsorption, the same diluted solution was prepared and heated up for 1h at 90°C in a water bath, and then stored at 4° C until its use. Before their use, both solutions were warmed up at room temperature during almost 15 min. Adsorption was then performed during 1h. If adsorption is made on the PEI anchoring layer, the surfaces were previously coated during 30 min with PEI 1mg/ml and were then rinsed in the buffer. After each kind of adsorption, surfaces were rinsed 7 times with ultrapure water by successive dilution and dried under N_2 flow for characterization.

For QCM-D results, the Col solutions were prepared in the same way as above but adsorption was performed *in-situ*. QCM flow was fixed at 30 µl/ml and temperature at 25°C. Col adsorption was performed during 1h, followed by buffer rinsing during 30 min. If adsorption was made on the PEI anchoring

layer, PEI solution was previously deposited during 30 min followed by rinsing in the buffer during 30 min.

5.2. Results and discussion

Results of the QCM-D monitoring: The results obtained by QCM-D monitoring are presented in Table II.1.7. Information on the influence of the buffer, of the denaturation and of the anchoring layer can be found in this table:

- Δf acetate > Δf Hepes >> Δf PBS for n-Col adsorption on PS and on PEI-coated PS. It means that total mass adsorbed on the surfaces, proteins and water, is higher in acetate buffer, then in Hepes, and finally in PBS. These differences can come from differences of surrounding ions depending on the buffer and, to a lesser extent, from difference of pH.
- In each type of buffer, Δf n-Col on PEI > Δf n-Col > Δf d-Col. There is thus probably a higher amount of n-Col adsorbed on PEI-coated PS than on PS. Adsorption of d-Col gives the smallest adsorbed mass.
- The Δ D measured for n-Col adsorption are very high compared to those of d-Col adsorption. It is probably due to the difference of conformation. As d-Col is not in triple helical conformation, it can be adsorbed in a flat conformation on the surface. The triple helical structure of n-Col gives more probably an extended conformation in solution, which catches easily water and thus dissipates much higher.

Table II. 1. 7: Results of the frequency shift (Δf) and dissipation (ΔD) measured by QCM-D for three different buffers and for n-Col adsorbed on PS or PEI and d-Col adsorbed on PS. Standard deviations are between brackets (n=3).

	PBS		**Hepes**		**Acetate**	
	$\Delta f_5/5$ [Hz]	Δ D	$\Delta f_5/5$ [Hz]	Δ D	$\Delta f_5/5$ [Hz]	Δ D
n-Col (on PEI)	-90 (10)	36 (4)	-590 (140)	140 (30)	-750 (220)	230 (10)
n-Col	-48 (3)	16 (2)	-150 (90)	50 (20)	-220 (40)	63 (7)
d-Col	-29 (1)	2 (0)	-60 (20)	11 (6)	-50 (10)	11 (2)

Thickness and water contact angle measurements: Measurement of thickness is presented in Fig. II.1.13. The results show that films of a same type built in different buffers have quite close thickness, except for PEI/n-Col films which are thinner in PBS than in Hepes or acetate buffer. The big differences observed above in QCM-D results between the buffers are thus not observed by ellipsometry measurements. They were thus probably linked to the swelling with water, measured thanks to QCM, and not to the adsorbed protein amounts. Films are thus more hydrated in acetate than in Hepes and films in Hepes are more hydrated than in PBS.

The thickness of PEI/n-Col films is higher than the thickness of n-Col films in Hepes and acetate buffer. The difference is due to the layer of PEI in itself. However, PEI layers measure only 1.19, 1.16 and 0.87 nm in PBS, Hepes and Acetate respectively. There is thus still more n-Col deposited on PEI-coated PS than on nude PS in Hepes and acetate. This conclusion was also found with the QCM-D results. PEI plays thus well the role of an anchoring layer.

The adsorption of d-Col gives always the thinnest films.

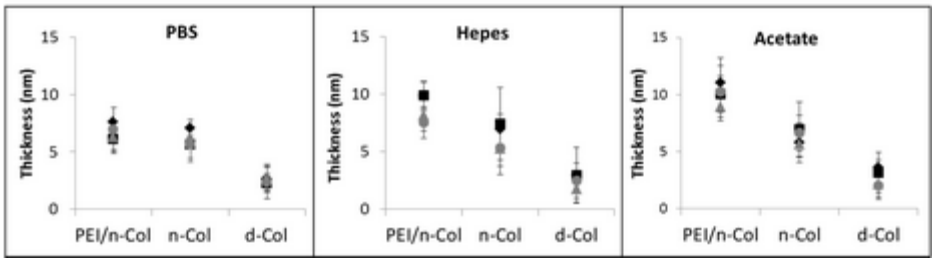

Figure II.1. 13: Ellipsometry measurement of the dry thickness after Col adsorption in different buffers. Ellipsometry graphs show four repetitions for each point. Symbols with the same colors (black or grey) refer to samples prepared the same day, with the same solution and the same condition. Samples denoted by a different color (black or grey) were prepared on different days. Each repetition has its own error bar representing standard deviation (n ≥ 3, on the same sample).

Water contact angles of the different film types, in the different buffers, are presented in Fig. II.1.14. They are quite close to each other. In Hepes and acetate, measured contact angles for the films with n-Col are slightly higher than the contact angles measured for d-Col film. They are also higher than the

contact angle measured for all the films types built in PBS. It is probably due to a different organization on the surface. All the measured contact angles are low which indicates a good protein adsorption in each case and good screening of PS.

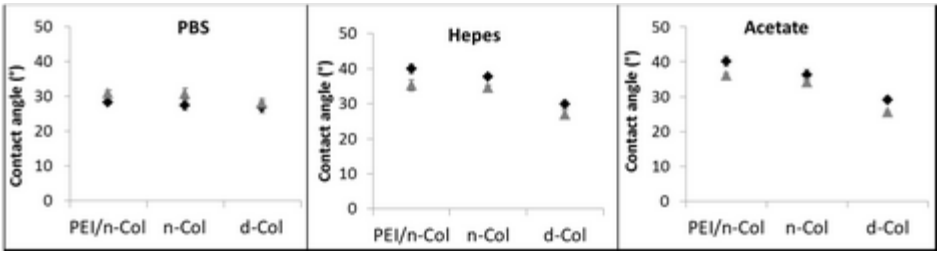

Figure II.1. 14: Water contact angle measurements after Col adsorption in different buffers. Contact angle measurement graphs show two repetitions, realized on different days. Each repetition has its own error bar representing standard deviation (n ≥ 5, on the same sample).

Morphology of the collagen layers: Morphologies of the films are presented in Fig. II.1.15. A first observation is that the films made with d-Col are very smooth compared to the films containing n-Col, probably because denaturation avoid fibrils formation. Then, n-Col fibrillation depends on the buffer. Fibrillation is the highest in PBS, good in Hepes and practically invisible in acetate buffer. Thereafter, fibrillation depends on the presence of an anchoring layer. Films with a PEI anchoring layer show less fibrils and present some heterogeneities coming from the PEI underlying layer. PEI could thus directly have an effect on Col fibrillation or could create a denaturation that prevents fibrillation. Finally, it is important to mention that the AFM pictures described here were obtained in air. Films are thus dried before imaging. Some of the morphological features observed on the samples can thus come from aggregation during drying. This could be confirmed by AFM imaging in buffer.

These results describe the different properties of Col layers. They can help us to better understand some of the result that will be presented in the next chapter, when Col will be combined with Fn.

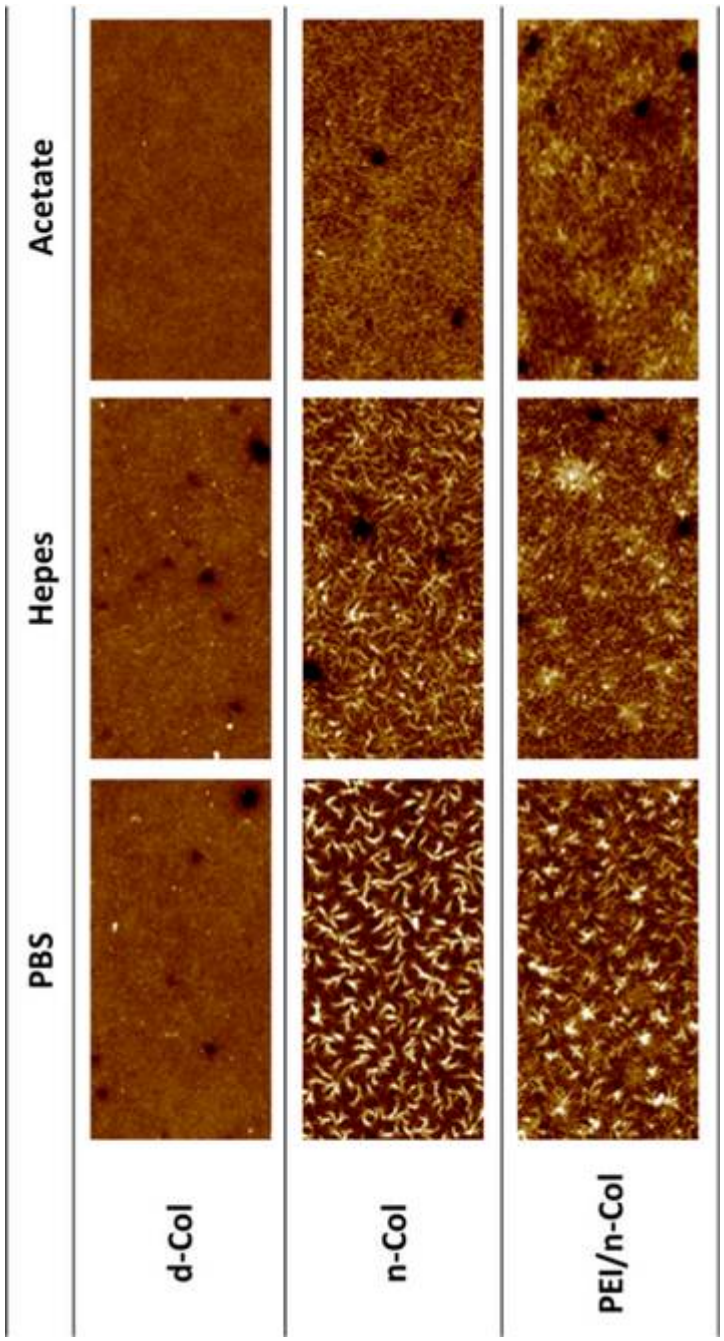

Figure II. 1. 15: AFM picture in tapping mode in air of d-Col or n-Col adsorbed on PS or on PEI-coated PS, in three different buffers. Image size is 5 x 2.5 µm² and Z-scale is 15 nm.

6. Conclusions

This chapter presents the developement of silanization and LbL building protocols. Each of these steps helped to determine the most interesting conditions to use or to study. These conditions will be applied to generate the results of next chapters. Moreover, some interesting behavior of n-Col and d-Col upon adsorption are already highlighted and will help to better understand results of next chapters.

References

1. Zuyderhoff, E.M. and C.C. Dupont-Gillain, *Nano-organized collagen layers obtained by adsorption on phase-separated polymer thin films.* Langmuir, 2012. **28**(4): p. 2007-2014.
2. Zuyderhoff, E.M., *Heterogeneous surfaces with organized collagen layers for the control of cell behavior*, 2012, Université catholique de Louvain: Louvain-la-Neuve.
3. Krongauz, V.V., S.R. Schmid, and J.T. Vandeberg, *Imaging in evaluation of polymer coatings adhesion to glass at high humidity.* Progress in Organic Coatings, 1995. **26**(2-4): p. 145-162.
4. Baujard-Lamotte, L., et al., *Kinetics of conformational changes of fibronectin adsorbed onto model surfaces.* Colloids and Surfaces B: Biointerfaces, 2008. **63**(1): p. 129-137.
5. Wang, M., et al., *Self-assembled silane monolayers: Fabrication with nanoscale uniformity.* Langmuir, 2005. **21**(5): p. 1848-1857.
6. Lhoest, J.B., et al., *Fibronectin adsorption, conformation, and orientation on polystyrene substrates studied by radiolabeling, XPS, and ToF SIMS.* Journal of Biomedical Materials Research, 1998. **41**(1): p. 95-103.
7. Ingham, K.C., R. Landwehr, and J. Engel, *Interaction of fibronectin with C1q and collagen.* European Journal of Biochemistry, 1985. **148**(2): p. 219-224.
8. Matsusaki, M., et al., *Fabrication of cellular multilayers with nanometer-sized extracellular matrix films.* Angewandte Chemie - International Edition, 2007. **46**(25): p. 4689-4692.
9. Elzbieciak-Wodka, M. and P. Warszyński, *Effect of deposition conditions on thickness and permeability of the multilayer films formed from natural polyelectrolytes.* Electrochimica Acta, 2013. **104**: p. 348-357.
10. Kolasińska, M., R. Krastev, and P. Warszyński, *Characteristics of polyelectrolyte multilayers: Effect of PEI anchoring layer and posttreatment after deposition.* Journal of Colloid and Interface Science, 2007. **305**(1): p. 46-56.
11. Mauquoy, S., et al., *Biointerfaces Designed Through Directed Collagen Assembly.* Journal of Bionanoscience, 2014. **8**(6): p. 407-418.
12. Li, Y., et al., *pH effects on collagen fibrillogenesis in vitro: Electrostatic interactions and phosphate binding.* Materials Science and Engineering C, 2009. **29**(5): p. 1643-1649.

13. Wood, G.C. and M.K. Keech, *The formation of fibrils from collagen solutions. 1. The effect of experimental conditions: kinetic and electron-microscope studies.* The Biochemical journal, 1960. **75**: p. 588-598.

Chapter 2:
Combination of collagen and fibronectin to design biomimetic interfaces: do these proteins form layer-by-layer assemblies?

Sara Mauquoy, Christine Dupont-Gillain

Published in: Colloids and Surfaces B : Biointerfaces, **2016**, Vol. 147, p. 54 - 64

Abstract:

Layer-by-layer (LbL) assembly is a surface modification method which may bring complexity to biointerfaces designed to control cell-material interactions. This work aims at investigating the LbL assembly of two extracellular matrix proteins, collagen (Col) and fibronectin (Fn), on polystyrene substrates. LbL assembly, which is widely applied to polyelectrolytes, is not easily transferred to proteins. Different buffers and conditions are tested, and LbL assembly is compared to the simultaneous adsorption of Fn and Col. Build-up and properties of the films are monitored using quartz crystal microbalance, ellipsometry, water contact angle measurements, and atomic force microscopy. Results show that denatured Col leads to smoother films, and that the addition of a polyethyleneimine anchoring layer increases film thickness. A more regular construction and thicker films are obtained with Hepes (pH 7.4) compared to other buffers. However, the LbL assembly is not sustainable and stops after the deposition of a few layers. Films obtained by simultaneous adsorption have lower water contact angles, different morphologies, lower water content and are as thick or thicker compared to the ones prepared by the LbL method. The present work shows that collagen and fibronectin are not involved in a true LbL assembly process. The obtained biointerfaces however exhibit different properties compared to those obtained by the one-step adsorption of these proteins. These differences could be exploited to control cell fate.

Key words: fibronectin, collagen, extracellular matrix, Layer-by-Layer, adsorption, biointerfaces

1. Introduction

The replacement of damaged or malfunctioning organs is a major challenge in medicine. The lack of donors and rejection problems related to allografts has led to the development of biomedical devices based on biomaterials, and more recently, to tissue engineering approaches. In these strategies, the optimization of cell-material interactions is a key point, in which integrins, transmembrane proteins of the cells, play an important role. These proteins recognize specific sequences, such as RGD sequences of adhesion proteins, which allow cell adhesion and spreading, and triggers signaling events [1, 2]. Biomaterial surfaces can be modified with molecules recognized by integrins to better control cell behavior.

A biomimetic way to modify material surfaces is to use extracellular matrix (ECM) components. In vivo, cells are embedded in the ECM , which delivers information to the cells related to adhesion, migration, proliferation, differentiation and apoptosis [3]. The ECM is composed of collagens of different types, glycoproteins (fibronectin (Fn), tenascein, elastin, fibrillin, laminin, etc), proteoglycans [3] and glycosaminoglycans [4]. Among these molecules, Fn is known to play a particularly important role for cell adhesion. For example, surface micropatterns of Fn were shown to modify cell shape and direct cell behavior from apoptosis to grow [5].

Collagen is one of the major proteins of the ECM (90 % in tendons and bone, 50 % in skin [6]), and gives structure to connective tissues [7]. The type I Collagen (Col) molecule (isoelectric point (iep): experimental values between 5.5 and 9.3[8], theoretical value ≈ 9.3) is a filament (mass ≈ 300 kDa; length = 300 nm; diameter = 1.5 nm [4]) composed of two identical α1 and one α2 chains put together in a triple helical conformation [6, 7]. The polypeptide α chains are made of Glycine-X-Y repeated sequences where X and Y are frequently proline and hydroxyproline, respectively [6]. Lysine residues are also frequently present in X or Y position [7]. The lack of side chain in glycine, forming the central axis of the helix, allows the packing of the triple helical structure. Proline and lysine are frequently hydroxylated during post-translational

modifications. Hydroxyproline residues are involved in hydrogen bonds which stabilize the triple helical structure and hydroxylysine residues offer glycosylation sites [6, 7].

Fibrillogenesis of native Col molecules occurs in vivo and produces well-ordered fibrils that give strength to tissues [7]. In vitro, collagen fibrillation is also largely observed in solution. Fibrillation rate and fibril size change according to pH, ionic strength, Col concentration, presence of specific ions and temperature [9-12]. Generally, fibrillation proceeds faster when temperature is higher [9] and is inhibited at low pH [12, 13]. When native Col is adsorbed, fibrillation can also be observed in the interfacial phase [14-16]. These interfacial fibrils are usually smaller than fibrils formed in solution, and fibrillation increases on more hydrophobic substrates [14]. Denaturation of Col prevents fibrillation in the adsorbed phase [15].

Fn (iep =5.2 ± 0.2 [17]) is also an important component of the ECM because it has the ability to interact with many other ECM molecules and with cells through specific interactions [18]. Fn is a dimeric glycoprotein with two subunits of 220 kDa linked together by disulfide bonds close to the carboxyl termini [18, 19]. Each subunit has a predicted length of 61 nm and a predicted diameter of about 2 nm [20]. Fn is composed of three types of repetitive motifs (type I, II, III) [3]. Combinations of these motifs constitute functional domains [4]. These globular functional domains are linked together by flexible polypeptide chains [18]. Among these domains, one is able to interact with Col and another one to bind to cells [3, 4, 18]. It is thus well known that Fn and Col interact with each other. This interaction was studied in vitro using a plate coated with type I Col, gelatinized by exposure to NH_3, and further incubated with labeled Fn. Its existence was demonstrated in a pH range from 2.6 to 10.6 and in a range of ionic strengths from 0.05 to 4 M NaCl [21]. The Fn-Col interaction is probably based on hydrophobic interactions [21]. Even if the interaction between Fn and native Col molecules of different types is well documented [22], other works also demonstrate that the interaction is stronger, and occurs in a wider range of conditions, with denatured Col [23-25]. Col indeed possesses multiple binding sites for Fn that can be masked in

the triple helical structure of the native molecules [26] . Col binding to Fn is reported to alter Fn folding and to increase its flexibility [27].

Developed by Decher in 1992 [28], layer-by-layer (LbL) assembly is a simple method to combine macromolecules on interfaces. Based on the successive dipping of the substrate in oppositely charged polyelectrolyte solutions, multilayered films can be built through electrostatic interactions [28, 29]. Theoretically, the technique can be applied to protein assembly and some success was obtained experimentally, usually by incorporating proteins together with other non-protein polyelectrolytes in multilayers [30]. For example, myoglobine, lysozyme, cytochrome, etc can be combined to polystyrenesulfonate to create multilayers film [30]. However, the use of proteins in LbL assembly, and especially the development of films exclusively based on proteins, is challenging because they are weak and amphoteric polyelectrolytes. Their charge density thus depends on the medium (pH, surrounding ions) and positive and negative charges may coexist, with a non-homogeneous distribution. Moreover, determination of the iep is not trivial. Theoretical determination based on amino acid composition does not take into account the shape of proteins, and experimental methods can give a broad range of results, especially in the case of anisotropic molecules such as collagen. LbL assembly involving Col was already performed. Many examples are reported in the literature. Col was combined with hyaluronic acid [31-33] to accelerate proliferation and differentiation of preosteoblast cells on titanium substrates [33]. Collagen and heparin were assembled to create coatings combining good endothelialization and blood compatibility properties [34-36]. Col was also combined to alginate [37, 38] and chondroitin sulfate [39]. Combination of Fn with gelatin, a compound obtained by collagen hydrolysis, was reported by Akashi and coworkers [40-47]. According to these studies, the assembly could be based on specific interactions that exist between Fn and gelatin. These films were further used in different applications, including the creation of cell multilayers. One study also reports the assembly of Fn and type I Col through a step-by-step procedure [48]. However, even if the protein coating improved the interaction with cells, the assembly was not studied in

enough details to conclude that the proteins were truly assembled in an LbL fashion.

Given their major signaling role in ECM, combining Fn and Col on a surface is expected to bring advances in the control of cell behavior, in a biomimetic approach. In addition to their presence on the interface, their spatial organization is of major interest because it affects the exposure of their binding sites to the cells. The aim of this second chapter is to assess the feasibility of organizing these two proteins at interfaces by the LbL method. Because of the difficulty to predict the electrostatic interactions between the two proteins (iep not well known and considerations above) and of the probable contribution of other interactions in the assembly, different conditions will be tested to compare their influence on the Col-Fn interaction.

Different LbL films are built on a polystyrene (PS) substrate, chosen as a material frequently used in biotechnological applications. Building of films with native Col is compared with the one based on denatured Col, to determine the influence of collagen denaturation on assembly. The effect of an anchoring layer made of a synthetic polyelectrolyte, poly(ethyleneimine), is also investigated. These films are built in three different buffers with similar ionic strength but different pH, to better understand the influence of pH and of the nature of the surrounding ions on Fn-Col interaction. Films obtained by simultaneous adsorption of Fn and Col are also prepared for the sake of comparison.

Film formation is monitored using quartz crystal microbalance with dissipation monitoring (QCM-D). The thickness and wettability of the obtained films is determined by ellipsometry and water contact angle measurements, and their morphology is observed by atomic force microscopy. Moreover, the availability of Fn in the films is assessed by immunodetection.

2. Materials and method

Materials: LbL assemblies are prepared using type I collagen from calf skin (Biochrom AG, Source Bioscience, Berlin, Germany, stored at 4°C) at 100 µg/mL and bovine fibronectin (Invitrogen, Life Technologies, Gent, Belgium, stored at -20°C) at 25 µg/mL. Denatured collagen (d-Col) is produced by denaturation of native collagen (n-Col) solution (100 µg/mL) during 1h at 90°C. When mixed solutions are prepared for simultaneous adsorption, concentration of Fn and Col are the same than above. Polyethyleneimine (PEI, Mr = 600,000-1,000,000 $g.mol^{-1}$; Fluka, Sigma-Aldrich) solutions are prepared at 1 mg/mL. The solutions are prepared in phosphate saline buffer (PBS), Hepes buffer or acetate buffer, as indicated. PBS is made from tablets (Gibco, Life technologies, Paisley, UK) dissolved in ultrapure water to give buffer at pH 7.4 with ≈ 0.14 M NaCl, 2.68 mM KCl and 10 mM phosphate. Hepes buffer (pH=7.4) is prepared from 10 mM of Hepes (Acros organic, Geel, Belgium) and 0.15 M NaCl (Sigma-Aldrich). Acetate buffer is prepared at pH 5.4 with 0.15 M sodium acetate (Prolabo, VWR, Leuven, Belgium) and 0.03204 M acetic acid (Sigma-Aldrich). All the protein solutions are prepared daily and stored at 4°C until being brought to working temperature 15 min before use. Ultrapure water is provided by Elga Purelab Ultra device (18.2 MΩ.cm, Veolia, UK). Spin-coated surfaces are prepared with PS (M_n= 140 000 $g.mol^{-1}$, M_w=230 000 $g.mol^{-1}$; Aldrich, Milwaukee, USA) dissolved in toluene (Prolabo, VWR, Leuven, Belgique).

Quartz crystal microbalance with dissipation monitoring (QCM-D) experiments: The assembly is performed on gold-covered quartz crystals spin-coated with polystyrene (PS). QCM-D crystals are AT-cut 5 MHz crystals coated with 100 nm Au from Q-Sense (Gothenburg, Sweden) or Fil-tech (Boston, USA). Crystals are washed by 3 x 5 min sonication in toluene to remove the PS film used in a precedent experiment and are submitted during 15 min to UV/O_3 (UVO cleaner, Jelight Company, USA) before spin-coating. The crystals are spin-coated with a WS-400B-6NPP/Lite spin-coater (Laurell technologies corporation, North Wales, USA) during 20 sec at 2000 rpm with PS 0.5 % w/w in toluene followed by a 30 min treatment at 80°C to evacuate the solvent.

Measurements are performed in a Q-Sense E4 system (Gothenburg, Sweden). Resonance frequencies of the crystal are obtained under buffer for the different overtones and the shifts of frequency (Δf) and of dissipation (ΔD) are then measured as a function of time and deposition steps. The flow was fixed at 30 µL/min using a peristaltic pump and temperature was fixed at 25°C.

For LbL assemblies, the adsorption of PEI, when needed, is performed during 30 min, followed by a rinsing step of 30 min in the corresponding buffer. The adsorption of each protein layer is performed during 1h, followed by a rinsing step of 30 min in the corresponding buffer. For simultaneous adsorption, the protein mixture is adsorbed during 1h followed by a rinsing step of 1h in the buffer. An adsorption time of 1h was chosen for LbL as a compromise between feasibility of the experiment (time constraints) and reaching the equilibrium. The same duration was then also used for simultaneous adsorption, for the sake of comparison. Results for the 5^{th} overtone are presented in the results.

Film preparation for ellipsometry, contact angle measurements and atomic force microscopy: Films are prepared on silicon wafers spin-coated with polystyrene. Silicon wafers are washed in piranha solution (H_2O_2 30% (Prolabo, VWR, Leuven, Belgium)/H_2SO_4 95% (Prolabo, VWR, Leuven, Belgium) 1:2) during max 20 min, thoroughly rinsed with ultrapure water then ethanol, dried under nitrogen flow, and further treated under UV/O_3 during 15 min. They are then silanized with octadecyldimethylchlorosilane (ODMS, Sigma-Aldrich) to prevent polymer film detachment. Silanisation is performed overnight in a glove box in an ODMS solution in anhydrous toluene (Prolabo, VWR, Leuven, Belgium) supplemented with a few drops of triethylamine (Fisher Scientific, Loughborough, UK). After rinsing 4 times in toluene, with a 2 min sonication during the second rinse, silicon wafers are dried under nitrogen flow. Then, spin-coating is performed with 20 g/L PS in toluene at 5000 rpm during 40 s to obtain a~70 nm-thick PS layer, as measured by ellipsometry.
The LbL films are constructed on these PS substrates at room temperature in 24 well plates (Greiner Bio-One, Wemmel, Belgique). 1 mL of solution is used at each adsorption step. PEI is adsorbed during 30 min when needed and n-Col, d-Col and Fn are adsorbed during 1h for each step. For simultaneous adsorption,

a mixture of both proteins is left in contact during 1h with PS or with PEI-treated PS. After each adsorption step, three rinses are performed during 1 min with the corresponding buffer. At the end of the construction, the films are rinsed 7 times with water, dried under a nitrogen flow and stored in a desiccator before analysis. Rinsing steps are always performed by withdrawing 0.8 mL of solution from the well and adding of 0.8 mL of rinsing solution (buffer or water), to avoid leaving the film in contact with air between steps.

Water contact angle measurement: Static contact angles are measured using the sessile drop method with a CDD camera and an image analysis processor (Electronisch Ontwerbureau De Boer, The Netherlands). A 0.3 µL drop of ultrapure water is deposited on the surface and the angle value is read after 5 s. On each sample, at least 5 measurements are performed on different locations.

Ellipsometry: For each sample, the thickness of the PS layer is measured before protein deposition and subtracted to the total thickness measured after protein deposition. A spectroscopic ellipsometer (Uvisel, Horiba-Jobin-Yvon, France) was used to make measurements from 1.5 to 5 eV with an incidence angle around 70°. Data are fitted with DeltapPsi 2 software. A layer of SiO_2 of 1.55 nm was considered and a Cauchy absorbent model was applied on 2 eV – 4 eV data to determine the PS or film thickness. Three measurements are performed on each sample before and after protein deposition. A single-wavelength ellipsometer (Horiba-Jobin-Yvon) was also used. To fit the data, the refractive index was considered constant before and after deposition and fixed at n=1.6. Five measurements are performed on each sample before and after protein deposition. No significant differences were observed between measurements performed on different ellipsometers.

Immunodetection of fibronectin: Immunodetection of Fn is performed on different films directly built in 96-well PS plates, with a view to detect Fn accessibility in the films. Films are built as described above, with a volume of 150 µL of PEI or protein solution. When the desired film is ready, 200 µL of bovine serum albumin solution (BSA 99%, Sigma-Aldrich) at 1 mg/mL is added

as the blocking agent. The primary antibody, 100 µL of monoclonal anti-Fn antibody produced in mouse (Sigma-Aldrich) at 10.4 µg/mL, is added. The next step consists in the addition of the secondary antibody, 100 µL of anti-mouse IgG produced in rabbit, coupled to peroxidase (Sigma-Aldrich), at 11.5 µg/mL. BSA and antibody solutions are prepared in the buffer used for film building. Between each step, rinsings are made 3 times with the corresponding buffer. The plate is emptied and filled again with 200 µL of the corresponding buffer. The last step of the test is the addition of 100 µL of o-phenylenediamine (Sigma-Aldrich) solution at 0.4 mg/mL. This solution is prepared in phosphate citrate buffer (0.05M, pH 5, sigma-Aldrich) containing 0.4 mL/L H_2O_2 30% (Prolabo, VWR, Leuven, Belgique). At the end, the obtained solution is diluted twice before measuring the absorbance at 492 nm in a plate reader (PowerWawe XS2, Biotek). Reference curves are established by adsorption of Fn solutions from 0 to 100 µg/mL in the bottom of the untreated PS wells followed by the immunodetection test as described above. Blanks that are subtracted from the data are obtained by the same protocol that described above, except that protein films are not built and thus BSA adsorption on PS plates as a blocking agent is the first step.

Atomic force microscopy: AFM topographic images are recorded on dried samples on a Nanoscope V multimode microscope (Digital instuments, Santa Barbara, USA) in moderate to light tapping mode, using AFM tips with a spring constant of 20 to 80 $N.m^{-1}$ and resonant frequency in air from 358 to 382 Hz (Veeco, Camarillo, Canada). Image sizes were 10 x 5 μm^2. Images are treated with the Nanoscope analysis software and submitted to 3rd order flattening.

3. Results

3.1. In situ monitoring of assembly with QCM-D

Fig. II.2.1 presents -Δf and the ΔD/-Δf values reached after each adsorption step during LbL assembly in each of the three different buffers. These parameters are extracted from graphs shown in Fig. II.2.2, presenting data recorded as a function of time. The -Δf parameter increases with the deposited mass, i.e. adsorbed molecules and water contained in the films. The second parameter, ΔD/-Δf, is characteristic of the film viscoelastic properties. When it increases, the film becomes softer and dissipates more energy.

Data recorded for the building of $(Fn/n\text{-}Col)_3$ film are presented in Fig. II.2.1.a and Fig. II.2.2.a. The -Δf parameter increases for first Fn and n-Col layers, showing deposition of the two proteins, but stabilizes after these two first protein layers. -Δf behavior is not strongly influenced by the buffer. The films become more viscoelastic after the first n-Col adsorption step, as shown by the large increase of ΔD/-Δf. Fig. II.2.2.a shows that Fn adsorption plateau is nearly reached at the end of the first step, except in acetate buffer. An almost complete Fn monolayer is thus probably built on the surface. Second step allows the adsorption of n-Col on Fn layer. However, the n-Col adsorption plateau is not reached.

The data recorded for the building of $(Fn/d\text{-}Col)_3$ films (Fig. II.2.1.b and Fig. II.2.2.b) show a more complex behavior. In Hepes and PBS, the three first protein layers give an increase of -Δf . But then, the building is characterized by a decreased of -Δf upon d-Col adsorption, slightly offset by the next Fn adsorption step. Stabilization of the frequency shift, and thus adsorption plateau, is almost reached for each adsorption step (Fig. II.2.2.b). In acetate buffer, the data are similar to the data obtained for $(Fn/n\text{-}Col)_3$ film (see Fig. II.2.1.a). Films constructed with d-Col are less soft than with n-Col, as shown by the lower ΔD/-Δf. This was expected, because filamentous n-Col molecules may extend in solution, and since they may be highly hydrated, they dissipate more energyy. The disruption of the triple helical structure gives to d-Col a less hydrated coiled conformation [8].

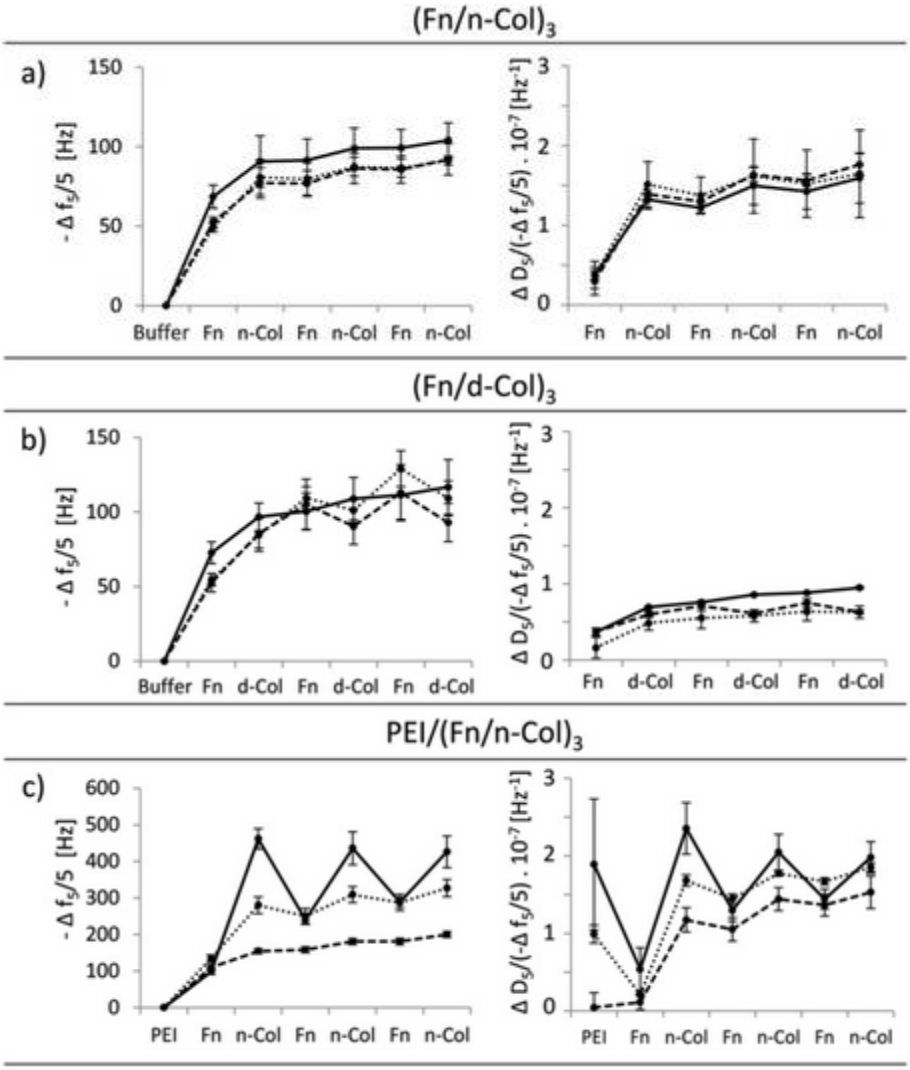

Figure II. 2. 1: QCM-D monitoring (left: cumulated -Δf5/5, right: cumulated ΔD5/(-Δf5/5)) for the construction of (a) (Fn/n-Col)3, (b) (Fn/d-Col)3 and (c) PEI/(Fn/n-Col)3 films. The assembly is performed in PBS (broken line), HEPES buffer (dotted line) and acetate buffer (plain line) on gold-covered quartz crystals spin-coated with polystyrene. Each point represented in the graphs is the value reached after each adsorption step of 1h and stabilization in the buffer during 30 min. For -Δf5/5 of PEI/(Fn/n-Col)3, baseline is artificially positioned after PEI adsorption. However, the -Δf5/5 used to compute ΔD5/(-Δf5/5) of PEI is the one measured from the real buffer baseline. Error bars are standard deviation (n=3).

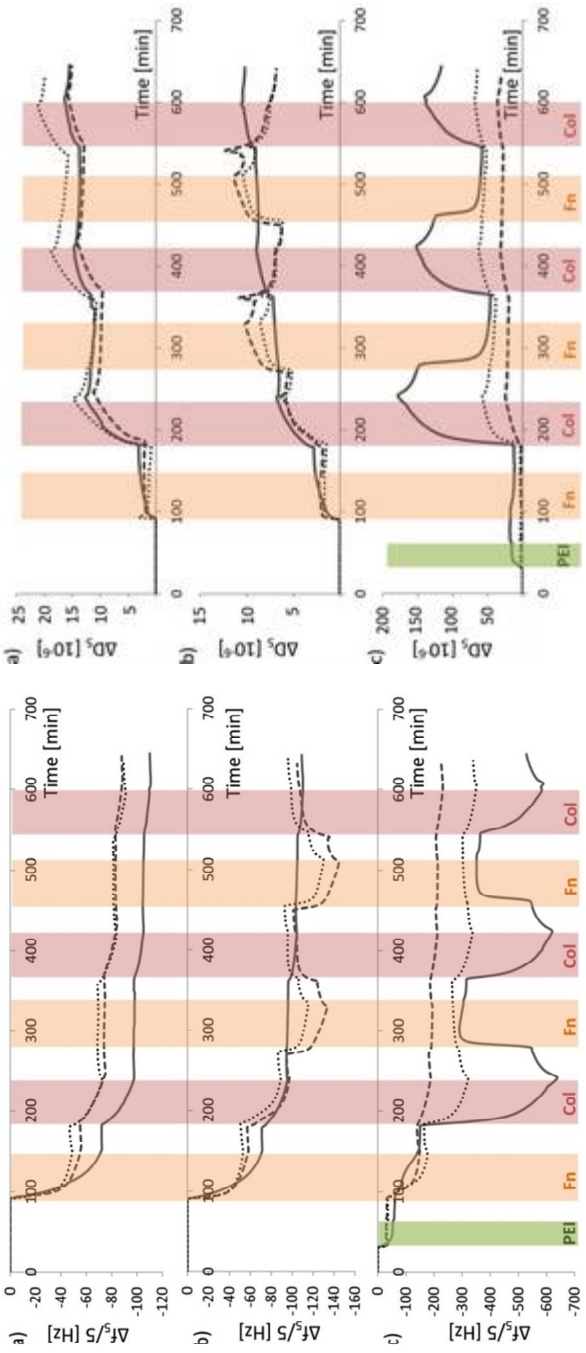

Figure II. 2. 2: Example of a real time QCM-D monitoring of $\Delta f_5/5$ and of ΔD_5 for the construction of (a) $(Fn/n\text{-}Col)_3$, (b) $(Fn/d\text{-}Col)_3$ and (c) $PEI/(Fn/n\text{-}Col)_3$ films. The assembly is performed in PBS (broken line), HEPES buffer (dotted line) and acetate buffer (plain line) on gold-covered quartz crystals spin-coated with polystyrene. After each adsorption step of 1h, rinsing is performed using the corresponding buffer.

The frequency shifts measured for the building of PEI/(Fn/n-Col)$_3$ films (Fig. II.2.1.c and Fig. II.2.2.c) differ completely from the ones of the two other film types. Frequency shifts are significantly higher. Even if the -Δf value recorded for first Fn adsorption step is similar in the three buffers, the behavior strongly depends on the buffer starting from the second adsorption step. n-Col adsorption is characterized by a |Δf| in Acetate buffer > |Δf| in Hepes buffer > |Δf| in PBS. Thereafter, in acetate and Hepes buffers, the building is characterized by a decreased -Δf during Fn addition. Interestingly, similar Δf values are reached in acetate and Hepes buffers at this stage of the process. In PBS, a slight increase of -Δf after each further adsorption step is observed. Adsorption kinetics (Fig. II.2.2.c) shows that a plateau is clearly not reached for n-Col adsorption step in acetate buffer and not either completely in Hepes and PBS. Viscoelasticity of the film is of the same order of magnitude than for films containing n-Col on PS. However, a decrease of viscoelasticity is observed here after each Fn adsorption step, particularly in acetate buffer.

In all the cases described above, the assembly occurs during the first two or three protein adsorption steps, but does not seem to be sustainable. Comparison with simultaneous adsorption of both proteins on PS or on PEI-coated PS can thus give more information about the interest of step-by-step construction. Frequency and dissipation shifts recorded after 1h of adsorption from a single Fn solution or mixed Fn+Col solutions and 1h of rinsing in the corresponding buffer are presented in Fig. II.2.3, where they are compared to the values obtained after LbL deposition ((Fn/Col)$_3$). Smaller shifts are observed for adsorption of Fn alone compared to adsorption from mixed Fn+Col solution, except when d-Col is used. Moreover, even if the differences are not significant, the -Δf recorded after 6 layers constructed with LbL protocols are almost always higher than after 1h of adsorption from mixed Fn+Col solution. This phenomenon is less marked for Fn/n-Col film on virgin PS.

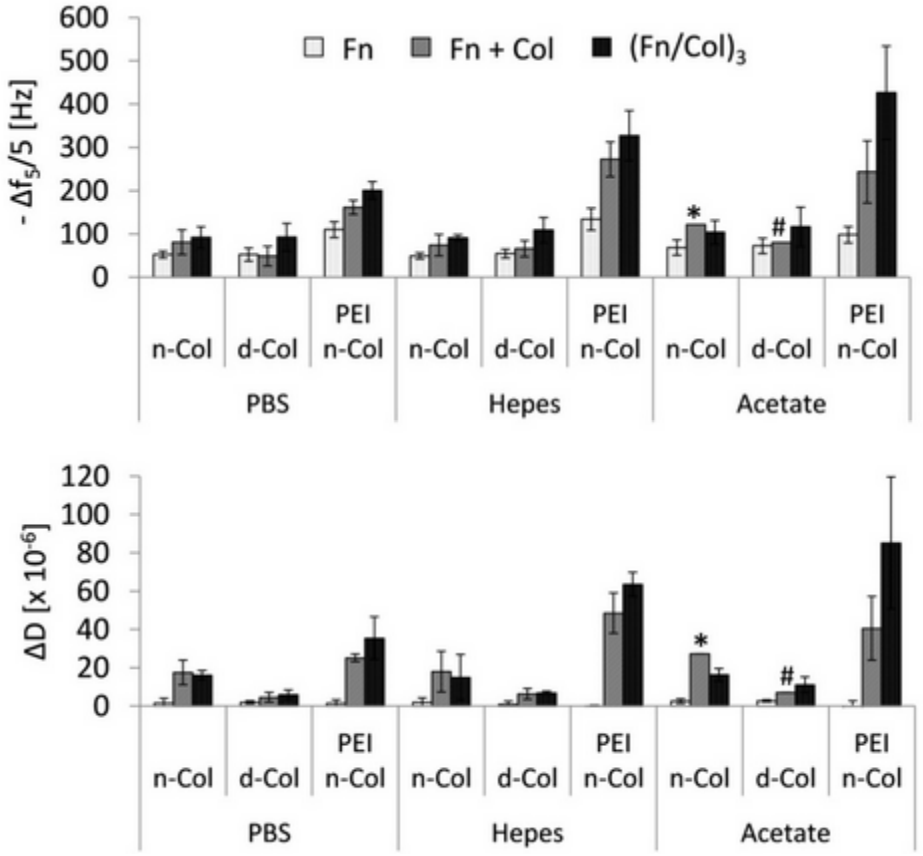

Figure II. 2. 3: QCM-D results after adsorption of Fn during 1h, adsorption from a mixture of Fn and Col during 1h and adsorption of three bilayers by LbL construction. The -Δf and ΔD values are extracted after the rinsing step in the corresponding buffer. Error bars show the 95% confidence interval (n=3). Results with * or # are the mean of only two measurements that differ respectively by 24.5 Hz and 10 Hz for $-\Delta f_5/5$ and 6.3.10-6 and $0.1.10^{-6}$ for ΔD.

3.2. Ex situ measurement of dry thickness and water contact angle

Dry thickness and water contact angle measurements are presented in Fig. II.2.4. Effect of the type of film is shown only in PBS. Films without a PEI anchoring layer are thinner than with the anchoring layer. None of the films prepared in PBS shows a regular growth of the thickness with the number of layers. Contact angle measurements present a slight saw-tooth profile for

(Fn/d-Col) film on PS, even less marked for (Fn/n-Col) film on PS, and that completely disappears for PEI/(Fn/n-Col) films. Saw-tooth profile can be the expression of a difference of chemistry according to the last layer, characteristic of LbL building. The water contact angles of Fn alone and Col alone are around 60°-70° and 30°-40°, respectively. A saw-tooth profile was thus expected, with a decrease or increase of the angle when Col or Fn is the last deposited layer, respectively.

Buffer effect is presented for PEI/(Fn/n-Col) films. In PBS, the thickness reaches a plateau after the first Fn adsorption step. In Hepes buffer, a regular increase of thickness with number of layers is observed but a plateau seems to be reached after two proteins bilayers. In acetate buffer, a saw-tooth profile is observed, similar to the one observed by QCM-D. Indeed, thickness decreases after Fn adsorption step and increases with n-Col adsorption step. Contact angle curves have approximatively the same shape whatever the buffer. It decreases for first Fn adsorption, still decreases for next n-Col adsorption, increases for next Fn adsorption and stays constant thereafter. The decrease is more important in acetate buffer.

In all cases, on PS or on PEI-coated PS, the thickness measured for simultaneous adsorption of Col and Fn (open circles in Fig. II.2.4) during only one hour is higher or equal to the thickness reached after four alternated steps of 1 h of adsorption. In the same line, contact angle values after simultaneous adsorption are always lower or equal to the lowest value reached after Col adsorption during step-by-step building.

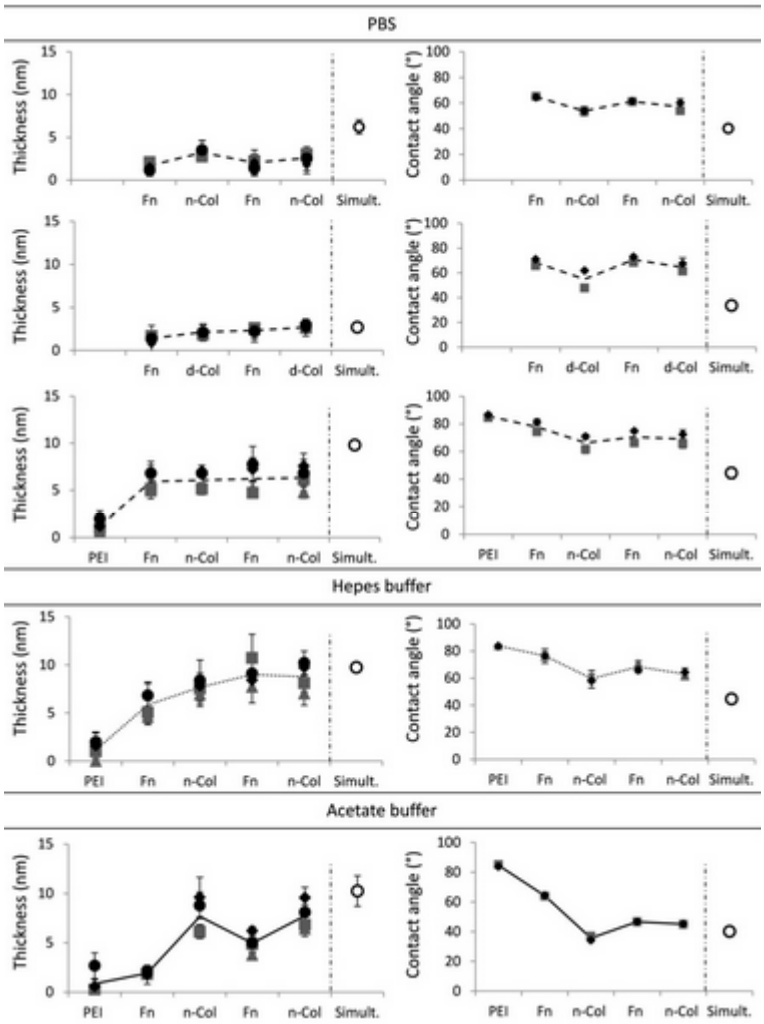

Figure II. 2. 4: Ellipsometry measurement of the dry thickness (left) and water contact angle measurement (right) after each adsorption step. Ellispometry graphs show four repetitions for each point. Symbols with the same colors (black or grey) refer to samples prepared the same day, with the same solutions. Samples denoted by a different color (black or grey) were prepared on different days. Each repetition has its own error bar representing standard deviation (n ≥ 3, on the same sample). Contact angle measurement graphs show two repetitions, realized on different days. Each repetition has its own error bar representing standard deviation (n ≥ 5, on the same sample). The open circles represent the thickness or the contact angle measured after simultaneous adsorption from a mixed Fn+Col solution, on PS or on PEI-treated PS (for films with an anchoring layer). Error bars represent standard deviation (n = 4) for thickness and the difference between the two measurements for contact angle (n = 2).

3.3. Immunodetection of Fn

To determine the amount and/or accessibility of adsorbed Fn, immunodetection of the protein is performed. First, reference curves were established on films obtained by adsorption on PS from Fn solutions at concentration ranging from 0 to 100 µg/mL. It showed that the maximum signal obtained on these adsorbed layers is found for 25 µg/mL solutions and higher (results not shown). This maximum signal may be interpreted as corresponding to the saturation of the interface with Fn. However, Fn adsorption isotherm on PS measured by Lhoest et al. have shown that the plateau is only reached for a concentration of about 50 µg/mL [49]. Saturation would thus not yet be obtained at 25 µg/mL. Steric hindrance due to the size of detection antibodies could cause signal saturation even if the surface is not already saturated with Fn.

Results are presented in Fig. II.2.5.a for films on PS and Fig. II.2.5.b for films on PEI-treated PS. The absorbance measured for a blank sample (ie native PS in absence of adsorbed protein film, with BSA adsorbed as a blocking agent) is subtracted from the absorbance measured for protein films on PS and PEI-treated PS. Moreover, data are normalized by the value measured for simple adsorption from a 25 µg/mL Fn solution on PS. Fig. II.2.5.a shows that n-Col adsorbed alone gives a signal while it is normally not recognized by the antibody specific to fibronectin. As d-Col is not detected at all with nevertheless the same amino acid sequence than n-Col, the detection of n-Col is probably not due to a specific recognition by the antibody. It could come from an embedment of the anti-Fn antibody in n-Col film leading to an increased non-specific signal. A second hypothesis can be that anti-Fn antibody recognizes sequences only presented if n-Col is in the triple helical structure, or involved in supramolecular aggregates (fibrils). The hypothesis of an embedment of the antibody leading to an increasing of non-specific signal can also explain the signal measured for PEI adsorbed on PS (Fig. II.2.5.b). This non-specific adsorption of the detection antibody makes the results more difficult to interpret.

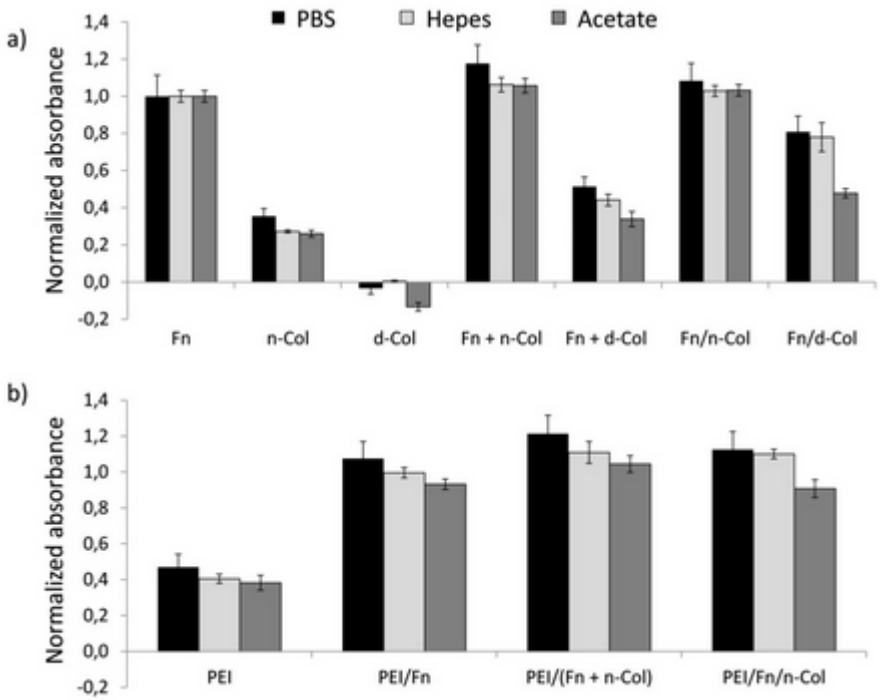

Figure II. 2. 5: Immunodetection of Fn in different adsorbed films. Graphs show the absorbance for a given film normalized by the absorbance measured for Fn adsorption on PS. Blank (uncoated PS, with blocking agent) is subtracted of both values before normalization. Values for adsorption on PS are presented in graph a) and for adsorption on PEI-coated PS in graph b). Error bars are 95% confidence intervals.

Films prepared in the three buffers show similar results. Films made by LbL deposition of Fn and n-Col give similar or higher signal compared to Fn adsorbed alone (Fig. II.2.5.a). It is however difficult to determine the non-specific part of this signal coming from n-Col. Still we can conclude that adsorption of n-Col does not completely mask the Fn adsorbed underneath, because the signal is much higher than for n-Col alone. On the contrary, films made by LbL adsorption of Fn and d-Col give a lower signal than Fn adsorbed alone. Fn is thus partially masked by d-Col in that case. The signal recorded for Fn + n-Col proves that there is Fn adsorbed on the surface after simultaneous adsorption. However, when d-Col is used, less Fn is detected after simultaneous adsorption than when a first layer of Fn adsorbed alone is covered by d-Col by

LbL deposition. The same conclusion than for films with n-Col on PS can be drawn for films made on PEI (Fig. II.2.5.b).

3.4. Film morphology depending on last deposited layer and on construction method

Fig. II.2.6 compares the morphology obtained for Fn/n-Col films on PEI-coated PS in the three different buffers. As shown in Fig. II.2.7, naked PS has a very smooth surface. PEI adsorbed on this PS layer forms aggregates in PBS (height ≈ 15 - 60 nm; diameter ≈ 100 - 500 nm), in Hepes (height ≈ 15 - 30 nm; diameter ≈ 100 - 300 nm) and in acetate buffer (height ≈ 5 – 20 nm; diameter ≈ 60 - 200 nm). The film morphology changes when protein layers are added on this PEI layer. This morphology is similar whatever the buffer but surfaces are smoother when prepared in acetate buffer. Not much difference is observed between LbL films terminated with Fn or n-Col. Simultaneous adsorption gives surfaces with a different morphology compared to LbL deposition: aggregates are observed and small fibrils are present between them. This morphology is less marked on films built in acetate.

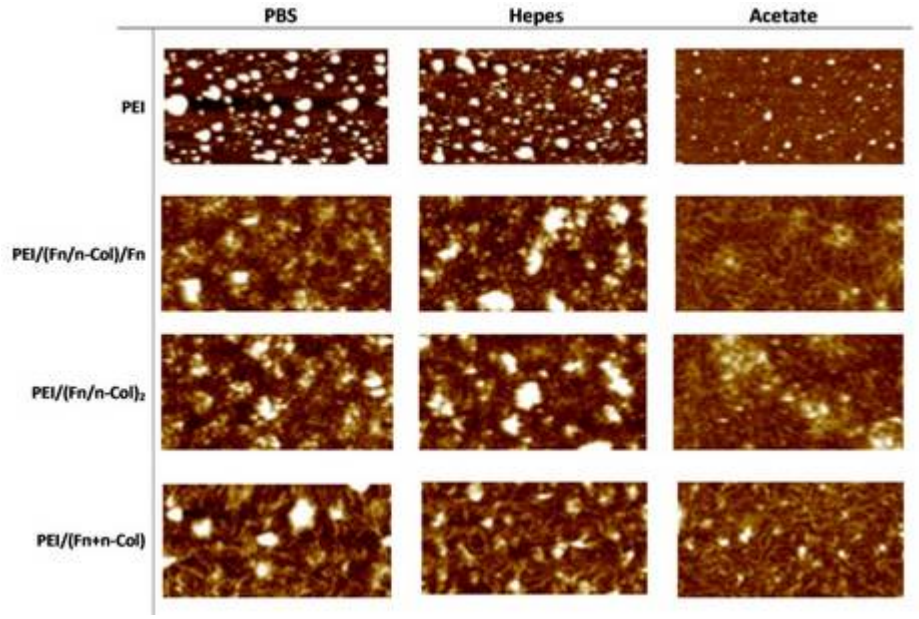

Figure II. 2. 6: AFM height images of films prepared from PBS (left), Hepes (middle) and acetate (right) buffers, at different steps of the assembly (as indicated) and after simultaneous adsorption on PEI-coated PS. Image size is 2.5 X 1.25 µm2 and Z-scale = 20 nm.

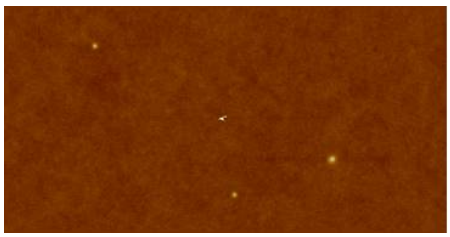

Figure II. 2. 7: AFM image of the naked PS surface (5 x 10 µm²; Z scale=20 nm)

Fig. II.2.8 compares the morphology obtained for Fn/n-Col and Fn/d-Col films built on PS in PBS. Smoother morphologies are observed compared to films built on PEI-coated PS. Films made of Fn and d-Col have the same morphology whatever the last layer and the building method. They are always very smooth. Films made of Fn/n-Col have different morphologies depending on the last deposited layer. When n-Col is the last layer, more fibrils are observed at the

interface. Depending on the sample, fibrils are short (0.5 -2 µm) and homogeneously distributed or long (more than 5 µm) and heterogeneously distributed on the surface. Simultaneous adsorption gives very reproducible images, with a lot of very small fibrils, homogeneously distributed at the interface.

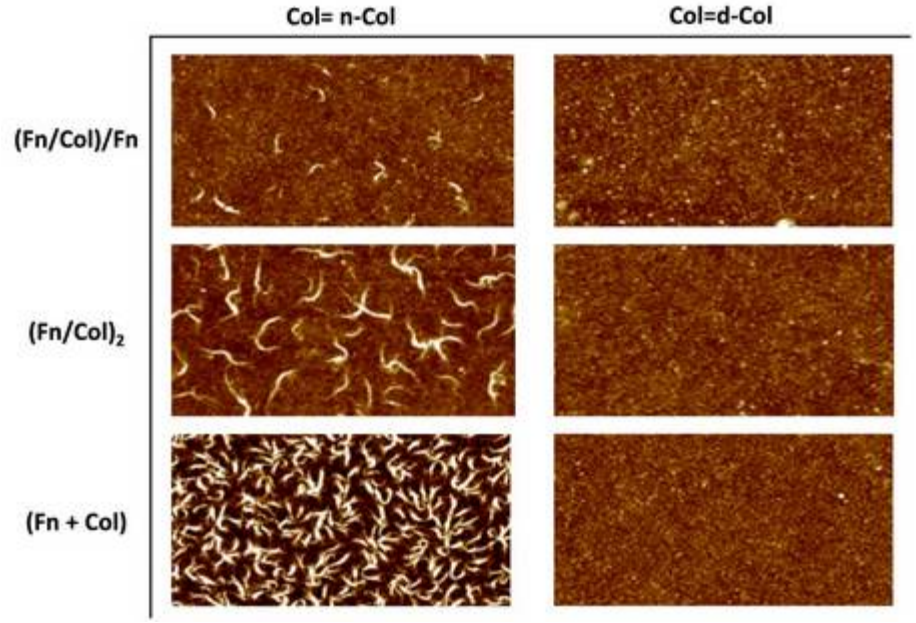

Figure II. 2. 8: AFM height images of films, prepared using PBS, at different steps of the assembly (as indicated) and after simultaneous adsorption on PS. Image size is 5 X 2.5 µm2 and Z-scale = 10 nm.

4. Discussion

4.1. Amount of water contained in the films

Computing the adsorbed mass based on QCM-D data is not trivial. Complex modelling process need to be used, particularly when dissipation is high, as it is the case in this study for some results. However, Sauerbrey equation, which is based on the assumption that the adsorbed layer behaves similarly as the quartz crystal, can be used to approximate the minimum adsorbed mass. The

Sauerbrey [50] equation is, $m_f = -C.(\Delta f_n/n)$, where n is the overtone number, m_f the adsorbed mass on the crystal, and C a constant roughly equal to 18 $ng.cm^{-2}Hz^{-1}$ for a 5 MHz crystal. With this equation, a $-\Delta f_5/5$ (Fig. II.2.1) of 100 Hz can be approximated to an adsorbed mass of 1800 $ng.cm^{-2}$. If a density of 1 $g.cm^{-3}$ is considered, it gives a thickness of 18 nm. This thickness can be compared to the thickness of the dry film measured by ellipsometry to obtain an estimation of the water content of the films as presented in Table II.2.1. This value is an approximation because (i) Sauerbrey model was applied, whose assumptions may not be completely met, and (ii) the dry films can still contain water, even after drying under N_2 flow. Nevertheless, films can be compared based on this estimated water content. The films are generally highly hydrated. Interestingly, the films created by simultaneous adsorption contain less water (58-80%) than the films created by LbL deposition (81-90%).

Table II. 2. 1: QCM-D and ellipsometry results obtained on films built through the LbL procedure or by simultaneous adsorption. Comparison of the thickness of the wet films, computed from QCM-D data, and of thickness of the dry films, measured by ellipsometry, is used to evaluate the amount of water trapped in the wet films.

Film	Buffer	$-\Delta f_5/5$ [Hz]	Thickness of wet film (nm)	Thickness of dry film (nm)	% of water in the film
Films created by LbL deposition method					
$(Fn/n\text{-}Col)_2$	PBS	86	15.5	2.6	83
$(Fn/d\text{-}Col)_2$	PBS	90	16.2	2.7	83
$PEI/(Fn/n\text{-}Col)_2$	PBS	181	32.6	6.3	81
$PEI/(Fn/n\text{-}Col)_2$	Hepes	310	55.8	8.8	84
$PEI/(Fn/n\text{-}Col)_2$	Acetate buffer	436	78.5	7.7	90
Films created by simultaneous adsoption					
Fn + n-Col	PBS	81	14.6	6.2	58
Fn + d-Col	PBS	49	8.8	2.7	69
PEI/(Fn + n-Col)	PBS	162	29.2	9.8	66
PEI/(Fn + n-Col)	Hepes	273	49.1	9.7	80
PEI/(Fn + n-Col)	Acetate buffer	244	43.9	10.3	77

4.2. Effect of collagen denaturation and of an anchoring layer on assembly

Results show that the conformation of the molecules involved in the build-up of the films influences the assembly profile. The use of d-Col is compared to the use of the native protein in assembly on PS, without anchoring layer. With the native protein, the assembly stops in its early stages and Fn seems only to adsorb during the first deposition step. d-Col is supposed to interact better with Fn than n-Col [23]. This can be attributed to the fact that denaturation disrupts the triple helical structure that can mask interaction sites of collagen. A better assembly was thus expected with d-Col compared to n-Col. Unfortunately, the use of d-Col does not give thicker films as shown by ellipsometry measurements. However, QCM-D data show a different behavior depending on the conformation of collagen. In PBS and Hepes, a decrease of -Δf (ie a loss of adsorbed mass) is observed after second and third d-Col adsorption steps. This behavior, already observed by Landoulsi at al.[8] for polystyrenesulfonate (PSS)/d-Col assembly for the PSS adsorption step, can originate from the high affinity of Fn with d-Col. The addition of d-Col could then desorb part of previously adsorbed Fn to form soluble Fn/d-Col complexes. Next step of Fn addition increases the adsorbed mass on the crystal and slightly offsets the desorption. But it decreases again thereafter and the assembly process is not sustainable. The first Fn layer is not desorbed from the substrate, probably because the adsorption on PS is almost irreversible. The first d-Col adsorption step thus forms a layer on Fn. Immunological detection of Fn confirms that Fn is partly masked by d-Col adsorption. Collagen denaturation also influences the film morphology. AFM images clearly show fibrillation of n-Col in Fn/n-Col films on PS. Films with d-Col are much smoother. Collagen self-assembly in the adsorbed phase is indeed a process related to the presence of the native molecule [15].

With a first layer of PEI, QCM-D data show an interesting profile in Hepes and acetate buffer. Decreased adsorbed mass and film viscoelasticity are observed after second and third Fn adsorption steps. This could be attributed to water loss, n-Col in the previous layer being highly hydrated, or loss of adsorbed

matter. The two phenomena are probably involved in acetate buffer because decrease of thickness, and thus desorption, is observed by ellipsometry. This desorption can be due to the formation of complexes between Fn in solution and previously adsorbed n-Col. Such complexes are however not formed without PEI anchoring layer. It can be assumed that, with a PEI anchoring layer, n-Col layers are thicker but less tightly linked to the previously adsorbed Fn than without PEI. Desorption through complexation is thus favored. To explain the saw-tooth profile in Hepes buffer, loss of water and film contraction are more probable because there is no thickness decrease, according to ellipsometry data.

The addition of an anchoring layer of PEI considerably increases the thickness of the films as confirmed by QCM-D and ellipsometry data. It is known that PEI generally improves the LbL assembly because it gives a first uniform layer that reduces the number of polyelectrolytes bilayers needed to obtain regular LbL assembly on the surface [51, 52]. Films are thus built more regularly from the first layer, and are thicker [51, 52] and smoother [52]. In the results presented here, LbL films obtained with a PEI anchoring layer are thicker but the assembly is not always improved, as in PBS where ellispometry data show a lack of adsorption after the first layer. In Hepes, the assembly works better but thickness seems to stabilize after the three first protein layers. Here, we show that PEI itself gives rough films, as shown by AFM, and does not seem to adsorb in a uniform layer. Aggregates are detected in AFM images and water contact angle after PEI adsorption is almost the same than the one of naked PS. The surface coverage by PEI is probably not complete, and the PS substrate is thus probably still apparent. This is somehow in contradiction with the reported use of PEI as a uniform first layer. These aggregates could however be artifacts produced during sample drying.

4.3. Effect of the buffer on assembly

PBS and Hepes buffers have the same pH, close to physiological conditions. Results of $(Fn/d\text{-}Col)_3$ films building on PS, obtained by QCM-D, are similar for these two buffers but different than in acetate buffer, which has a lower pH. pH

thus influences assembly. The high affinity of d-Col for Fn, which generates the saw-tooth pattern upon assembly in PBS and Hepes buffers (Fig. II.2.1.b), is then weaker between Fn and d-Col in acetate buffer, far from physiological conditions. On the contrary, PEI/(Fn/n-Col) assembly is highly modified by the buffer, even at constant pH, as illustrated by both QCM-D and ellipsometry data (Fig. II.2.1.c and Fig. II.2.4). Assembly is thus not only influenced by pH but also by the nature of surrounding ions. It was reported that phosphate ions, present in PBS, can bind to collagen molecules. Li et al. show that addition of 10 mM Na_2HPO_4 in 12 mM NaCl changes the isoelectric point of n-Col from 9.2 to 7.4 [13]. Fibrillation behavior can thus be altered, as well as electrostatic interactions with Fn. Among the buffers tested here, Hepes is the best one to trigger assembly. According to the iep values measured by Li et al. [13] and reported above, it is only in Hepes that Fn and d-Col have opposite charges, allowing LbL assembly through electrostatic interaction.

4.4. True LbL assembly or step-by-step saturation of the interface?

The results presented in this chapter are not pointing to a true LbL assembly, that grows indefinitely after each layer or bilayer adsorption. However, more than a protein monolayer is built on the surface and the obtained biointerfaces are stable under Hepes buffer during 20h (as determined by QCM-D; result not shown), which is already very promising because proteins generally adsorb in monolayers. QCM results show that saturation of the interface is almost reached after Fn adsorption (Fig. II.2.2) and that adsorption continues thereafter in most of the cases. Col is not smaller than Fn and should not have space to adsorb between Fn molecules. The surface should thus not be only saturated by a protein monolayer after the Col adsorption step, because collagen cannot adsorb in the holes left between Fn molecules. We are probably in an intermediate situation between a few well-defined multilayers and a mixed monolayer of Fn and Col. Depending on the buffer, presence of PEI anchoring layer and use of n-Col or d-Col, we are more close to the first or the second mode of deposition.

Charge reversal after each deposition step is a key to the formation of multilayered structures based on electrostatic interactions [29]. In some cases however, molecules with a very low charge density or no charges at all can be involved in a sustainable LbL assembly, based on other types of interactions (hydrophobic interactions, hydrogen bonds, host-guest interactions etc) [53]. The growth of LbL assemblies is known to proceed according to two different modes. Linear growth is observed when the same amount of polyelectrolyte is adsorbed at each bilayer deposition step; it is mainly the case for strong polyelectrolytes. Exponential growth, often observed with polysaccharides or polypeptides, is characterized by an increasing thickness increment after each new bilayer deposition step, owing to the ability of one of the species to diffuse within the film [53, 54].

In this work, we show that collagen and fibronectin do not undergo linear nor exponential assembly. The lack of sustainability of the assembly may have several origins. If electrostatic interactions are mainly involved, it is probable that charge reversal is not taking place, preventing further assembly. Proteins undoubtedly do not behave as classical polyelectrolytes given their amphoteric character and their more defined conformation. Since specific interactions are expected between these two proteins, it is moreover thought that once those established for one bilayer, the amount of available sites for further binding is limited. As far as we know, the mechanism of assembly within LbL films fully made of proteins is not yet unraveled. It is more common to create LbL films using a combination of one protein and one synthetic or natural polyelectrolyte [8, 30].

4.5. Comparison of simultaneous adsorption and LbL assembly

The results show that simultaneous adsorption generally gives thicker films (Fig. II.2.4, left, dry thickness) than LbL adsorption, and that LbL building is not sustainable. These observations can thus question the utility to construct Fn and Col-containing films by the LbL method. However, simultaneous adsorption gives more wettable (Fig. II.2.4 Right) and less hydrated (Table II.2.1) films than LbL deposition. Moreover, film morphology depends on the film formation

method (Fig. II.2.6 and II.2.8). The structure of the obtained films is thus different. This could be explained by the following hypotheses. First, simultaneous adsorption could only give a monolayer while a few multilayers would be obtained by LbL assembly. Second, AFM results for simultaneous adsorption show more features which are characteristic of collagen adsorption, such as fibrils. Moreover, immunodetection on Fn + d-Col adsorbed simultaneously on PS shows less Fn than on Fn/d-Col film. Simultaneous adsorption thus leads to the preferential adsorption of Col, the major component of the mixed solution and the largest protein. With LbL deposition, more Fn is adsorbed, and the assembly process of collagen is altered.

5. Conclusion

Results presented in this second chapter show that construction of protein multilayers by classical LbL procedure is not trivial. Here, three different buffers were tested as well as the influence of collagen denaturation and of a PEI anchoring layer in a view of understanding assembling mechanisms and identifying good assembly conditions. None of these conditions allows sustainable multilayer growth. The assembly process stops after a few layers and sometimes even before. However, multilayers are obtained, which is already very promising given that proteins are generally known to adsorb only in monolayers. Moreover, interesting behaviors are highlighted, such as the saw-tooth profile observed in QCM-D results with d-Col, the increased thickness when PEI is used and the influence of pH and phosphate ions on the assembly. Additionally, construction of fibronectin and collagen-containing films using the LbL procedure gives surfaces with different structure and properties than simultaneous adsorption. This is expected to affect cell behavior, which is known to be very sensitive to the extracellular matrix compounds organization. Next step of this work will be the evaluation of cell adhesion, proliferation and differentiation on these surfaces. This will aim at evidencing specific cell behaviors linked to protein organization with foreseen applications in biotechnology and medicine. These results will be presented in the third chapter.

References

1. Giliberti, D.C., K.K. White, and K.C. Dee, *Control of cell-biomaterial interactions*, in *Polymeric Biomaterials*, S. Dumitriu, Editor. 2002, Marcel Dekker: New-York. p. 361-375
2. García, A.J., *Interfaces to Control Cell-Biomaterial Adhesive Interactions*, in *Polymers for Regenerative Medicine*, C. Werner, Editor. 2006, Springer Berlin Heidelberg. p. 171-190.
3. Aumailley, M. and B. Gayraud, *Structure and biological activity of the extracellular matrix.* Journal of Molecular Medicine, 1998. **76**(3-4): p. 253-265.
4. Alberts, B., et al., *Molecular Biology of The Cell*. 5th ed. 2008, New-York: Garland Sciences.
5. Chen, C.S., et al., *Geometric control of cell life and death.* Science, 1997. **276**(5317): p. 1425-1428.
6. Piez, K.A., *Collagen*, in *Encyclopedia of polymer sciences and engineering*, J. Kroschwitz, Editor. 1985, Willey: New-York. p. 699-727.
7. Beckman, M.J., K.J. Shields, and R.F. Diegelmann, *Collagen*, in *Encyclopedia of biomaterials and biomedical engineering*, G.E. Wnek and G.L. Bowlin, Editors. 2004, Marcel Dekker: New-York p. 324-334.
8. Landoulsi, J., S. Demoustier-Champagne, and C. Dupont-Gillain, *Self-assembled multilayers based on native or denatured collagen: Mechanism and synthesis of size-controlled nanotubes.* Soft Matter, 2011. **7**(7): p. 3337-3347.
9. Wood, G.C. and M.K. Keech, *The formation of fibrils from collagen solutions. 1. The effect of experimental conditions: kinetic and electron-microscope studies.* The Biochemical journal, 1960. **75**: p. 588-598.
10. Gross, J. and D. Kirk, *The heat precipitation of collagen from neutral salt solutions:Some Rate-regulating factors.* Journal of biological chemistry, 1958. **233**(2): p. 355-360.
11. Harris, J.R. and A. Reiber, *Influence of saline and pH on collagen type I fibrillogenesis in vitro: Fibril polymorphism and colloidal gold labelling.* Micron, 2007. **38**(5): p. 513-521.
12. Harris, J.R., A. Soliakov, and R.J. Lewis, *In vitro fibrillogenesis of collagen type I in varying ionic and pH conditions.* Micron, 2013. **49**: p. 60-68.

13. Li, Y., et al., *pH effects on collagen fibrillogenesis in vitro: Electrostatic interactions and phosphate binding.* Materials Science and Engineering C, 2009. **29**(5): p. 1643-1649.
14. Gurdak, E., P.G. Rouxhet, and C.C. Dupont-Gillain, *Factors and mechanisms determining the formation of fibrillar collagen structures in adsorbed phases.* Colloids and Surfaces B: Biointerfaces, 2006. **52**(1): p. 76-88.
15. Gurdak, E., et al., *Influence of collagen denaturation on the nanoscale organization of adsorbed layers.* Journal of Colloid and Interface Science, 2006. **302**(2): p. 475-484.
16. Dupont-Gillain, C.C., I. Jacquemart, and P.G. Rouxhet, *Influence of the aggregation state in solution on the supramolecular organization of adsorbed type I collagen layers.* Colloids and Surfaces B: Biointerfaces, 2005. **43**(3-4): p. 179-186.
17. Tooney, N.M., et al., *Solution and surface effects on plasma fibronectin structure.* Journal of Cell Biology, 1983. **97**(6): p. 1686-1692.
18. Hynes, R.O. and K.M. Yamada, *Fibronectins: Multifunctional modular glycoproteins.* Journal of Cell Biology, 1982. **95**(2 I): p. 369-377.
19. Pearlstein, E., L.I. Gold, and A. Garcia-Pardo, *Fibronectin: A review of its structure and biological activity.* Molecular and Cellular Biochemistry, 1980. **29**(2): p. 103-128.
20. Engel, J., et al., *Shapes, domain organizations and flexibility of laminin and fibronectin, two multifunctional proteins of the extracellular matrix.* Journal of Molecular Biology, 1981. **150**(1): p. 97-120.
21. Gold, L.I. and E. Pearlstein, *Fibronectin-collagen binding and requirement during cellular adhesion.* Biochemical Journal, 1980. **186**(2): p. 551-559.
22. Dessau, W., et al., *Identification of the sites in collagen α-chains that bind serum anti-gelatin factor (cold-insoluble globulin).* Biochemical Journal, 1978. **169**(1): p. 55-59.
23. Ingham, K.C., R. Landwehr, and J. Engel, *Interaction of fibronectin with C1q and collagen.* European Journal of Biochemistry, 1985. **148**(2): p. 219-224.
24. Engvall, E., M.L. Bell, and E. Ruoslahti, *Affinity chromatography of collagen on collagen-binding fragments of fibronectin.* Collagen and Related Research, 1981. **1**(6): p. 505-516.

25. Engvall, E., E. Ruoslahti, and E.J. Miller, *Affinity of fibronectin to collagens of different genetic types and to fibrinogen.* Journal of Experimental Medicine, 1978. **147**(6): p. 1584-1595.
26. Ingham, K.C., S.A. Brew, and M. Migliorini, *Type I collagen contains at least 14 cryptic fibronectin binding sites of similar affinity.* Archives of Biochemistry and Biophysics, 2002. **407**(2): p. 217-223.
27. Williams, E.C., et al., *Conformational States of Fibronectin: Effects of pH, Ionic Strenght, and Sollagen Binding.* The journal of biological chemistry, 1982. **257**(24): p. 14973-14978.
28. Decher, G., J.D. Hong, and J. Schmitt, *Buildup of ultrathin multilayer films by a self-assembly process: III. Consecutively alternating adsorption of anionic and cationic polyelectrolytes on charged surfaces.* Thin Solid Films, 1992. **210-211**(Part 2): p. 831-835.
29. Decher, G., *Fuzzy nanoassemblies: Toward layered polymeric multicomposites.* Science, 1997. **277**(5330): p. 1232-1237.
30. Lvov, Y., *Electrostatic layer-by-layer assembly of proteins and polyions*, in *Protein architecture: Interfacing molecular assemblies and immobilization biotechnology*, Y. Lvov and H. Möhwald, Editors. 2000, Marcel Dekker: New-York. p. 125-167.
31. Johansson, J.Å., et al., *Build-up of collagen and hyaluronic acid polyelectrolyte multilayers.* Biomacromolecules, 2005. **6**(3): p. 1353-1359.
32. Zhang, J., et al., *Natural polyelectrolyte films based on layer-by layer deposition of collagen and hyaluronic acid.* Biomaterials, 2005. **26**(16): p. 3353-3361.
33. Li, X., et al., *The responses of preosteoblasts to collagen/hyaluronic acid polyelectrolyte multilayer coating on titanium.* Polymers for Advanced Technologies, 2012. **23**(4): p. 756-764.
34. Lin, Q., et al., *Heparin/collagen multilayer as a thromboresistant and endothelial favorable coating for intravascular stent.* Journal of Biomedical Materials Research - Part A, 2011. **96**(1): p. 132-141.
35. Chou, C.-C., H.-J. Zeng, and C.-H. Yeh, *Blood compatibility and adhesion of collagen/heparin multilayers coated on two titanium surfaces by a layer-by-layer technique.* Thin Solid Films, 2013. **549**: p. 117-122.
36. Chen, J., et al., *Collagen/heparin coating on titanium surface improves the biocompatibility of titanium applied as a blood-contacting biomaterial.* Journal of Biomedical Materials Research - Part A, 2010. **95**(2): p. 341-349.

37. Li, W., et al., *Natural Polyelectrolyte Self-Assembled Multilayers Based on Collagen and Alginate: Stability and Cytocompatibility.* Biomacromolecules, 2013. **14**(8): p. 2647-2656.
38. Chaubaroux, C., et al., *Collagen-based fibrillar multilayer films cross-linked by a natural agent.* Biomacromolecules, 2012. **13**(7): p. 2128-2135.
39. Mhanna, R.F., J. VörÖs, and M. Zenobi-Wong, *Layer-by-layer films made from extracellular matrix macromolecules on silicone substrates.* Biomacromolecules, 2011. **12**(3): p. 609-616.
40. Matsusaki, M., et al., *Fabrication of cellular multilayers with nanometer-sized extracellular matrix films.* Angewandte Chemie - International Edition, 2007. **46**(25): p. 4689-4692.
41. Matsusaki, M., et al., *Layer-by-layer assembly through weak interactions and their biomedical applications.* Advanced Materials, 2012. **24**(4): p. 454-474.
42. Kadowaki, K., M. Matsusaki, and M. Akashi, *Control of cell surface and functions by layer-by-layer nanofilms.* Langmuir, 2010. **26**(8): p. 5670-5678.
43. Matsuzawa, A., M. Matsusaki, and M. Akashi, *Effectiveness of nanometer-sized extracellular matrix layer-by-layer assembled films for a cell membrane coating protecting cells from physical stress.* Langmuir, 2013. **29**(24): p. 7362-7368.
44. Chetprayoon, P., et al., *Survival and structural evaluations of three-dimensional tissues fabricated by the hierarchical cell manipulation technique.* Acta Biomaterialia, 2013. **9**(1): p. 4698-4706.
45. Matsusaki, M., *Development of three-dimensional tissue models based on hierarchical cell manipulation using nanofilms.* Bulletin of the Chemical Society of Japan, 2012. **85**(4): p. 401-414.
46. Matsusaki, M., C.P. Case, and M. Akashi, *Three-dimensional cell culture technique and pathophysiology.* Advanced Drug Delivery Reviews, 2014. **74**: p. 95-103.
47. Nishiguchi, A., et al., *Effects of angiogenic factors and 3D-microenvironments on vascularization within sandwich cultures.* Biomaterials, 2014. **35**(17): p. 4739-4748.
48. Omorphos, N.P., L. Kahn, and D.M. Kalaskar, *Design of extracellular protein based particles for intra and extra-cellular targeting.* Colloids and Surfaces B: Biointerfaces, 2015. **136**: p. 440-448.

49. Lhoest, J.B., et al., *Fibronectin adsorption, conformation, and orientation on polystyrene substrates studied by radiolabeling, XPS, and ToF SIMS.* Journal of Biomedical Materials Research, 1998. **41**(1): p. 95-103.
50. Reviakine, I., D. Johannsmann, and R.P. Richter, *Hearing what you cannot see and visualizing what you hear: Interpreting quartz crystal microbalance data from solvated interfaces.* Analytical Chemistry, 2011. **83**(23): p. 8838-8848.
51. Elzbieciak-Wodka, M. and P. Warszyński, *Effect of deposition conditions on thickness and permeability of the multilayer films formed from natural polyelectrolytes.* Electrochimica Acta, 2013. **104**: p. 348-357.
52. Kolasińska, M., R. Krastev, and P. Warszyński, *Characteristics of polyelectrolyte multilayers: Effect of PEI anchoring layer and posttreatment after deposition.* Journal of Colloid and Interface Science, 2007. **305**(1): p. 46-56.
53. Borges, J. and J.F. Mano, *Molecular interactions driving the layer-by-layer assembly of multilayers.* Chemical Reviews, 2014. **114**(18): p. 8883-8942.
54. V. Klitzing, R., *Internal structure of polyelectrolyte multilayer assemblies.* Physical Chemistry Chemical Physics, 2006. **8**(43): p. 5012-5033.

Chapter 3: Adipose-derived stem cell response to biointerfaces based on collagen and fibronectin

Abstract:

With a view to improve tissue engineering approaches, the development of biomimetic surfaces, inspired of extracellular matrices, is of major interest. In this work, the use of collagen and fibronectin to design these biointerfaces was investigated. Layer-by-layer assembly of these two proteins was compared to the simultaneous adsorption of both proteins, with or without an anchoring layer of poly(ethyleneimine) (PEI), in Hepes buffer. Results showed that films made on PEI are thicker and rougher whatever the deposition method. Films obtained by simultaneous adsorption have at least the same thickness than films obtained by LbL deposition. Moreover, more fibrils are observed in the case of simultaneous adsorption, and measured water contact angles are lower. The behavior of adipose-derived mesenchymal stem cell was then investigated on the different films. All the protein films allow a better adhesion and proliferation than naked PS. Films built on PEI decrease the proliferation rate of the cells at the beginning of growth. However, differentiation was shown to be improved by the presence of this anchoring layer. The impact of the deposition method on cell behavior was less noticeable. It does not alter proliferation but in the case of differentiation, without the PEI layer, films built by LbL assembly show very poor performances compared to films built by simultaneous adsorption. This study shows that the organization and the nature of molecules at interfaces can influence cell behavior.

1. Introduction

In the context of damaged organ replacement, two strategies are developed to overcome the lack of donor and rejection problems: biomaterial-based devices and tissue engineering. For both strategies, the control of cell-material interactions plays an important role. There is a large amount of approaches that can be used to govern cell behavior. Changing the topography [1-4], the mechanical properties [5-7] and the chemistry [8] of the interface can actually modify cell behavior. In many works, the material surface is functionalized with biomimetic molecules. *In vivo*, cells are indeed embedded in an extracellular matrix (ECM) and mimicking this matrix is a promising approach to improve cell-material interactions.

The ECM is mainly composed of proteins and polysaccharides [9]. Collagen is one of the most important proteins of the matrix. Different types of collagen exist, most of them being able to form fibrils. These fibrils give strength to tissues such as bones and tendons [10]. The ECM is also composed of elastin fibers, that give elasticity to tissues such as blood vessel walls, skin and ligaments [10]. Then, fibronectin is a glycoprotein mainly responsible of the adhesion of cells to the matrix and is known to regulate cell characteristics and behavior [10]. Finally, polysaccharides of the ECM are mainly glycosaminoglycans (GAG), polymers of disaccharide units [9] which are hydrophilic and are swelled with water.

Integrins constitute the link between ECM proteins and cells. These proteins, localized in the cell membrane, are composed of two subunits (α and β). They exist in an active and an inactive form and can be activated both by internal and external signals. When integrins are activated, they are linked outside of the cell to a signaling sequence of the ECM and on the cytoplasmic side to actin filaments via talin. They thus make the link between the ECM and the cell cytoskeleton [9]. Integrins can move laterally to cluster, thereby forming focal adhesion points in which protein complexes gather together a large number of intracellular proteins such as vinculin, tensin, paxillin, etc. The formation of focal adhesion points triggers the phosphorylation of important intracellular proteins, thereby influencing cell behavior [11].

Collagen is a major component of the ECM. Many types of collagen exist but the most used in biomaterial research is type I collagen (Col). The Col molecule is composed of three chains, coiled together in a triple helical structure, composed of two α1 and one α2 chains [12], with a length of 300 nm and a diameter of 1.5 nm [13]. Each polypeptide chain of the molecule has a repetitive structure of Glycine-X-Y where X is often proline and Y is often hydroxyproline [12]. Glycine is a small amino acid residue located in the central part of the helix which allows the close packing of the triple helix. Col molecules have the property to self-assemble to form fibrils [12]. This fibrillation happens *in vivo* as well as *in vitro*. The main sequence recognized by integrins in Col is Gxx'GEx'' with x being a hydrophobic residue, x' usually a hydroxyproline and x'' usually R [14]. A few RGD sequences and probably DGEA sequences also play a role in interactions with integrins [14].

Fibronectin (Fn) is considered as the interaction protein of the matrix. This glycoprotein is a dimer composed of two subunits of 250 kDa each, having a length of 61 nm and a diameter of 2 nm [15], linked together by two disulfide bonds [16]. Fn is composed of repeated units of type I, type II and type III motifs. Some of these motifs, taken together, form recognition domains for fibrin, heparin, cell integrins, collagen, etc. [17]. Fn thus presents a specific collagen-binding site, generating a specific interaction between these two proteins. However, Fn links more easily to denatured compared to native Col [16, 18]. Fn is also well known to present cell adhesion sites such as amino acid sequences RGD, that work in synergy with PHRSN sequence [16, 19]. Other recognition amino acid sequences, such as LDV and REDV present on an alternatively spliced region of Fn, also contribute to the cell adhesion properties of Fn [16, 20].

Mesenchymal stem cells (MSC) are more and more used in tissue repair because they can differentiate into a large diversity of cell types [21]. Adipose-derived mesenchymal stem cells (AMSC) are MSC extracted from adipose tissue. Being easily isolated from the patient in large amount, they are promising for regenerative medicine [22]. Schubert et al. have already shown that these cells can undergo osteogenic differentiation [23]. They also proved that AMSC, seeded on demineralized bone matrix, form an implant that can,

after osteogenic differentiation, be used as therapeutic solution for bone defect reconstruction [24]. To improve the clinical applications involving AMSC, a better understanding of the mechanisms influencing AMSC behavior is needed. In this aim, studying cell behavior on specific biointerfaces has an interest. Indeed, first phases of clinical applications are very often an *in vitro* cell expansion and differentiation in culture plates. Improvement of cell adhesion and differentiation on flat substrates is thus a key to develop new strategies involving these AMSC.

In this work, Col and Fn will be used to create biomimetic interfaces to improve the interaction of AMSC with materials. The strategy is to combine these two proteins on the interface, where AMSC behavior will be investigated. Two deposition methods will be tested: simultaneous adsorption of both proteins and layer-by-layer (LbL) deposition. LbL deposition of extracellular matrix components was used previously to create biointerfaces. Assemblies were built with either Col [25-33] or Fn [34-36] as building block, but never with another protein as the second building block, because assembly of two proteins by LbL deposition is indeed very challenging. Until now, only one research group succeeded to combine two proteins using the LbL approach by using gelatin, derived from Col by denaturation, and Fn to create biointerfaces [37-41]. The study of the feasibility of LbL assembly between Fn and Col was investigated in chapter 2 of this thesis.

The first aim of this chapter is thus to characterize the properties of biomimetic films built with Col and Fn in Hepes buffer on polystyrene (PS), with different methods of deposition (simultaneous adsorption vs LbL) and with/without an anchoring layer of PEI. These films will be compared to a simple Fn layer, on PS and PEI-coated PS. The second purpose is to evaluate cell behavior on these films by studying adhesion, growth and osteogenic differentiation of AMSC and to identify specific conditions that could improve cell behavior. More specifically, films that will improve cell adhesion, increase proliferation rate and avoid differentiation during expansion phase, and decrease the time needed for differentiation during osteogenic differentiation phase, are looked for. Films with these properties could decrease the time of *in vitro* culture needed before clinical application.

2. Materials and method

2.1. Preparation of biointerfaces by layer-by-layer method or simultaneous adsorption

The protocols used to prepare biointerfaces are already described in details in the previous chapter. In this section, the most important steps will be summarized and more details will be given on film preparation details required for cell culture, not described before.

Substrates: Biointerfaces are all prepared starting from a PS surface, whose preparation depends on the experiment. For film characterization by contact angle, ellipsometry and atomic force microscopy, films are built on silicon wafers coated with a thin PS layer. Silicon wafers are first washed in piranha solution (H_2O_2 30 % (Prolabo, VWR, Leuven, Belgium):H_2SO_4 95% (Prolabo, VWR, Leuven, Belgium), 1:2) and treated under UV/O_3. They are then silanized with octadecyldimethylchlorosilane (ODMS, Sigma-Aldrich) and are spin-coated with 20 g/L PS (M_n= 140 000 g.mol^{-1}, M_w = 230 000 g.mol^{-1}, Aldrich, Milwaukee, USA) in toluene (Prolabo, VWR, Leuven, Belgium) at 5000 rpm during 40 s to obtain a~70 nm-thick PS layer.

For characterization by QCM-D monitoring, a PS film is deposited on a gold-coated quartz crystal by spin-coating from a 0.5% w/w PS solution in toluene during 20 s at 2000 rpm, followed by a 30 min treatment at 80° C to evacuate the solvent.

For cell culture experiments, if fluorescent staining is performed, glass coverslips (diameter = 12 mm) are used. They are also washed in piranha solution, silanized with ODMS and spin-coated during 40 s at 5000 rpm with PS 20 g/L. To be used in cell culture, these PS-coated glass coverslips are sterilized in ethanol 70 %, prepared with absolute ethanol (Prolabo, VWR, Leuven, Belgium) and ultrapure water (Elga Purelab Ultra device, 18.2 MΩ.cm, Veolia, UK), during 30 min under laminar flow hood. They are then put on a 96-wells sterile plate to dry under the hood. For other cell culture experiments, the PS substrate is directly the PS of the bottom of sterile untreated 24-wells plates (Greiner). Tissue-culture polystyrene (TCPS) 24-wells plate (Falcon, VWR) are

also used as control. TCPS is PS that has undergone oxidizing treatment to favor cell adhesion.

Buffer and proteins: The buffer used is Hepes prepared from 10 mM of Hepes salt (Acros organic, Geel, Belgium) and 0.15 M NaCl (Sigma-Aldrich). The buffer pH is then adjusted to 7.4 using NaOH. This buffer is used to prepare the proteins and PEI solutions for film building. PEI (Mr = 600 000 – 1 000 000 $g.mol^{-1}$, Fluka, Sigma-Aldrich) solution is prepared at 1 mg/ml, Col (type I from calf skin, Biochrom AG, Source Bioscience, Berlin, Germany) solution is prepared at 100 µg/ml and Fn (bovine fibronectin, Invitrogen, Life Technologies, Gent, Belgium) solution at 25 µg/ml. Protein solutions are stored at 4°C until use.

Protein film building (except for QCM): Building of the film is performed by two different methods, LbL assembly or simultaneous adsorption. In both cases, when a PEI anchoring layer is added, PEI is adsorbed from solution on PS during 30 min, followed by three rinsing steps in Hepes buffer. Proteins are then adsorbed on this anchoring layer, or directly on PS. For LbL deposition method, Fn is adsorbed (1h), followed by Col adsorption (1h), Fn adsorption (1h) and Col adsorption (1h). Between each adsorption step, three rinsing steps in Hepes buffer are performed. It gives PEI/$(Fn/Col)_2$ and $(Fn/Col)_2$ films, abbreviated as **PEI/LbL** and **LbL** film respectively. If adsorption is stopped after the first Fn layer, **PEI/Fn** and **Fn** films are obtained. Finally, simultaneous adsorption is performed by adsorption from a mixed solution of Fn and Col, at 25 µg/ml and 100 µg/ml respectively, during 1h. It gives **PEI/Fn+Col** and **Fn+Col** films. After protein adsorption, the different films are rinsed in water and dried under nitrogen flow before characterization.

For cell culture experiments, film preparation is based on the same protocols except that all the protein solutions are prepared in sterile Hepes buffer, sterilized by filtration on 0.22 µm filters. PEI solution is also sterilized by filtration. All the adsorption steps are performed under laminar flow hood to assure aseptic conditions. At the end of the deposition, films are rinsed in Hepes and are kept immersed under buffer during a few hours or overnight. Then, cells are seeded on the films as detailed hereunder.

2.2. Film characterization

The different methods used to characterize the films are already described in the previous chapter. This section summarizes the main information.

QCM-D monitoring: QCM-D experiments are performed on AT-cut 5 MHz quartz crystals coated with 100 nm of Au from Q-Sense (Gothenburg, Sweden) or Fil-tech (Boston, USA). These crystals are spin-coated with PS as explained above. Q-Sense E4 system (Gothenburg, Sweden) is used to measure changes in resonant frequency (Δf) and dissipation (ΔD). Flow is fixed at 30 µl/min and temperature at 25°C. Between deposition steps of 30 min for PEI and 1h for proteins, a rinsing step of 30 min in Hepes buffer is performed. Results of the 5^{th} overtone are used.

Ellipsometry: Ellipsometry measurements of the film thickness are performed on two types of ellipsometers, a spectroscopic ellipsometer (Uvisel, Horiba-Jobin-Yvon, France) and a single-wave ellipsometer (Horiba-Jobin-Yvon), with no significant difference observed between the ellipsometers. Thickness of the PS layer is measured first and a second measurement is done after protein film deposition. Thickness of the PS layer is then subtracted to obtain the thickness of the protein-based film.

Contact angle measurement: Sessile drop method, with a CDD camera and an image analysis processor (Electronisch Ontwerpbureau De Boer, The Netherlands), is used to measure contact angle. A drop of ultrapure water of 0.3 µl is deposited on the surface and the value is read after 5 s.

Atomic force microscopy: A Nanoscope V multimode microscope (Digital instruments, Santa Barbara, USA) is used to obtained AFM topographic images. Image treatment is performed with the Nanoscope analysis software. A 3^{rd} order flattening is applied to each image.

2.3. Cell culture

Adipose-derived mesenchymal stem cells (AMSC) culture: Cell culture is performed with AMSC provided by Dr. D. Dufrane and P. Palacios (UCL, Belgium). All procedures were approved by the Ethical Committee of the Medical Faculty (Université catholique de Louvain) for tissue procurement (B40320108280). Cells are extracted from the abdominal lipoaspirate of a 39-years-old woman. This lipoaspirate is washed, digested with collagenase, filtered and centrifuged to obtain cells at P0. Passages are performed until P4. At P4, cells are frozen until use. All the experiments are performed with this same batch of cells to avoid experimental variation due to donor or cell population. Thawing of the cells is made a few days before their use. Cells are then expanded in T25 plates until they reach around 80 % confluency. After trypsinisation (Trypsin-Versene (EDTA), 200 mg/ml Versene (EDTA), 170 000U/L Trypsin, Lonza), they are seeded at 2500 cells/ml at P5 in 24-wells plates. 1 ml is added in each well. Wells are aseptically coated with protein films (for Alamar blue assay and differentiation studies) or contain a sterilized PS-coated glass slide with the protein-based films (for fluorescent staining). 24-wells plates directly coated with protein films are made of pure PS (Greiner), without oxidizing treatment. For some controls, or when coated glass slide are used, tissue culture polystyrene (TCPS) multiwall plates are used.

***Culture medium*:** Proliferation medium is Dubelco modified Eagle Medium (4.5 g/L glucose, without glutamine, Lonza) supplemented with 10% fetal bovine serum (certified, heat inactivated, US origin, Life technologies), 1 % antibiotics (Penicillin-Streptomycin, 10K/10K, Lonza), 1 % L-glutamine (0.2mol/L, Lonza) and 0.1 % fungizone (Amphotericin B, 250µg/ml, Lonza). Differentiation medium is prepared from proliferation medium. The addition of 0.05 g/L of sodium ascorbate (Sigma-Aldrich), 1 µM of dexamethasone (Sigma-Aldrich) and 0.35 g/L of sodium dihydrophosphate (Sigma-Aldrich) allows differentiation to be induced [24].

Fluorescent staining: Cell culture is performed on PS-coated glass coverslips, coated with protein films. Uncoated glass coverslips are used as positive

controls and PS-coated glass coverslips, without protein films, as negative control. After 20h and 4 days of culture, cells are fixed for staining as follows. Nuclei, vinculin and actin filaments are stained by DAPI, FITC-antibody and TRITC-phallodin, respectively. Cell layers are washed three times in PBS (Tablet, Gibco, Life technologies, Paisley, UK), are fixed during 30 min in 4 % paraformaldehyde (Sigma-Aldrich), are rinsed three times with PBS and are stored at 4°C in PBS. For the fluorescent staining, cells are washed with a washing buffer (0.05% Tween-20, Sigma-Aldrich), and then permeabilized with 0.1 % TritonX-100 (Sigma-Aldrich) during 5 min. After two washing steps in washing buffer, a blocking solution made of bovine serum albumin (BSA, Sigma-Aldrich) 1 % in PBS, is added during 30 min. The primary antibody, mouse anti-vinculin antibody (FAK100 kit, Millipore), diluted at 5.7 µg/ml in 1 % BSA solution, is then added for 1h. After three washing steps with washing buffer, the secondary antibody, FITC-conjugated goat anti-mouse antibody (Millipore), at 5 µg/ml , mixed in PBS with TRITC-phalloidin (FAK100 kit, Millipore), at 0.6 µg/ml, are added during 1h. After three washing steps in washing buffer, glass coverslips are mounted on glass lamella in an antifading medium containing DAPI (vectashield, Vector lab, UK) and are sealed with nailpolish.

Alamar blue test: Alamar blue is used to measure the metabolic activity of the cells. In a first experiment, it will be used to quantify cell proliferation on the different types of protein-based films designed. Positive and negative controls are thus TCPS and pure PS, respectively. In a second experiment, Alamar blue assay is also used to measure metabolic activity in specific conditions to test PEI cytotoxicity. Specific conditions are first PEI-coated TCPS at 1mg/ml on which cells are seeded. Second specific conditions are cell layers on TCPS put in contact with culture medium containing 2 µg/ml PEI at different moment of the culture (0, 4 and 8 days). Concentration of 2 µg/ml in the medium is chosen because 1 ml of this solution approximately represents the amount of PEI contained in the PEI anchoring layer.

The Alamar blue protocol itself is based on the conversion of non-fluorescent resazurin into fluorescent resorufin by cell metabolic activity. Medium containing 5 % resazurin (in vitro toxicology assay kit, VWR) is put on cells

washed once with PBS. Reaction is performed during 4 h at 37°C. Supernatant is then collected and fluorescence intensity is measured (excitation wavelength: 560 nm - emission wavelength: 590 nm). As the test is nondestructive for the cells, cells are washed two times with PBS at the end of the experiment and fresh medium is added to continue their culture.

Differentiation induction: Differentiation medium is usually added when cells are 100 % confluent. In this work, a compromise had to be found due to the difference of proliferation between the protein films without the anchoring layer (confluence reached 6 -7 days after cells seeding) and films with PEI as well as for TCPS control, for which proliferation is slower. Differentiation was thus induced 9 days after cell seeding. For the differentiation results, time is expressed in days after differentiation induction.

Differentiation characterization: Two main tests were performed to characterize the osteogenic differentiation of AMSC. The first is based on the detection of the **alkaline phosphatase (ALP) activity**, normally produced from the beginning of differentiation phase. This enzyme has the function to degrade pyrophosphates to increase the concentration of phosphate ions [42]. This activity need to be normalized by a value related to the cell number. Proteins concentration, measured by bicinchoninic acid assay (BCA), was used for this normalization. The second test is the staining of mineralized part of the matrix by **Alizarin red** that links calcium to form a red complex. These tests were performed at different time after differentiation induction. Positive controls are cells on TCPS in differentiation medium and negative controls are cells on TCPS in proliferation medium.

Measurement of ALP activity and protein concentration are performed on cell lysate supernatant after differentiation during 14, 21 and 28 days. Cell lysate are obtained by sonication of the cell layers in 500 µl of lysis buffer. The lysis buffer is made of Triton X-100 (Sigma-Aldrich) 1% diluted in PBS buffer with a cocktail of protease inhibitor (1 tablet in 10 ml, Complete, mini, EDTA free, Roche, Sigma-Aldrich). After the lysis, the lysate is centrifuged 10 min at 13 000 rpm. 100 µl of the supernatant is used to determine de total protein amount and is thus mixed to the BCA reactants (Pierce BCA protein assay kit,

ThermoFisher Scientific). Reaction is performed 1h at 60°C and absorbance is read after cooling at 559 nm. Calibration curve is obtained using bovine serum albumin. ALP quantification is also performed on 100 µl of the supernatant (+ 100 µl for the blank) obtained after centrifugation of cell lysate. Reaction with p-nitrophenyl phosphate (pNPP) 10 mM is performed in Tris buffer (SigmaFast, p-nitrophenyl phosphate tablets, Sigma-Aldrich) during 30 min in the dark. Reaction is then stopped with NaOH 3 N. Absorbance, coming from the p-nitrophenol (pNP) produced by the transformation of pNPP by ALP present in the samples, is measured at 405 nm. Blanks values are measured with the same protocol, but NaOH is added in each well before the reaction to block the production of pNP. Blanks are subtracted to each absorbance value. Calibration curve of absorbance depending on the concentration of pNP (sigma-Aldrich) is established to compute the produced pNP concentration.

Alizarin red staining is directly performed on fixed cell layers**.** Cells are rinsed 3 times with PBS, fixed with paraformaldehyde 4% during 30 min and rinsed 3 times with ultrapure water. Alizarin red staining solution (Merck-Millipore) is then added on the cells during 45 min in the dark. Four rinsing steps with water are then performed and PBS is added on the cells. Macroscopic image of the plates are taken as well as image with a binocular and a microscope.

Statistical analysis: Statistical analysis is performed to determine significant differences between the results. Fisher test is used to determine whether the variances are equal between the samples and t-student test are then performed to compare the means. Differences are considered as significant if P-values < 0.05. When several hypothesis tests are performed on the same data set, Bonferroni correction is applied to determine the α to use. When three comparisons are done on the same data set, α of 0.017 is used.

3. Results and discussion

3.1. Film characterization

3.1.1. *In situ monitoring of assembly by QCM-D and stability study*

The building of the films made of Col and Fn is first monitored by QDM-D. Films are studied with or without the anchoring layer and the two deposition methods are compared. These QCM-D results were already described in details in chapter 2. The build-up of two typical films, LbL and PEI/LbL films, is shown as examples in Fig. II.3.1.

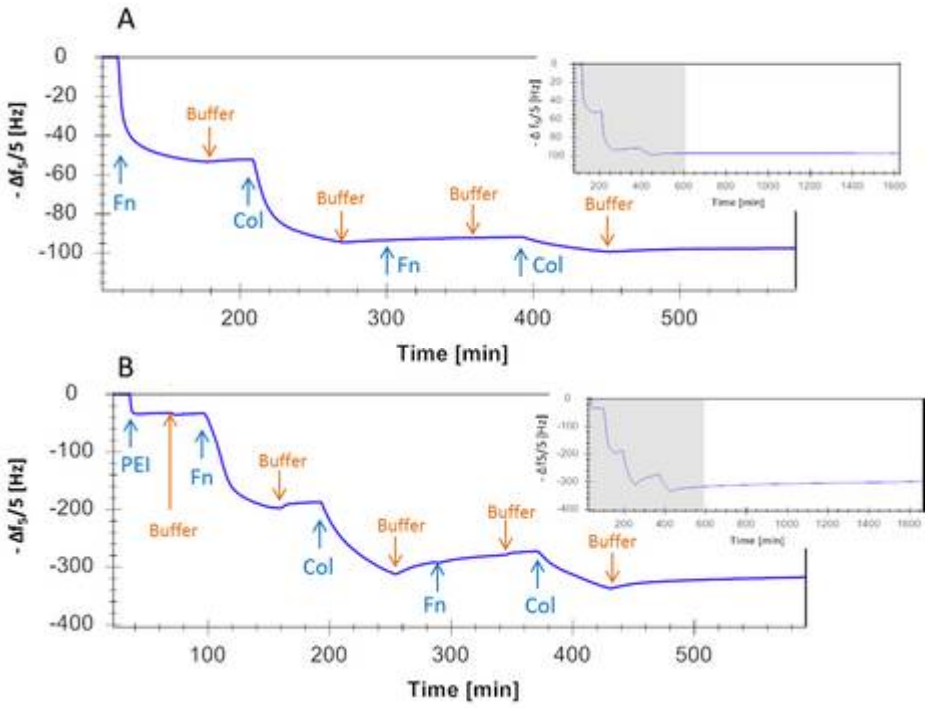

Figure II. 3. 1: QCM-D monitoring of the 5th overtone during building of LbL film (A) and PEI/LbL film (B) in Hepes. Insets represent the complete experiment which includes stability study in the buffer during around 20h after the end of film build-up.

As described in details in chapter 2, the addition of an anchoring layer allows to obtain higher frequency shifts for each deposition method. While the LbL building on pure PS stops after one bilayer, film growth continues for a few more steps with the anchoring layer. Results of the comparison between the deposition methods, not presented in this chapter, show that the frequency shifts measured for simultaneous adsorption are higher than for Fn adsorption alone but lower than for LbL deposition of 3 bilayers. The differences between simultaneous and LbL deposition are however quite small.

The stability of the different films: Fn, Fn+Col, LbL, PEI/Fn, PEI/(Fn+Col) and PEI/LbL is also monitored by QCM. Results are shown in Fig. II.3.1 for LbL and PEI/LbL films only but are the same for the other deposition method. The frequency shift measured at the end of film deposition stay constant during 20h. It proves that the assemblies are stable under buffer.

3.1.2. Measurement of dry thickness and water contact angle

Dry thickness measurements are presented in Fig. II.3.2. The PEI anchoring layer allows to obtain a thicker film and a more regular building of the layers. It seems that three distinct protein layers can be assembled on the PS substrate. Saturation is reached after the third layer, at a thickness of around 10 nm. Interestingly, the same thickness is also reached by simultaneous adsorption of Fn and Col during only 1h. Without the anchoring layer, thickness stabilizes around 4 nm for LbL assembly as well as for simultaneous adsorption.

Contact angle measurements, also presented in Fig. II.3.2, show a slight saw-tooth profile. This saw-tooth profile is characteristic of true LbL assemblies because it proves that the chemistry of the surface changes with the last deposited layer. It should be noted that Fn and Col layers adsorbed alone have different contact angles. Fn on PS and on PEI-coated PS has a contact angle of 71.5° and 76.5°, respectively. Col on PS and on PEI-coated PS has a contact angle of 36° and 37.5°, respectively. If there is an enrichment of one of these proteins depending on the last deposited layer, it could explain the saw-tooth profile. In these results, the saw-tooth profile is clearly more present for films

with a PEI anchoring layer. Besides, contact angles measured after simultaneous adsorption are smaller than after LbL deposition. It is particularly the case on films with the anchoring layer. The contact angles for simultaneous adsorption are both closer to the value measured for Col adsorption alone.

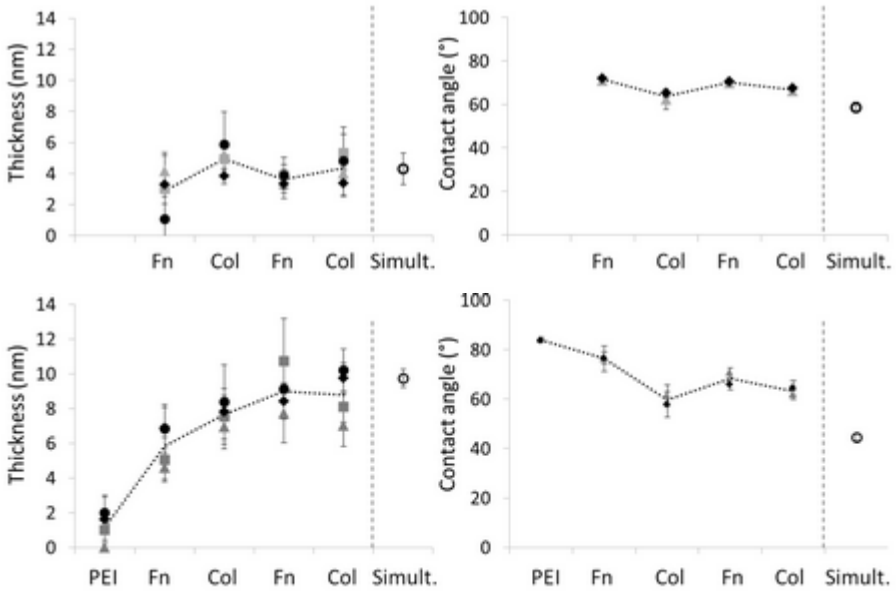

Figure II. 3. 2: Ellipsometry measurement of the dry thickness (left) and water contact angle measurements (right) after each adsorption step. A PEI anchoring layer was used (bottom) or not (top). Ellipsometry graphs show four repetitions for each step. Symbols with the same color (black or grey) refer to samples prepared the same day, with the same solutions and in the same conditions. Samples denoted by a different color (black or grey) were prepared on different days. Each repetition has its own error bar representing standard deviation (n ≥ 3, on the same sample). Contact angle measurement graphs show two repetitions, realized on different days. Each repetition has its own error bar representing standard deviation (n ≥ 5, on the same sample). The open circles represent the thickness or the contact angle measured after simultaneous adsorption from a mixed Fn+Col solution, on PS or on PEI-treated PS (for films with an anchoring layer). Error bars represent standard deviation (n = 4) for thickness and the difference between the two measurements for contact angle (n = 2).

3.1.3. Film morphology

Different types of films are studied by AFM: films obtained after Fn adsorption alone, films built by simultaneous Col and Fn adsorption and films built by LbL deposition. AFM images are presented in Fig. II.3.3. Films with a PEI anchoring layer are rougher than films without anchoring layer. This roughness comes from the PEI layer that forms kind of aggregates at the surface, as already shown in the previous chapter. Moreover, morphology of the films depends on the film type. First, without the anchoring layer, film made of Fn only is very smooth compared to the other films. Second, films obtained by simultaneous adsorption generally present more Col fibrils than by LbL deposition. This was already reported in the previous chapter.

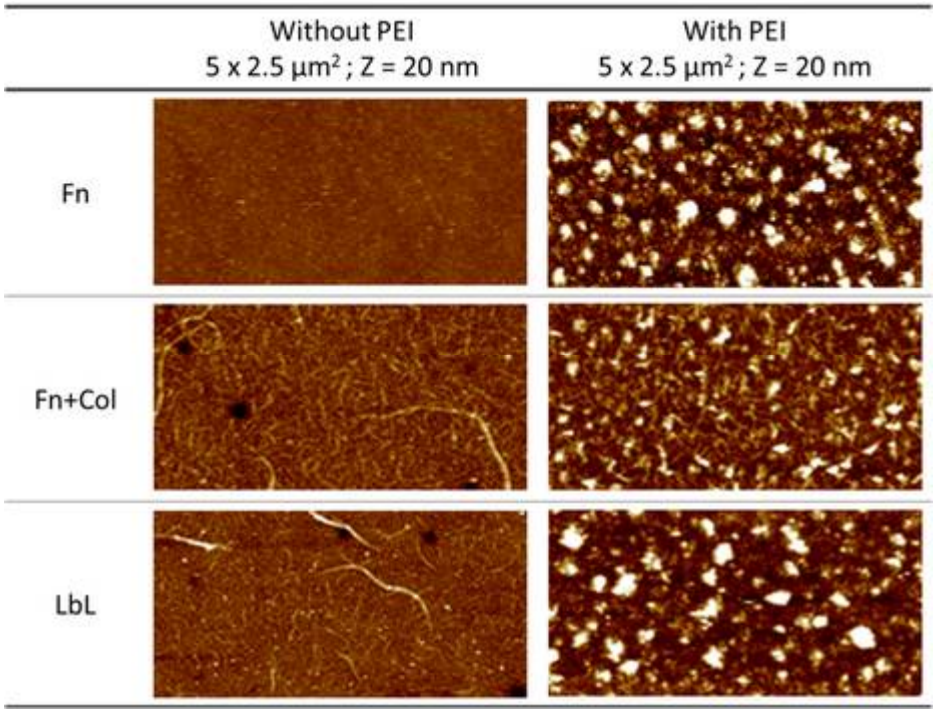

Figure II. 3. 3: AFM height images of films prepared from Hepes buffer for different types of assemblies (Fn alone, simultaneous adsorption and LbL deposition) on PS or on PEI-coated PS. Image size is 5 X 2.5 µm² and Z-scale = 20 nm.

3.1.4. Impact of the anchoring layer and of the deposition method

In this chapter, a first comparison is made between films built on a PEI anchoring layer or not. The results show that this layer has an influence on the films. Firstly, the use of PEI anchoring layer allows to obtain thicker films, a more regular assembly and a more visible saw-tooth profile for contact angles (Fig. II.3.2, right). This film formation is thus closer to a true LbL construction compared to films without the anchoring layer. Secondly, the PEI anchoring layer changes the film morphology, giving rougher films.

A second comparison is made between the two different methods of adsorption. Simultaneous adsorption gives films with at least the same thickness as films made of four protein layers deposited by LbL method. Moreover, water contact angles measured after simultaneous adsorption are lower. Finally, film morphology is different, with more fibrils detected for simultaneous deposition. These two last differences, *ie* related to morphology and contact angle value, seem to show than Col adsorbs more than Fn when simultaneous adsorption is performed. This is especially true for PEI/Fn+Col film because fibrils are more visible and contact angle is very close to the one of a single Col layer.

3.2. Study of cell behavior

Cell behavior is studied on the six different types of films characterized above: Fn, Fn+Col and LbL films, without or with a PEI anchoring layer. Adhesion and proliferation will be first studied. Thereafter, osteogenic differentiation will be triggered and assessed.

3.2.1. Fluorescent imaging of AMSC: Adhesion and proliferation

A fluorescent cell staining was performed with DAPI for nucleus, phalloïdine for actin filaments and antibodies for vinculin, after 20h and 4 days of culture. Observation of cell morphology shows well spread cells, with a star shape, for almost all conditions, even after 20h. Examples are shown in Fig. II.3.4. No

significant differences of morphologies can be highlighted depending on the conditions and time.

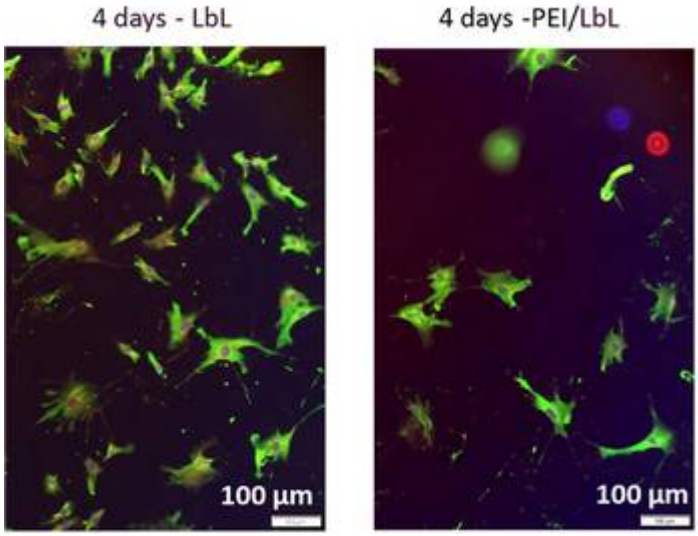

Figure II. 3. 4: Examples of the fluorescent images (1.1 x 0.7 mm2) are shown for the film obtained by LbL deposition method, after 4 days of culture. Vinculin, actin filaments and nuclei are respectively stained in green, red and blue.

Besides morphology observation, cell staining allows also cell counting as presented in Fig. II.3.5. After 20h of culture, cell number is almost the same for each condition, except for the control samples which show a lower cell density. Cells adhesion is thus almost the same on the different types of modified surfaces. After 4 days, some differences appear depending on the conditions. On PS control and on a pure PEI layer (no protein added), there are only a few cells after 4 days. On PS, this is probably due to a lack of initial adhesion. On PEI, cells adhered after 20h but cell number decreased thereafter. PEI alone does thus not support cell adhesion. Moreover, even if cell number generally increases between 20 h and 4 days for the protein films on PEI, cell growth is slowed for the conditions with this anchoring layer compared to films prepared without PEI. The number of cells obtained after 4 days for Fn or LbL is significantly higher than for PEI/Fn or PEI/LbL respectively, with unilateral p-value of 0.013 and 0.002 < 0.017. The same trend exists for Fn+Col and

PEI/Fn+Col but the difference is not significant (unilateral p-value 0.047 > 0.017). This lower cell number after 4 days on the protein films built on a PEI anchoring layer could be due to a cytotoxic effect of PEI.

Finally, an interesting observation on Fig.II.3.5 is that cell proliferation on glass is very high. It comes probably from a proper adsorption on glass of adhesion biomolecules from the medium or secreted by cells, these proteins being in configuration and high amount.

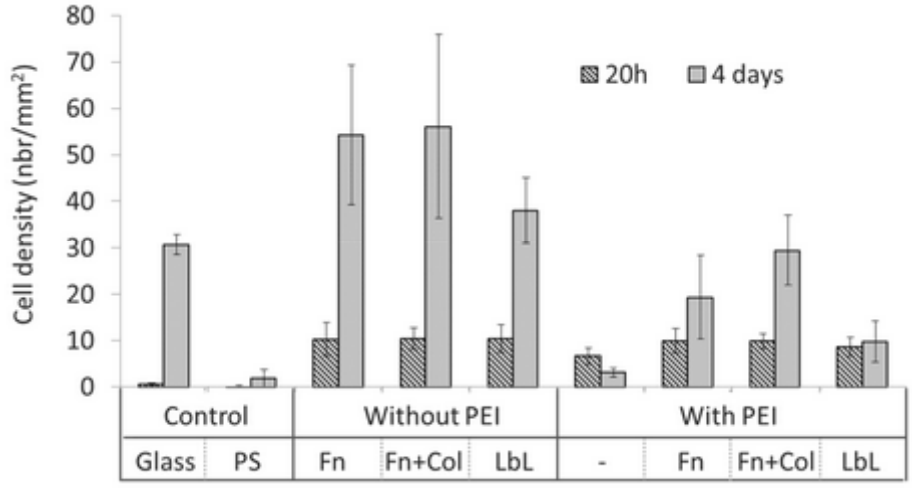

Figure II. 3. 5: Cell density after 20h and 4 days on different surfaces. Cell density is measured by counting cells after fluorescent staining and imaging. Glass is the positive control, PS the negative control. Error bars represent standard deviation.

3.2.2. Measurement of AMSC metabolic activity by Alamar blue assay

Alamar blue assay allows the metabolic activity of the cells to be measured. This value is directly linked to cell number if the cells have the same metabolic activity in each condition and at each moment, which is not always the case. A calibration curve was established to compute the metabolic activity in function of cell number in suspension (Fig. II.3.6). This curve shows that there is a linear correlation between the metabolic activity and the cell number. However, the curve was made with a number of cells in suspension at a specific moment, just

after trypsinisation, not representative of adhesive cells. Use this calibration curve to interpret the data must thus be done with caution. Here, total metabolic activity, expressed by the fluorescent units measured by alamar blue assay, will be use to evaluate cell growth.

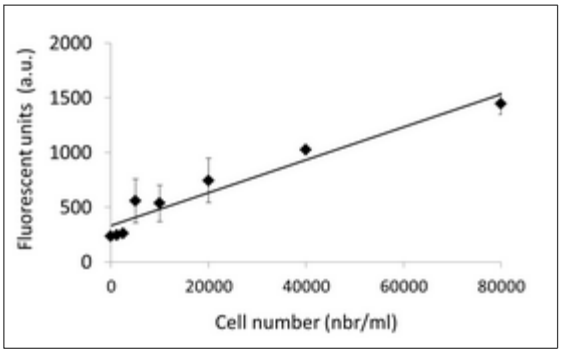

Figure II. 3. 6: Metabolic activity of AMSC in suspension measured by Alamar blue assay. Fluorescence measured after the reaction is correlated to on cell number, as highlighted by the linear fit.

The results of metabolic activity evolution with culture time are presented in Fig. II.3.7. Results after 2 days are not taken into account because they are too close to the blank value. Effects of deposition method (simultaneous adsorption vs LbL) are not observed in these results but the negative effect of PEI on the cell proliferation in the beginning of the growth phase is confirmed. Metabolic activity is indeed lower for films with an anchoring layer, compared to the films without anchoring layer, after 4, 6 and 8 days. Statistical analysis are performed to check if cell metabolic activities with or without PEI anchoring layer present significant differences. The results are presented in Table II.3.1. The differences after 4 days are non-significant. After 6 and 8 days however, differences are significant, except for 8 days LbL. However, p-value is very close to the exclusion α value.

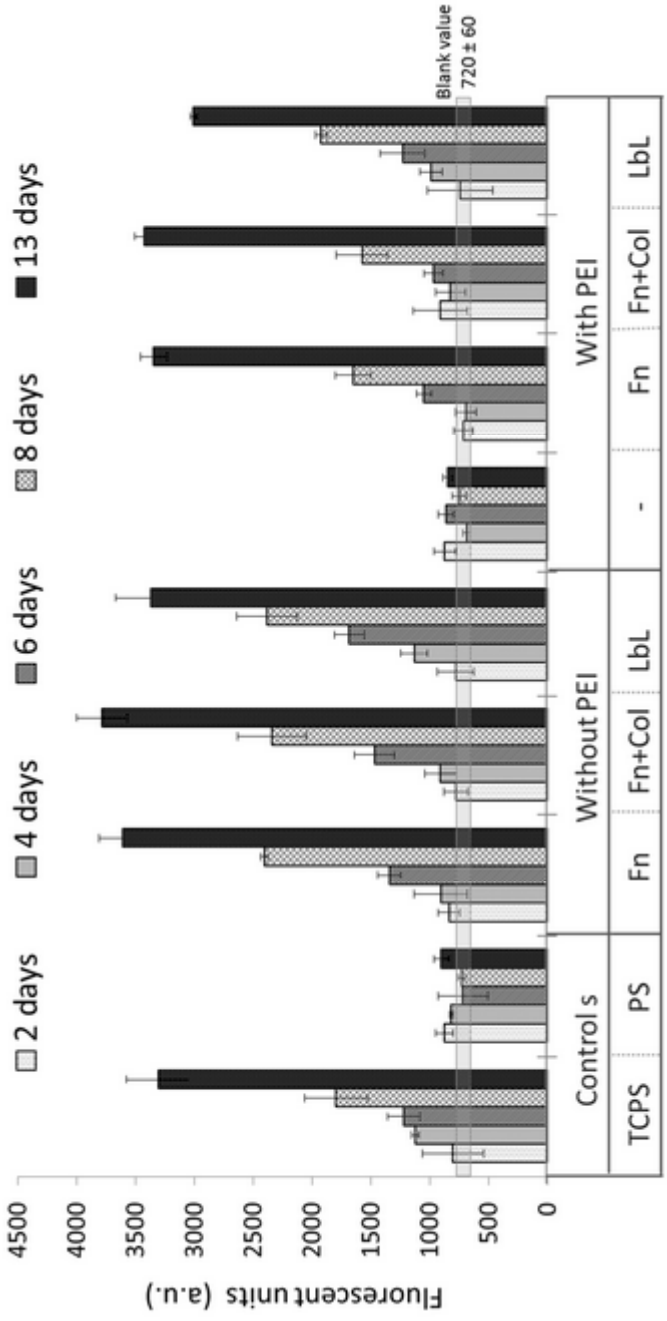

Figure II. 3. 7: Metabolic activity of the AMSC after different days of culture measured by Alamar blue assay on the different film types. Positive control is TCPS, negative control is pure PS. Error bars represent the standard deviation. The transparent bar represents the confidence interval at 95% of the blank (culture medium without cells).

Nevertheless, after 13 days, the metabolic activity reaches almost the same level with and without PEI. Conditions with PEI after 13 days do not present a lower metabolic activity than without PEI according to the statistical analysis. It shows that PEI is probably cytotoxic in the beginning of growth but that this negative effect disappears later. Different hypothesis can explain this behavior. First, a degradation of the film followed by the release of PEI molecules can be evoked. After 13 days, all PEI would have disappeared, as well as its cytotoxic effect. Another hypothesis would be that the PEI anchoring layer could be completely buried by proteins secreted during growth. Finally, cell resistance to PEI could appear later in the growth phase and explain the observed results. The next section will present attempts to clarify these hypotheses.

Table II. 3. 1: Statistical analysis of metabolic activity depending on the presence of the anchoring layer. Unilateral p-values are summarized in the table for statistical test to prove that fluorescence for condition without PEI > fluorescence condition with PEI. If p-value is <0.017, the difference is significant, as indicated by *.

Days	Fn vs PEI/Fn	Fn+Col vs PEI/Fn+Col	LbL vs PEI/LbL
4	0.101	0.230	0.084
6	0.006*	0.005*	0.014*
8	0.001*	0.011*	0.019
13	0.060	0.028	0.084

3.2.3. Effect of PEI addition at different time of culture

This test is performed to better understand the influence of PEI on the cells. Different conditions were tested on TCPS used here as a substate. Positive control for the study is nude TCPS. The first condition is adsorbed PEI to mimic the anchoring layer used in the protein films. As shown in Fig. II.3.8, this layer is cytotoxic for the cells and stops cell growth.

The second condition tested is PEI in solution in the culture medium at 2 µg/ml. This concentration was chosen to be representative of the amount of PEI that would be released in solution if the total amount of PEI contained in the anchoring layer would be desorbed. In one case, the culture is performed from the beginning in PEI containing medium. In other cases, culture is performed in

normal culture medium until PEI containing culture medium is used after 4 days or 8 days. If PEI is directly added in the culture medium, the cell growth stops as for adsorbed PEI. If medium with PEI is used 4 days after the beginning of growth, metabolic activity continues to increase with time but not as fast as for the control. If medium with PEI is used 8 days after the beginning of growth, there is no statistical influence on metabolic activity compared to the control after 13 days (p-value = 0.087).

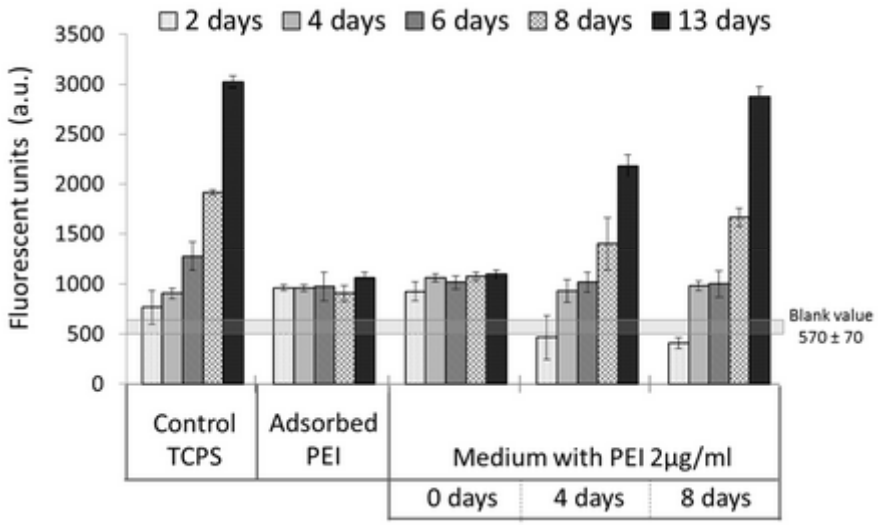

Figure II. 3. 8: Metabolic activity of the AMSC after different time in culture measured by Alamar blue assay on TCPS. Positive control is nude TCPS with cell culture performed in classical culture medium. This control is compared to PEI-coated TCPS. The control is also compare to culture realized on TCPS, in medium containing 2 µg/ml of PEI. This medium supplemented with PEI is used directly after cell seeding or 4 and 8 days after cells seeding. Error bars represent the standard deviation. The transparent bar represents the confidence interval at 95% of the blank (culture medium without cells).

3.2.4. PEI cytotoxicity analysis

It is clearly observed that the PEI anchoring layer decreases proliferation in the beginning of growth. In fact, PEI layer was already shown to be deleterious for cells. For example, Brunot et al. have shown that a deposited PEI layer on titanium or nickel-titanium alloy samples decreases adhesion and proliferation of cells [43].

PEI can be used as a carrier for gene delivery in cells and study of its cytotoxicity is often performed in this application . As shown by Ahn et al. [44], PEI can combine with DNA and these complexes can be used for transfection of AMSC. They are not toxic except if the PEI/DNA ratio increases because free PEI can be released from the complexes and disrupt the negatively charged membranes. This information can thus be transposed to the observation of this work. If adsorbed PEI molecules are released from the films, they can be cytotoxic for the cells. In the context of gene transfer, Moghimi et al. [45] have studied PEI cytotoxicity in more details. They have shown that cytotoxicity of PEI is divided in two phases. The first phase, after 30 min, is perturbation of the cell membrane, characterized by an increased phosphatidylserine exposure at the outside of the cells. A second phase, after 24h, is characterized by the activation of a “mitochondrially-mediated apoptotic program”. Effect of PEI on the cells is already observed at a concentration of 0.1 µg/ml.

In this work, an investigation of PEI toxicity was made. The aim is to understand why PEI influences proliferation only in the beginning of growth. Different answers can be found based on the results of Fig. II.3.8. First, when PEI is adsorbed on TCPS, its cytotoxicity prevents cell growth even after 13 days. It is not the case with proteins films on PEI-coated PS (Fig. II.3.7). The protein films thus probably preserve the cells of a too high cytotoxicity of PEI. This allows cell growth to happen, even if growth is slower than without a PEI anchoring layer. A second interesting fact is that cell behavior is less affected by addition of PEI in the medium at the end of the growth phase. Indeed, if culture medium with PEI is added after 4 days and 8 days, the toxic influence of PEI is less and less visible compared to the use of culture medium with PEI since the beginning of the growth phase. It is probably because the PEI amount becomes too low compared to the cell number.

Based on these considerations, a hypothesis can be formulated to explain the results of Fig. II.3.7. The hypothesis is that the PEI anchoring layer is cytotoxic for the cells. However, the protein films (Fn, Fn+Col or LbL) deposited on the anchoring layer protect the cells from this cytotoxic effect. The proliferation is thus slowed down but does not completely stop. Owing to proliferation, there

are more and more cells and the ratio PEI/cells number decreases. Moreover, some degradation and/or covering with secreted molecules of PEI anchoring layer also help to decrease the amount of PEI in contact with the cells. Global cytotoxicity of the anchoring layer thus decreases with culture time.

3.2.5. Osteogenic differentiation study

Cell density determined by protein amount: After cell proliferation on the films, osteogenic medium is used to induce cell differentiation, except on negative control. The total amount of protein present in the cell lysate is measured 14, 21 and 28 days after the induction of cell differentiation. Results are presented in Fig. II.3.9. The total protein content can be linked to the total cell activity. It is difficult to know if it can be linked to cell density because activity of each cell probably changes during differentiation. It is thus impossible to know if an increased protein amount is due to an increased cell activity or to an increased number of cells.

Firstly, results show that the protein amount is higher on PS coated with protein films compared to the controls realized on TCPS. Second, they show that the positive and negative control give very similar results. The difference after 14 days is significant but not after 21 or 28 days (p-values of 0.005, 0.209 and 0.421 respectively). The total protein amount thus does not change, whether cell differentiation is induced (differentiation medium, positive control) or not (proliferation medium, negative control). Then, they show that there is always a slight increase in protein content with time during differentiation but this increase is very slow. And finally, results show that there is no influence of PEI anchoring layer or of deposition method on protein amount after differentiation induction.

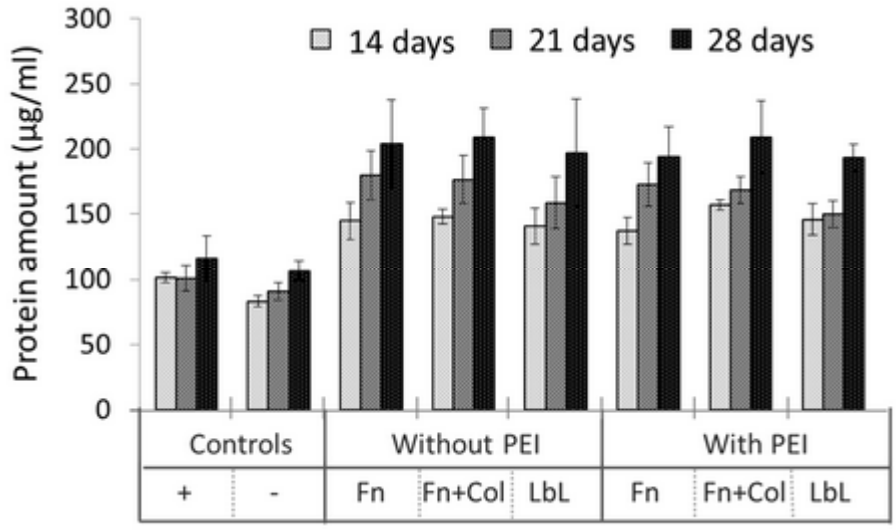

Figure II. 3. 9: Total protein amount in µg/ml measured by BCA test on cell lysates after differentiation during 14, 21 ad 28 days. Positive controls are cells on TCPS in differentiation medium and negative controls are cells on TCPS in proliferation medium. Error bars are standard deviation (n = 3).

Alizarin red staining: Alizarin red is used to stain the mineralized part of the matrix, characteristic of the osteogenic differentiation of cells. As shown in Fig. II.3.10, that presents macroscopic images of films, the positive control already presents a well differentiated state after 21 days. For the protein films, 28 days are needed to observe matrix mineralization. Even after 28 days, matrix mineralization is less marked than for the positive control.

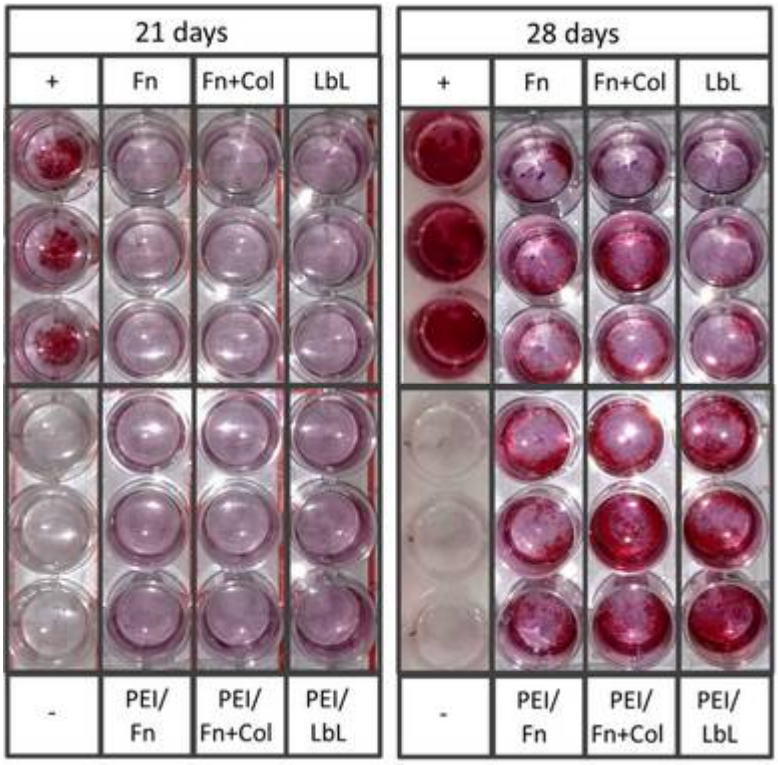

Figure II. 3. 10: Macroscopic images of alizarin red staining for the different films

To better observe the differences between the different types of film, images obtained with binocular and microscope are used. Fig. II.3.11 shows these images. Binocular images allow to obtain a global image of each well and microscope image allow to zoom on some part of the film. On each picture, red staining of the matrix can be observed clearly. Thanks to image treatment software, the percentage of the red fraction of each sample area, equivalent to the mineralization level of each sample, can be determined. The results are presented in Table II.3.2. Here, the impact of the film deposition method can be observed. For films without PEI, LbL deposition method gives a significantly less advanced differentiation compared to films with only Fn or simultaneous adsorption of Fn and Col. These results also show that the PEI anchoring layer improves differentiation of the AMSC in each case.

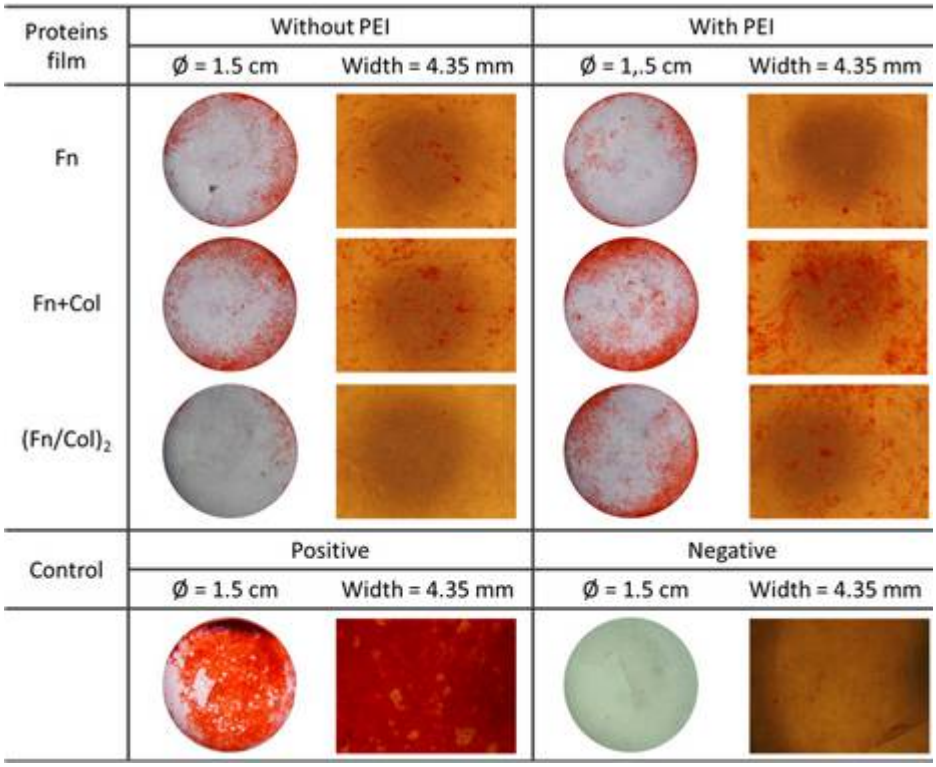

Figure II. 3. 11: Binocular and microscope images of alizarin red staining for the different films

Table II. 3. 2: Percentage of mineralization by alizarin red staining of the films obtained by image treatment of binocular images with ImageJ software.

	Without PEI % red color (s.d.)	With PEI % red color (s.d.)
Fn	14 (3)	17 (3)
Fn+Col	15 (9)	21 (5)
LbL	4 (3)	19 (3)

***Measurement of alkaline phosphatase activity*:** ALP activity was measured on different days after osteogenic induction. Results are presented in Fig. II.3.12. An unexpected behavior is observed for the controls given that the positive control gives a lower signal than the negative control. Yet, alizarin red staining

proves that there is cell differentiation in all cases except for negative control. The results are thus very difficult to explain.

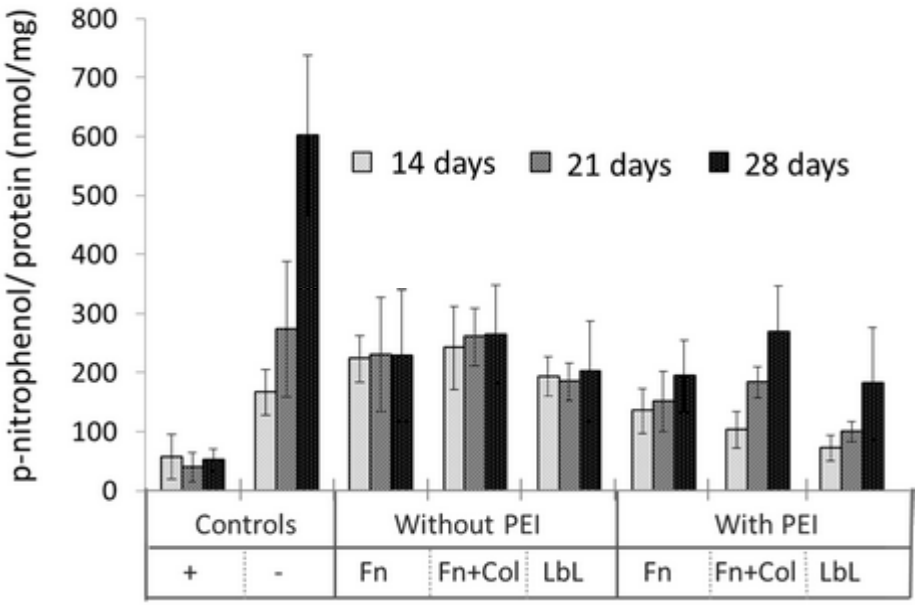

Figure II. 3. 12: Alkaline phosphatase activity measured by colorimetric assay. The assay is based on the transformation of p-nitrophenol phosphate in p-nitrophenol. The results are reported to total amount of proteins in each sample measured by BCA test.

A first hypothesis is that 14 days is already too late to measure ALP activity. ALP is indeed normally produced from the beginning of the differentiation phase. Measurements were thus also performed after 7 days to check if the activity peak was missed. Results however gave lower values than after 14 days for each type of film and this hypothesis is thus not confirmed. A second hypothesis is that the ALP enzyme is denatured or degraded during the lysis process. The measurements could thus be very low compared to normal values and only reveal the noise related to the measurement. Comparison is thus made with literature. Kim et al. [46], who worked on osteoblast (MG-63) differentiation on a fibrin network in a collagen sponge, have measured an ALP activity of 0.1 to 1.2 nmol pNP/mg protein in 30 min. However, Jain et al. [47], who worked on mesenchymal stem cell osteogenic differentiation on a

composite scaffold, have measured between 2 and 20 µmol pNP/min/mg protein, equal to 60 000 to 600 000 nmol pNP/mg protein in 30 min. The values in literature are thus completely different, very low or very high compared to the data of this paper.

Because of the weirdness of the ALP results, they will not be taken into account to discuss the effect of the film on differentiation.

3.2.6. Summary of the impact of the PEI anchoring layer and of the protein deposition method on cell behavior

Influence of PEI on cell behavior: The results obtained in this study show that even if the PEI anchoring layer slows down proliferation, it increases cell differentiation. Two hypotheses can be formulated to explain the results.

The first one is based on the proliferation data: a decreased proliferation may have a positive impact on cell differentiation. The effect can be directly linked to changes of metabolism, which can favor differentiation. It can also be linked to the lower number of cells on the surface when differentiation is induced. As explained in materials and method, differentiation medium is added on each film type a few days after 100% confluency was reached on the films without a PEI anchoring layer. At this point, films with a PEI anchoring layer and controls are not yet confluent. It would mean that inducing differentiation before total confluence is reached would be benificial.

A second hypothesis is based on the film morphology. Films with the anchoring layer are rougher. Even if this roughness is very small (nm range) compared to etched titanium implant generally studied (µm range), it could improve cell differentiation as it is the case in the study of Lossdörfer et al. [1] in which micro-roughness allows to increase osteoblast differentiation. In fact, roughness can influence cell behavior because it can change the protein recognition by integrins. Depending on how proteins are organized, which depends on roughness, integrin clustering can be altered and focal adhesion

organization can vary. Signals transmitted to the cell nucleus can thus be modified.

Influence of the protein deposition method on cell behavior: The influence of the protein deposition method is unfortunately not visible on adhesion and proliferation data. However, for the films without anchoring layer, there is an influence of the deposition method on differentiation. Films constructed by simultaneous adsorption lead to better differentiation than film built by LbL. It proves that proteins organization at an interface can change cell behavior. Unfortunately, more experiments are needed to understand better why in this specific case.

4. Conclusion

In this chapter, the aim was to compare different kinds of interfacial assemblies made of Fn and Col to study their physico-chemical properties and the cell response to these properties. The results show that the anchoring layer of PEI improves the LbL building of the films. It allows more regular and thicker LbL films to be obtained. It also changes the morphologic properties of the films, giving rougher surfaces. Moreover, physico-chemical characterization also shows that the protein deposition method influences surface properties. Surfaces obtained by simultaneous adsorption have a lower contact angle and a morphology with more Col fibrils. In a second part of the work, cell behavior is studied. Results mainly show that the PEI anchoring layer slows down the proliferation rate. But after 13 days of culture, metabolic activity reaches the same level for each type of protein film. Interestingly, differentiation is improved by this PEI anchoring layer. Differentiation is also influenced by the deposition method, with LbL deposition method giving a less advanced differentiation compared to simultaneous deposition when a PEI anchoring layer is not used. We thus show that the nature of molecules present in the film and their organization both influence cell behavior. This kind of interfaces can be of interest to improve *in vitro* differentiation of cells in view of biomedical applications.

Acknowledgment

Thanks to Dr D. Dufrane and Dr. P. Palacios for providing the AMSC and to Dr. P. Palacios for her help and advices in cell culture experiments.

References

1. Lossdörfer, S., et al., *Microrough implant surface topographies increase osteogenesis by reducing osteoclast formation and activity.* Journal of Biomedical Materials Research - Part A, 2004. **70**(3): p. 361-369.
2. Charest, J.L., A.J. García, and W.P. King, *Myoblast alignment and differentiation on cell culture substrates with microscale topography and model chemistries.* Biomaterials, 2007. **28**(13): p. 2202-2210.
3. Dalby, M.J., et al., *Nucleus alignment and cell signaling in fibroblasts: Response to a micro-grooved topography.* Experimental Cell Research, 2003. **284**(2): p. 274-282.
4. Janson, I.A. and A.J. Putnam, *Extracellular matrix elasticity and topography: Material-based cues that affect cell function via conserved mechanisms.* Journal of Biomedical Materials Research - Part A, 2014.
5. Engler, A.J., et al., *Matrix Elasticity Directs Stem Cell Lineage Specification.* Cell, 2006. **126**(4): p. 677-689.
6. Degand, S., B. Knoops, and C.C. Dupont-Gillain, *Design and characterization of surfaces presenting mechanical nanoheterogeneities for a better control of cell-material interactions.* Colloids and Surfaces A: Physicochemical and Engineering Aspects, 2014. **442**: p. 164-172.
7. Almodóvar, J., et al., *Gradients of physical and biochemical cues on polyelectrolyte multilayer films generated via microfluidics.* Lab on a Chip - Miniaturisation for Chemistry and Biology, 2013. **13**(8): p. 1562-1570.
8. Lin, M., et al., *Adsorption Force of Fibronectin on Various Surface Chemistries and Its Vital Role in Osteoblast Adhesion.* Biomacromolecules, 2015. **16**(3): p. 973-984.
9. Alberts, B., et al., *Molecular Biology of The Cell*. 5th ed. 2008, New-York: Garland Sciences.
10. von der Mark, K. and J. Park, *Engineering biocompatible implant surfaces: Part II: Cellular recognition of biomaterial surfaces: Lessons*

from cell–matrix interactions. Progress in Materials Science, 2013. **58**(3): p. 327-381.
11. Giliberti, D.C., K.K. White, and K.C. Dee, *Control of cell-biomaterial interactions*, in *Polymeric Biomaterials*, S. Dumitriu, Editor. 2002, Marcel Dekker: New-York. p. 361-375
12. Piez, K.A., *Collagen*, in *Encyclopedia of polymer sciences and engineering*, J. Kroschwitz, Editor. 1985, Willey: New-York. p. 699-727.
13. Beckman, M.J., K.J. Shields, and R.F. Diegelmann, *Collagen*, in *Encyclopedia of biomaterials and biomedical engineering*, G.E. Wnek and G.L. Bowlin, Editors. 2004, Marcel Dekker: New-York p. 324-334.
14. Hamaia, S. and R.W. Farndale, *Integrin recognition motifs in the human collagens*, in *Advances in Experimental Medicine and Biology*2014. p. 127-142.
15. Engel, J., et al., *Shapes, domain organizations and flexibility of laminin and fibronectin, two multifunctional proteins of the extracellular matrix.* Journal of Molecular Biology, 1981. **150**(1): p. 97-120.
16. Pankov, R. and K.M. Yamada, *Fibronectin at a glance.* Journal of Cell Science, 2002. **115**(20): p. 3861-3863.
17. Aumailley, M. and B. Gayraud, *Structure and biological activity of the extracellular matrix.* Journal of Molecular Medicine, 1998. **76**(3-4): p. 253-265.
18. Ingham, K.C., R. Landwehr, and J. Engel, *Interaction of fibronectin with C1q and collagen.* European Journal of Biochemistry, 1985. **148**(2): p. 219-224.
19. Redick, S.D., et al., *Defining Fibronectin's Cell Adhesion Synergy Site by Site-Directed Mutagenesis.* The Journal of Cell Biology, 2000. **149**(2): p. 521-527.
20. Akiyama, S.K., K. Olden, and K.M. Yamada, *Fibronectin and integrins in invasion and metastasis.* Cancer and Metastasis Reviews, 1995. **14**(3): p. 173-189.
21. DiMarino, A.M., A.I. Caplan, and T.L. Bonfield, *Mesenchymal Stem Cells in Tissue Repair.* Frontiers in Immunology, 2013. **4**.
22. Mizuno, H., M. Tobita, and A.C. Uysal, *Concise review: Adipose-derived stem cells as a novel tool for future regenerative medicine.* Stem Cells, 2012. **30**(5): p. 804-810.

23. Schubert, T., et al., *The enhanced performance of bone allografts using osteogenic-differentiated adipose-derived mesenchymal stem cells.* Biomaterials, 2011. **32**(34): p. 8880-8891.
24. Schubert, T., et al., *Critical size bone defect reconstruction by an autologous 3D osteogenic-like tissue derived from differentiated adipose MSCs.* Biomaterials, 2013. **34**(18): p. 4428-4438.
25. Li, W., et al., *Natural Polyelectrolyte Self-Assembled Multilayers Based on Collagen and Alginate: Stability and Cytocompatibility.* Biomacromolecules, 2013. **14**(8): p. 2647-2656.
26. Lin, Q., et al., *Heparin/collagen multilayer as a thromboresistant and endothelial favorable coating for intravascular stent.* Journal of Biomedical Materials Research - Part A, 2011. **96**(1): p. 132-141.
27. Chen, J., et al., *Collagen/heparin coating on titanium surface improves the biocompatibility of titanium applied as a blood-contacting biomaterial.* Journal of Biomedical Materials Research - Part A, 2010. **95**(2): p. 341-349.
28. Chou, C.C., H.J. Zeng, and C.H. Yeh, *Blood compatibility and adhesion of collagen/heparin multilayers coated on two titanium surfaces by a layer-by-layer technique.* Thin Solid Films, 2013.
29. Mhanna, R.F., J. VörÖs, and M. Zenobi-Wong, *Layer-by-layer films made from extracellular matrix macromolecules on silicone substrates.* Biomacromolecules, 2011. **12**(3): p. 609-616.
30. Johansson, J.Å., et al., *Build-up of collagen and hyaluronic acid polyelectrolyte multilayers.* Biomacromolecules, 2005. **6**(3): p. 1353-1359.
31. Zhang, J., et al., *Natural polyelectrolyte films based on layer-by layer deposition of collagen and hyaluronic acid.* Biomaterials, 2005. **26**(16): p. 3353-3361.
32. Landoulsi, J., S. Demoustier-Champagne, and C. Dupont-Gillain, *Self-assembled multilayers based on native or denatured collagen: Mechanism and synthesis of size-controlled nanotubes.* Soft Matter, 2011. **7**(7): p. 3337-3347.
33. Li, X., et al., *The responses of preosteoblasts to collagen/hyaluronic acid polyelectrolyte multilayer coating on titanium.* Polymers for Advanced Technologies, 2012. **23**(4): p. 756-764.
34. Nishiguchi, A., M. Matsusaki, and M. Akashi, *Cell-cell crosslinking by bio-molecular recognition of heparin-based layer-by-layer nanofilms.* Macromolecular Bioscience, 2015. **15**(3): p. 312-317.

35. Ai, H., et al., *Biocompatibility of layer-by-layer self-assembled nanofilm on silicone rubber for neurons.* Journal of Neuroscience Methods, 2003. **128**(1-2): p. 1-8.
36. Li, G., P. Yang, and N. Huang. *Layer-by-layer construction of the heparin/fibronectin coatings on titanium surface:Stability and functionality*. in *Physics Procedia*. 2011.
37. Matsusaki, M., et al., *Fabrication of cellular multilayers with nanometer-sized extracellular matrix films.* Angewandte Chemie - International Edition, 2007. **46**(25): p. 4689-4692.
38. Kadowaki, K., M. Matsusaki, and M. Akashi, *Control of cell surface and functions by layer-by-layer nanofilms.* Langmuir, 2010. **26**(8): p. 5670-5678.
39. Matsuzawa, A., M. Matsusaki, and M. Akashi, *Effectiveness of nanometer-sized extracellular matrix layer-by-layer assembled films for a cell membrane coating protecting cells from physical stress.* Langmuir, 2013. **29**(24): p. 7362-7368.
40. Uchida, N., et al., *Nanometer-sized extracellular matrix coating on polymer-based scaffold for tissue engineering applications.* Journal of Biomedical Materials Research - Part A, 2015.
41. Matsusaki, M., et al., *Layer-by-layer assembly through weak interactions and their biomedical applications.* Advanced Materials, 2012. **24**(4): p. 454-474.
42. Marie, P., *Différenciation, fonction et contrôle de l'ostéoblaste.* Medecine sciences, 2001. **17**(12): p. 1252-1259.
43. Brunot, C., et al., *Cytotoxicity of polyethyleneimine (PEI), precursor base layer of polyelectrolyte multilayer films.* Biomaterials, 2007. **28**(4): p. 632-640.
44. Ahn, H.H., et al., *Polyethyleneimine-mediated gene delivery into human adipose derived stem cells.* Biomaterials, 2008. **29**(15): p. 2415-2422.
45. Moghimi, S.M., et al., *A two-stage poly(ethylenimine)-mediated cytotoxicity: Implications for gene transfer/therapy.* Molecular Therapy, 2005. **11**(6): p. 990-995.
46. Kim, B.S., J.S. Kim, and J. Lee, *Improvements of osteoblast adhesion, proliferation, and differentiation in vitro via fibrin network formation in collagen sponge scaffold.* J Biomed Mater Res A, 2013. **101**(9): p. 2661-6.

47. Jain, K.G., et al., *Culture & differentiation of mesenchymal stem cell into osteoblast on degradable biomedical composite scaffold: In vitro study.* Indian J Med Res, 2015. **142**(6): p. 747-58.

Part III:

Conclusions

and future prospects

1. Main achievements

This first section will summarize the main achievements of this thesis and will highlight the most interesting conclusions. First, main achievements related to the elaboration of the biointerfaces will be described and then, the main trends regarding the behavior of cells on these interfaces will be summed up.

1.1. Elaboration of biomimetic films containing fibronectin and collagen

The first topic that was investigated for the elaboration of the biointerfaces was the development of the experimental protocol for the **preparation of PS substrates** by spin-coating. The main issue to solve was the lack of polymer film adhesion on glass or silicon. We have shown that the nature of the silane used to modify glass or silicon before spin-coating is important. The use of ODMS, with a silanization protocol in liquid phase, greatly improves polymer adhesion on glass or Silicon compared to the use of MOPTMS.

After obtaining PS substrates suitable for protein adsorption, first tests of LbL building were performed with Fn and Col. Development steps were performed to improve the **LbL deposition protocol** including study of the effect of temperature, adsorption time, protein concentration, etc. It was also shown that the use of Fn as the first layer of the assembly gives more reproducible results. At the end of this protocol development, it was decided to test three interesting buffers: Hepes, PBS and Acetate buffer. The aim was to compare three widely-used buffers, two with the same pH but featuring different ions (Hepes and PBS) and one with another pH (Acetate buffer). Moreover, the use of denatured Col and of an anchoring layer of PEI was also shown to be relevant for future developments.

The different parameters highlighted during protocol development were applied to LbL building to give protein films that were analyzed as presented in chapter 2. The **characterization of films obtained by LbL deposition method** was thus performed for these different conditions. Most of the approaches tested for LbL assembly allow at least the construction of one bilayer even if

the assembly process is not sustainable. The obtained assemblies were **compared to interfaces obtained through simultaneous adsorption of Col and Fn**. Several conclusions can be drawn from the obtained results:

(i) The use of denatured or native collagen influences the assembly of Col with Fn. A saw-tooth profile is observed by QCM-D monitoring in Hepes and PBS for LbL building with denatured Col, probably due to the formation of soluble complexes between Fn and denatured Col. Moreover, the use of denatured Col gives very smooth film morphologies because denaturation prevents Col fibrillation.

(ii) The use of PEI allows thicker films to be obtained. QCM-D monitoring also shows a saw-tooth profile for LbL building, this time in Hepes and Acetate buffer. In acetate, it is also probably due to soluble complex formation. However, in Hepes, hypothesis of film contraction/swelling depending of the last layer is more probable. Film morphology observation shows that films on PEI are rougher, due to PEI aggregation.

(iii) There is a real influence of the buffer on the assembly. LbL building in PBS and Hepes are similar in some conditions but give very different results for LbL building on PEI anchoring layer. In acetate buffer, LbL building shows a different behavior. It proves that pH as well as the nature of surrounding ions has an influence on assembly. Combination of all the results described in chapter 2 shows that Hepes is the buffer that allows more regular assemblies to be obtained.

(iv) Deposition method greatly influences the film design. Even if film with the same thickness, or even thicker, are obtained by simultaneous adsorption compared to LbL deposition, properties of the interfaces are not the same. Indeed, films obtained by simultaneous adsorption are less hydrated, have a lower contact angle but expose more Col fibrils than films obtained by LbL deposition.

Even if true LbL assemblies are not obtained, i.e. assemblies presenting sustainable linear or exponential growth, different biointerfaces are designed with different properties depending of the experimental conditions. Moreover, multilayers were built, which is promising since proteins generally adsorb in monolayers only. These interfaces are thus more complex than a simple protein monolayer and could possess interesting properties to modulate cell behavior.

Three main **hypotheses can explain the lack of LbL assembly**. First, if assembly is based on electrostatic interactions, there is probably no charge reversal at each adsorption step. This hypothesis could be checked by zeta potential measurements. Then, if assembly is based on specific interactions between Fn and Col, there may not be enough interaction sites on each molecule to allow multilayer assembly. All interaction sites may be involved in the creation of the first bilayer and may then not be available for further interaction. Finally, formation of soluble complexes after deposition of a few layers could also explain the non-sustainability of the assembly. It could explain the saw-tooth profile that is sometimes observed, as was already reported as a problem for LbL construction by other authors [1].

As **Hepes** was the buffer that allows the most regular assemblies to be obtained, this buffer was used for further experiments. The use of PEI was also shown to be very interesting to increase the thickness of the films. The assemblies obtained in Hepes buffer, with or without PEI, by LbL deposition method or simultaneous adsorption, were thus analyzed in more details and compared to adsorption of Fn alone. These results were presented in chapter 3. A stability analysis of the different films was also performed to prove that they are stable in the buffer during 20h. As these different films present interesting properties depending on the conditions, they will be used for cell culture experiments with a view to understand how film properties can influence cell behavior.

1.2. Influence of the films on AMSC behavior

The behavior of AMSC was studied on films built in Hepes buffer, by simultaneous adsorption or LbL deposition method, with or without PEI anchoring layer. Adhesion, proliferation and differentiation were tested on the films. Moreover, the cytotoxicity of PEI was also assessed. Several conclusions can be drawn from the obtained results:

(i) PEI anchoring layer has an impact on cell proliferation. It decreases proliferation rate in the beginning of growth. It can be related to a cytotoxic effect of PEI. However, the use of the PEI anchoring layer improves cell osteogenic differentiation. First hypothesis to explain this behavior is that a decreased proliferation in the beginning of growth is beneficial for differentiation. Second hypothesis is that induction of differentiation before 100 % confluence, which is the case for protein films built on PEI, but not for the other ones, would improve differentiation. The last hypothesis is that the higher roughness of the film built on PEI would improve differentiation.

(ii) Impact of deposition method on adhesion, proliferation and differentiation is very low. There is just one observation showing that differentiation is influenced by deposition method when PEI anchoring layer is not used. Differentiation would be disadvantaged on films obtained by LbL deposition method.

(iii) Study of PEI cytotoxicity shows that the ratio between PEI and cell number has an impact on cytotoxicity. If there are more cells adherent to the surface, PEI has less impact on these cells. Owing to these results, hypothesis can be made to explain cell proliferation profile on films with a PEI anchoring layer. Proteins coated on PEI partly protect cells from the cytotoxic effect of PEI. The proliferation rate is thus slowed down but protected cells can divide and proliferate. Moreover, some degradation of PEI, or covering by secreted molecules will happen. Total amount of PEI in contact with cells will thus become very

low after a few days compared to cell number, and cytotoxic effect disappears.

These conclusions thus show that molecules at the interface, as well as their organization, have an impact on cell behavior. The major influence on the cells comes from the use of an anchoring layer. Even if, at first sight, PEI seems to have a negative impact of cells, we show that, finally, its use can help to improve osteogenic differentiation. The design of substrates on which stem cell osteogenic differentiation occurs faster than on currently used substrates is of major interest to improve several biomedical applications that use *in vitro* cultured cells.

With this work, it was thus possible to demonstrate the influence of different parameters on the organization of proteins at the interfaces. Even if true LbL assemblies were not built, we have already better understood the assembly mode of proteins in multilayers, and we have designed interfaces presenting interesting properties to study cell behavior. Next section will describe approaches that could be used to improve the deposition of proteins and possibly obtain a true LbL assembly. Moreover, other possible improvements and future prospects will be presented.

2. Future prospects

This last section aims at describing some strategies that can be applied to directly improve the LbL building, or to improve the properties of the assemblies.

2.1. Strategies for improvement of LbL deposition

2.1.1. Improvement of the current LbL deposition protocol

Even if a high amount of different parameters was already experimented in this thesis, it is always possible to test other experimental protocols. It could be interesting to assess very methodically the influence of pH, ionic strength, surrounding ions, etc on the assembly. For example, testing buffers with the

same composition and with the same pH but with different ionic strengths, or the opposite, would increase our understanding and control of assembly mechanisms. Testing of other anchoring layers could also be of major interest to better understand how the anchoring layer influences the interfacial properties.

Several methods of characterization could also improve the understanding of the LbL building process. Measurement of the surface zeta potential after each deposition step could give more knowledge about electrostatic interactions involved in the assembly. Moreover, the precise quantification of each protein type in the layer could reveal exchanges during the assembly. Labeled proteins could be used for such quantification, even though labelling can change their properties. Finally, performing morphological studies of the films in liquid could help to better understand if there is rearrangement during drying of the surfaces or not.

2.1.2. Use of another polyelectrolyte in the films

To build a true LbL assembly, the use of a third molecule could be a solution. The use of a synthetic polyelectrolyte, with a well-known charge, homogeneously distributed on the chain, could be envisioned. However, in this work, we have supposed that Fn and Col have opposite charges (negative for Fn and positive for Col) at pH 7.4. It would thus be impossible to find a polyelectrolyte that interacts with both proteins to build LbL with three components. Nevertheless, we are not sure about the iep of Col and about its charge. A negative charge on Col at pH 7.4 could moreover explain the problem of assembly observed in this thesis.

In the literature, assembly between gelatin, considered as negative at pH 7.4, and PEI was already proved at pH 7.4 [2-4]. We thus think it could be possible to combine n-Col and PEI. Assembly with Fn and PEI have not been already studied but could be possible because Fn is negative at pH 7.4 and PEI positive. We thus have decided to test $(Fn/PEI/n\text{-}Col/PEI)_n$ assemblies. The results show an assembly that is not sustainable. This is thus not a solution to improve LbL building based on Fn and n-Col.

The use of other polyelectrolytes is also reported in literature in combination with Col or Fn. For example, Col can be also associated to other molecules in LbL assembly, such as poly(styrene sulfonate)(PSS), but at pH 4.7 [5]. Fn can be associated to Poly(L-lysine)(PLL) at pH 7.4 [6]. Moreover, PSS and PLL can be associated in films around pH 6 [7]. We can thus imagine combining both proteins, by working at different pH and with two different polyelectrolytes. However, this building process becomes very complex and the strategy described in the next section seems then more interesting to use.

2.1.3. Protein-polyelectrolyte complexes

Another strategy, close to the first one but probably more versatile, is the creation of protein-polyelectrolyte complexes. The main principle is to create soluble charged complexes made of a protein core surrounded by polyelectrolytes. These complexes could then be used as building blocks for LbL assembly. As a proof of concept, polyelectrolyte complexes were already used in the lab to create films including a globular protein: lysozyme [8]. Lysosyme was complexed with PSS, and LbL assembly was performed between these complexes and poly(allylamine). In the case of this thesis, we could imagine forming complexes including Col and other complexes, of opposite charge, including Fn. For example, as previously described, Fn could be combine to PLL into complexes, and Col to PSS. Complexes could be built at two different pH values and then, be assembled together. However, due to the complex structure of collagen, building of complexes will probably be very challenging, but still interesting to test.

2.1.4. Cross-linking

Another strategy that could be used to improve LbL assembly is the cross-linking of the films. On one hand, if films only made of Col and Fn are desired, cross-linking can be performed after each protein layer deposition. Indeed, the addition of a cross-linking agent will allow the exposure of reactive groups at the top of the films that can promote chemical reaction with the next protein layer. It could thus be possible to create a kind of LbL assembly made of Fn and Col by chemical reaction between each layer. On the other hand, cross-linking

can be used to stabilize films made by true electrostatic interactions. For example, if films are built with different polyelectrolytes in addition to Fn and Col, or with protein-polyelectrolyte complexes, or/and if building needs to be done at different pH values during the deposition, cross-linking could help to stabilize the layers.

Different kinds of cross-linking agents could be used. However, they need to be compatible with cell culture. Cross-linking with EDC/NHS, or with glutaraldehyde, need thus to be avoided because there are potentially cytotoxic [9]. Genipin would have to be favored as a cross-linking agent [9]. In the literature, it was shown that genipin can be used to cross-link Col [10, 11] and Fn [12]. It could thus be interesting to test this cross-linking agent to build LbL films.

2.1.5. Chemical modification of proteins

A last possibility to improve the assemblies is the chemical modification of the proteins. If proteins are modified, it could be possible to maximize the interactions between Col and Fn. For example, we can imagine adding polypeptide chains at the end of each protein. One would be negatively charged, and the other one positively charged. Proteins would thus interact electrostatically trough these additional arms. Another example could be the grafting of biotin on Fn and Col, coupled to LbL building with streptavidin between each layer of Fn or Col. These modifications are theoretically possible but constitute uncertain approaches. Indeed, it is difficult to predict if modification will not change protein conformation, or if the modified part will not be buried in the core of the protein after folding.

2.2. Study of other cell types behavior

To validate the results obtained in this thesis, the cell culture needs to be performed on cells from other origins. The use of other kind of mesenchymal stem than AMSC thus be interesting to confirm the properties of the films. During his master thesis, Cédric Vrankckx has used dental-derived mesenchymal stem cells (DPSC) and, to a lesser extent, stem cells from apical

papilla (SCAP). He studied their behavior on films build with protocols very close to the one used in this thesis. His results are presented in Appendix 2. Briefly, he has also demonstrated an impact of PEI anchoring layer on cell behavior. This influence was very close to the one described in this thesis. PEI anchoring layer decreases slightly proliferation but improves cell osteogenic differentiation. His study thus confirms the influence of PEI on the cells but studies with more cell types should now be performed to draw more general conclusions.

2.3. Inclusion of specific signals in the films

2.3.1. Bone morphogenetic protein -2 (BPM-2)

Inclusion of specific proteins into the films could impart properties to promote osteogenic differentiation without the use of differentiation medium. BMP-2 is well known to induce osteogenic differentiation. For example, BMP-2 can be used as a pre-conditioning agent for the cells to promote AMSC osteogenic differentiation in growth medium [13]. Addition of this molecule in the films could be of major interest to allow a controlled and slow delivery of BMP-2.

A study of Cai et al. [14] has shown that poly(allylamine hydrochlorine)/poly(sodium 4-styrenesulfonate) multilayers can be loaded with BMP-2. The release of the molecule in the culture medium was then measured and was shown to be very slow. The authors have also proved that these loaded multilayered films improve osteogenic differentiation of MSC in differentiation medium compared to the unloaded films in the same medium. Immobilization inside the film thus improves differentiation. Another study performed by Crouzier et al. was based on cross-linked poly(L-lysine)/hyaluronan films. Loading of the multilayered films with recombinant human BMP-2 was optimized by adjustments of pH, ionic strength, recombinant human BMP-2 concentration and multilayer thickness. Release from the films was shown to be low, even with cells cultured on the films. In this work, films without recombinant human BMP-2 were shown to induce myoblasts differentiation into myotubes. However, on the films loaded with

recombinant human BMP-2, myoblasts differentiated into osteoblasts, when cultured in a simple growth medium, as shown by ALP production measurements.

The addition of BMP-2 inside multilayered films is thus promising to improve the osteogenic properties of these films. Future improvements of this work could study the addition of BMP-2 in the Fn and Col assemblies, with the aim to induce osteogenic differentiation.

2.3.2. Demineralized bone matrix

As explained previously, the addition of specific signals inside the films could be very interesting to trigger cell osteogenic differentiation. Even if BMP-2 is a good candidate to be included in the films, proteins from demineralized bone matrix (DBM) could be more interesting and cheaper. This DBM contains probably a cocktail of signaling molecules that trigger osteogenic differentiation very specifically. During the thesis, we have studied the extraction of proteins from DBM. More information about the extraction process and characterization of the extracts are presented in Appendix 3. To summarize, we have shown that extraction of proteins from DBM is possible in mild conditions. However, characterization of the nature of the proteins present in the extract was not easy. Results have shown that a small concentration of BMP-2 and VEGF are detected in the extracts. More detailed characterization of these extracts needs to be performed. Moreover, their integration in the films could be tested to determine if it improves cell differentiation.

2.4. Future applications

The different films designed in this thesis could have some interesting future use. They could be used as a coating of materials for tissue engineering processes. As shown in chapter 3, PS plates coated with the protein films are not better than TCPS to support cell culture. Nevertheless, the advantage of these films it that they can probably be used on other materials than PS and on other shapes than flat surfaces. The building of the films on other materials needs to be characterized but it is probable that it will be applicable on

different kinds of polymers. We can thus imagine coating scaffolds for tissue engineering with Fn and Col assemblies to improve their osteogenic properties. Moreover, if some improvements are performed to obtain true LbL assembly, with specific signals for differentiation, the films could be very interesting in bone reconstruction. They can be used as a coating for acellular bone scaffold or for scaffold designed to fit exactly the bone defect and created by 3D-printing.

References

1. Sukhishvili, S.A., E. Kharlampieva, and V. Izumrudov, *Where Polyelectrolyte Multilayers and Polyelectrolyte Complexes Meet.* Macromolecules, 2006. **39**(26): p. 8873-8881.
2. Zhu, H., et al., *Protein electrostatic self-assembly on poly(DL-lactide) scaffold to promote osteoblast growth.* Journal of Biomedical Materials Research - Part B Applied Biomaterials, 2004. **71**(1): p. 159-165.
3. Zhong, X., et al., *Surface modification of poly(propylene carbonate) by aminolysis and layer-by-layer assembly for enhanced cytocompatibility.* Colloids and Surfaces B: Biointerfaces, 2012. **93**: p. 75-84.
4. Ai, H., et al. *Coating bio-nanofilm on PDMS through layer-by-layer self-assembly*. in *Annual International Conference of the IEEE Engineering in Medicine and Biology - Proceedings*. 2002.
5. Landoulsi, J., S. Demoustier-Champagne, and C. Dupont-Gillain, *Self-assembled multilayers based on native or denatured collagen: Mechanism and synthesis of size-controlled nanotubes.* Soft Matter, 2011. **7**(7): p. 3337-3347.
6. Soumetz, F.C., L. Pastorino, and C. Ruggiero, *Human osteoblast-like cells response to nanofunctionalized surfaces for tissue engineering.* Journal of Biomedical Materials Research - Part B Applied Biomaterials, 2008. **84**(1): p. 249-255.
7. Tezcaner, A., et al., *Polyelectrolyte multilayer films as substrates for photoreceptor cells.* Biomacromolecules, 2006. **7**(1): p. 86-94.
8. Vander Straeten, A. and C. Dupont-Gillain, *Protein-polyelectrolyte complexes for the surface immobilization of proteins: lysozyme as a proof of concept*, to be published, UCL.
9. Gaudière, F., et al., *Genipin-cross-linked layer-by-layer assemblies: Biocompatible microenvironments to direct bone cell fate.* Biomacromolecules, 2014. **15**(5): p. 1602-1611.
10. Chaubaroux, C., et al., *Collagen-based fibrillar multilayer films cross-linked by a natural agent.* Biomacromolecules, 2012. **13**(7): p. 2128-2135.
11. Chen, M.C., et al., *A novel drug-eluting stent spray-coated with multi-layers of collagen and sirolimus.* Journal of Controlled Release, 2005. **108**(1): p. 178-189.
12. Ravi, S., et al., *Incorporation of fibronectin to enhance cytocompatibility in multilayer elastin-like protein scaffolds for tissue engineering.* Journal

of Biomedical Materials Research - Part A, 2013. **101 A**(7): p. 1915-1925.

13. Lu, Z., et al., *Synergistic effect of nanomaterials and BMP-2 signalling in inducing osteogenic differentiation of adipose tissue-derived mesenchymal stem cells.* Nanomedicine: Nanotechnology, Biology, and Medicine, 2015. **11**(1): p. 219-228.
14. Cai, P., et al., *Adsorbed BMP-2 in polyelectrolyte multilayer films for enhanced early osteogenic differentiation of mesenchymal stem cells.* Colloids and Surfaces A: Physicochemical and Engineering Aspects, 2013. **434**: p. 110-117.

Part IV: Appendices

Appendix 1:

Silanization of polystyrene with methacryloxypropyltrimethoxy-silane with a view to improve polymer adhesion

In this work, protein adsorption is performed on PS substrates. These substrates need to be prepared by spin-coating of polymer to obtain smooth polymer films, on which it is easier to make protein films characterization. For this purpose, PS solution is spin-coated on thin 12 mm in diameter glass coverslips or pieces of silicon wafer. However, a well-known problem appears when polymer films are deposited on a hydrophilic substrate: the polymeric film detaches from the support. This detachment comes from accumulation of water in the polymer-glass interface. This accumulation decreases the contact area between glass and polymer, leading to a decrease of adhesion force between them [1]. In the work of Zyuderhoff et al. [2], this problem was already raised. To solve it, methacryloxypropyltrimethoxy silane (MOPTMS, see Fig. IV.1.1) was used as a coupling agent to increase adhesion.

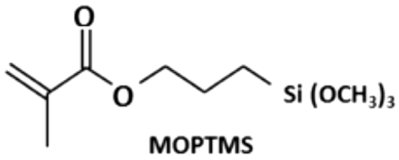

Figure IV.1. 1: MOPTMS structure

1. Initial silanization protocol with MOPTMS

Method: Silanization was performed on piranha-cleaned (20 min in a 1:2 H_2O_2/H_2SO_4 mixture) glass coverslips (12 mm in diameter) with MOPTMS silane dissolved at 0.01M in dioxane. Surfaces were immersed during 4 h in this silane solution and were then rinsed one time in dioxane and then four times in ethanol, with sonication each time in an ultrasonic bath. Surfaces were then

dried in a N_2 flow. PS was then deposited by spin-coating. PS was dissolved in toluene at a concentration of 10 g/l and was spin-coated at a speed of 5000 rpm during 40 s.

Results and discussion: By applying this protocol, a very high number of film detachments were observed during the first experiment. A first hypothesis to explain these detachments is that handling of the glass coverslips was very challenging. Cautious handling is needed to avoid scratches of the PS layer. And if there are scratches on the surface, the film probably detaches faster because water will penetrate easier toward the interface. Some optimization of the protocol was thus performed to improve PS adhesion.

2. Protocol optimization with MOPTMS

Method: Several solutions were tested, in addition to the silanization, to facilitate handling or to give more resistance to scratches to the films:

- The **increase of silane concentration** was tested with the aim to improve grafting of the silane on glass and potentially improve polymer film adhesion.
- The use of **thicker glass substrates** was tested. Indeed, handling of thin glass coverslips is much more difficult than handling of glass pieces cut from thicker microscope slides.
- The **coating with polymer of the two sides of the glass coverslips** was then tested. If the two sides are coated, water will penetrate less easily by the edges of the coating to detach the film.
- The **increase of the polymer concentration** in the spin-coated solution was also tested. If the PS concentration increases in solution, the thickness of the PS film on glass will increase. Scratches could thus be less problematic. The concentration will be increased from 10 g/L to 20 g/L. Based on the equation (I) presented in the introduction part (see section 3.1.2), thickness is expected to double.

To evaluate film detachment, spin-coated glass coverslips were immersed in PBS during a few hours. Several times during the immersion, PBS was withdrawn and delivered again (abbreviated as "pipetting") and/or spin-coated glass pieces were handled with tweezers (abbreviated as "handeling"), to mimic the procedure and sample handling used when several adsorption steps are performed. After the immersion, surfaces were dried under nitrogen flow and water contact angles were measured. Depending on the results, it is possible to determine if the films were detached (low contact angle) or not (contact angle around 90°).

Results and discussion: Results of these different tests are presented in Tables IV.1.1 and IV.1.2. As shown in Table IV.1.1, the adhesion is very bad on thick glass. Moreover, the use of an increased silane concentration does not improve adhesion. Spin-coating of the two sides of the surface seems to improve a little bit adhesion on thin glass but detachments are always observed. Results of Table IV.1.2 confirm this last observation. However, they show that increasing the polymer concentration seems to greatly improve adhesion. A PS concentration of 20 g/L will thus be used for the rest of the work.

Table IV. 1. 1: Results of PS film adhesion experiment on glass. For the results of this table, handling and pipetting were performed on the same samples. Immersion in PBS with pipetting was first performed. Contact angle was measured and detachment was evaluated. Handling is then performed on the samples without films detachments after pipetting. The influence of the thickness of the glass substrate, of silane concentration and of spin-coating on 1 or 2 sides was tested. PS concentration is fixed at 10 g/L. The scorings in the table indicate number of adherent films on the number of tested films. Green color highlights best conditions, orange, the intermediate one, and red, the worst one.

Thick or thin glass substrate	[silane]	Spin-coating	Pipetting 6 times every 30 min	Handling 6 times every 30 min
Thick microscope slide	0.01 M	1 side	0/3	-
		2 sides	1/3	0/1
	0.1 M	1 side	1/3	0/1
		2 sides	0/2	-
Thin coverslip	0.01 M	1 side	3/3	1,5/3
		2 sides	2/2	1,5/2
	0.1 M	1 side	2/3	0/2
		2 sides	3/3	2,5/3

Table IV. 1. 2: Results of PS film adhesion experiment on thin glass coverslips. For the results of this table, handling and pipetting test were performed on different surfaces, three for each. The influence of the thickness of the polymer concentration and of spin-coating on 1 or 2 sides was tested. Silane concentration was fixed at 0.01M. The scorings in the table indicate number of adherent films on the number of tested films. Green color highlights best conditions, orange, the intermediate one, and red, the worst one.

[PS]	Spin-coating	Pipetting + 3 days in solution	Handling 6 times every 30 min
10 g/L	1 side	0/3	1.5/3
	2 sides	0.5/3	2.5/3
20 g/L	1 side	2/3	2/3
	2 sides	3/3	3/3

The different results presented here show that the only significant improvement of adhesion comes from increasing polymer concentration used for spin-coating. To better understand why the MOPTMS silane does not improve so much PS adhesion, measurements of water contact angle after silanization, on glass and on silicon, were performed to determine if it really makes surfaces more hydrophobic. They are presented in Fig. IV.1.2. Water contact angle of Si and glass before silanization was also determined. We measured Θ of 12 ± 5° on Si just after cleaning and of 26 ± 4° after a few days of storage in dessicator. For glass, surfaces are too hydrophilic to measure Θ. Based on these results, it was shown that MOPTMS silanization does not increase much the hydrophobicity of the substrate. Ethanol rinsing performed in the MOPTMS grafting protocol, especially with sonication, could be a reason to this very contact angles values. These rinsing steps were probably too strong and detached the grafted silane. This hypothesis was tested and results are presented in Fig. IV.1.2. Without any rinsing in ethanol after MOPTMS silanization, contact angles were higher on glass but not on silicon.

.

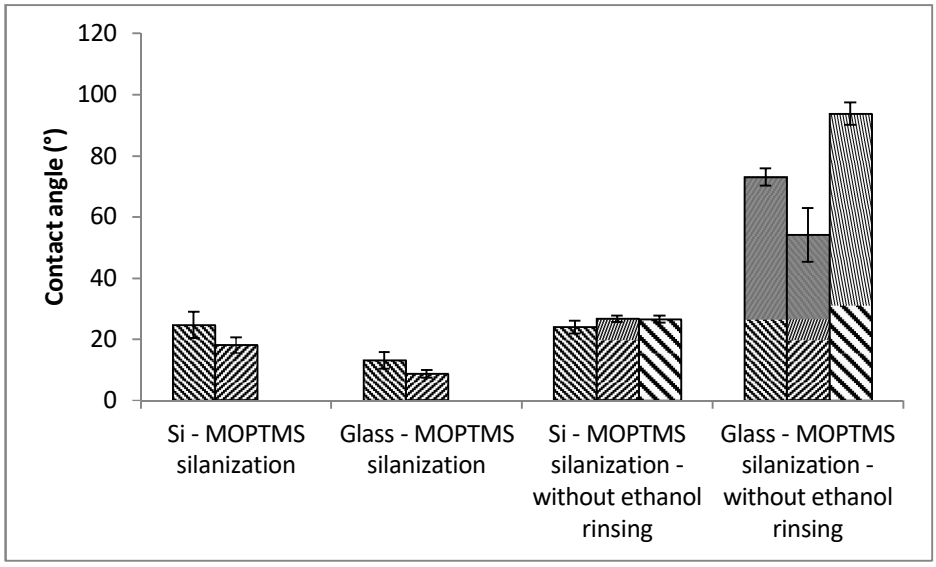

Figure IV. 1. 2: Contact angle measurements after silanization of glass and silicon with MOPTMS, with or without rinsing steps in ethanol. Error bar represent confident interval at 95%. Results for two or three different surfaces are shown in the figure and are represented by the different bars of the histogram. Θ of 12 ± 5° was measured on Si just after cleaning and Θ of 26 ± 4° after a few days in dessicator. Glass surfaces are too hydrophilic to measure Θ.

3. Conclusion

Based on the data presented in this Appendix, we conclude the MOPTMS is not the best choice to hydrophobize the glass substrate surface in a view of increasing polystyrene adhesion, even after improvements brought to the original protocol of silanization.

1. Krongauz, V.V., S.R. Schmid, and J.T. Vandeberg, *Imaging in evaluation of polymer coatings adhesion to glass at high humidity.* Progress in Organic Coatings, 1995. **26**(2-4): p. 145-162.
2. Zuyderhoff, E.M., *Heterogeneous surfaces with organized collagen layers for the control of cell behavior*, 2012, Université catholique de Louvain: Louvain-la-Neuve.

Appendix 2: Study of dental stem cell behavior on the designed interfaces

This section aims at summarizing the work of Cédric Vranckx [1] realized in the context of this thesis. During his work, he studied the behavior of dental stem cells on the same interfaces that the one designed here. However, some modifications were applied to the protocol that can change the morphology of the designed interfaces. In the cell culture experiments of this thesis, the films were prepared under aseptic conditions on sterile substrates. There was thus no need for sterilization before cell seeding. Before physico-chemical characterization, films were dried under N_2 flow. For practical reasons, in the work of Cédric, the films were prepared under non-aseptic conditions and were sterilized after the protein film building. Before cell seeding, they were immersed in ethanol and rinsed with sterile water. Before physico-chemical characterization, they were immersed in ethanol and dried gently in air. These differences of protocols could have some impact on the obtained results.

The first part of this appendix will present the cells used in the work. The second part will describe the differences obtained in the results for physico-chemical characterization of the films. Finally, the last part will detail the results obtained during cell culture experiments.

1. Dental mesenchymal stem cells

In the work of Cédric, two types of stem cells were used. The first are stem cells from the dental papilla (DPSC), isolated from the dental pulp as shown on Fig. IV.2.1. They proliferate fast and can differentiate *in vitro* into odontoblasts, adipocytes, neural cells, osteoblasts, chondrocytes, myocytes, cardiomyocytes, melanocytes and hepatocyte-like cells [2]. The second cell type consists in stem cells from the apical papilla (SCAP), shown on Fig. IV.2.1. These cells come from the apical part of the developing teeth. They have a higher proliferation rate and better mineralization potential than DPSC. They can differentiate into adipocytes, odontoblasts, osteoblasts, hepatocyte-like cells, and even express neural cell markers [2]. SCAP cells need to be extracted from immature teeth

because the apical papilla disappears in mature teeth. DPSC can be extracted from mature teeth but are also generally extracted from immature ones. Indeed, wisdom teeth are generally used as a source of both cell types because their extraction is needed for other reasons than stem cell recovery. Many other cell types can be extracted from teeth but they were not used in this work.

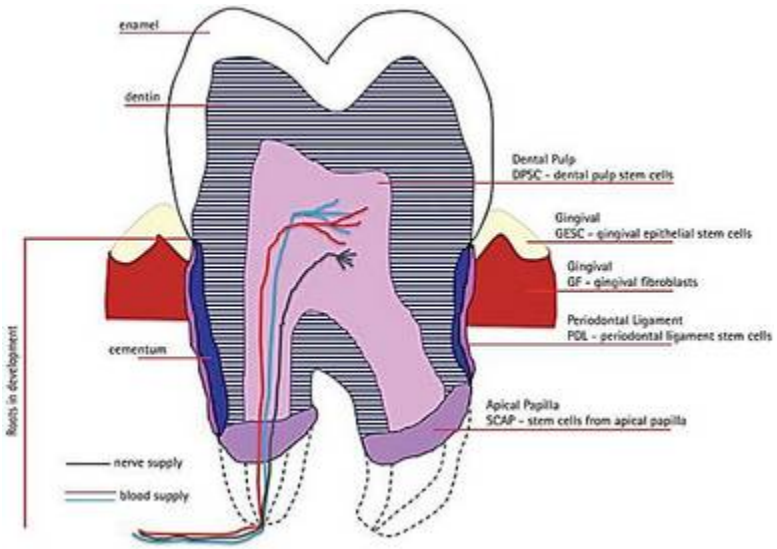

Figure IV. 2. 1: Representation of immature human molar with the different stem cells that can be recovered from it [3].

2. Comparison of the results

The characterization of the physico-chemical properties of the designed interfaces revealed some differences between the results obtained by Cédric and the one of this thesis.

- **Contact angle:** For the films with a PEI anchoring layer, higher contact angles were measured in the work of Cédric compared to the one obtained here. It is especially the case for PEI/Fn+Col films, for which Cédric measured values around 71.5° compared to 44.5° measured in

this work. Measurements without the anchoring layer are closer between the two works.

Organization of the films probably changes due to the drying step under ethanol before contact angle measurement. An aggregation of proteins, which let more PS domains exposed at the outermost surface, probably happens easier with a slow drying in ethanol than with the N_2 drying used in this work. This phenomenon can be facilitated on a PEI anchoring layer because, as shown in this thesis, this polymer has already a tendency to aggregate.

- **Thickness:** Measurements are performed with the same protocol and apparatus than in the thesis. PEI anchoring layer also gives thicker proteins films than without PEI. Even if the results are of the same order of magnitude, some differences can be observed. The major difference appears from films prepared by simultaneous adsorption. In this thesis, simultaneous adsorption gives films of the same thickness or even thicker than LbL adsorption. However, in the work of Cédric, simultaneous adsorption gives films with the same thickness than for Fn adsorption alone, but thinner than LbL adsorption.

- **Film morphology:** Morphological analysis of the films also reveals some differences. Films made of Fn or PEI/Fn present the same morphology in both works. The PEI anchoring layer also gives rougher films like in this thesis. However, general observation when Col is used is that Col fibrils are less visible in the work of Cédric. It is especially the case for simultaneous adsorption. In the results of this thesis, this kind of film is the one where fibrillation is the most favored. It is not the case in the work of Cédric, in which almost no fibril is observed in this condition.

To summarize, the major difference between the two works is observed for the results of simultaneous adsorption of Fn+Col. The differences can come from the experimental procedure, depending of the operator, or from the drying procedure. The use of slow drying in ethanol compared to fast drying under

nitrogen flow can change protein organization in the film and thus change contact angle, thickness and morphology. For cell culture experiments, this drying is not performed but protein films are also immersed in ethanol. It could thus influence film properties.

However, main differences observed in this thesis for cell behavior come from the use or not of the anchoring layer. And the main conclusions regarding the use of the anchoring layer are the same in both works (thicker assembly, rougher surfaces). It is thus interesting to study the reaction of different cell types to such layer characteristics.

3. Study of cell behavior

The study of cell behavior is based on two main experimental tests. The first one is the measurement of cell metabolism by MTS assay (3-(4,5-dimethylthiazol-2-yl)-5-(3-carboxymethoxyphenyl)-2-(4-sulfophenyl)-2H-tetrazolium). The second one is characterization of the osteogenic differentiation by alizarin red staining.

MTS results are often linked to cell proliferation. It is true if all the cells have the same metabolic activity and if this activity stays constant during growth. The results of these measurements are presented in Fig. IV.2.2 for DPSC and Fig. IV.2.3 for SCAP. The impact of PEI on cells, highlighted in the thesis, is also observed here. Indeed, cells seem to die on a simple PEI layer. With protein films built on this PEI layer, the metabolic activity increases more slowly than without PEI anchoring layer. PEI anchoring layer probably thus decreases proliferation rate. However, this decrease is not so important and is even very low in the second repetition of Fig IV.2.2. It thus remains interesting to study cell differentiation on these films.

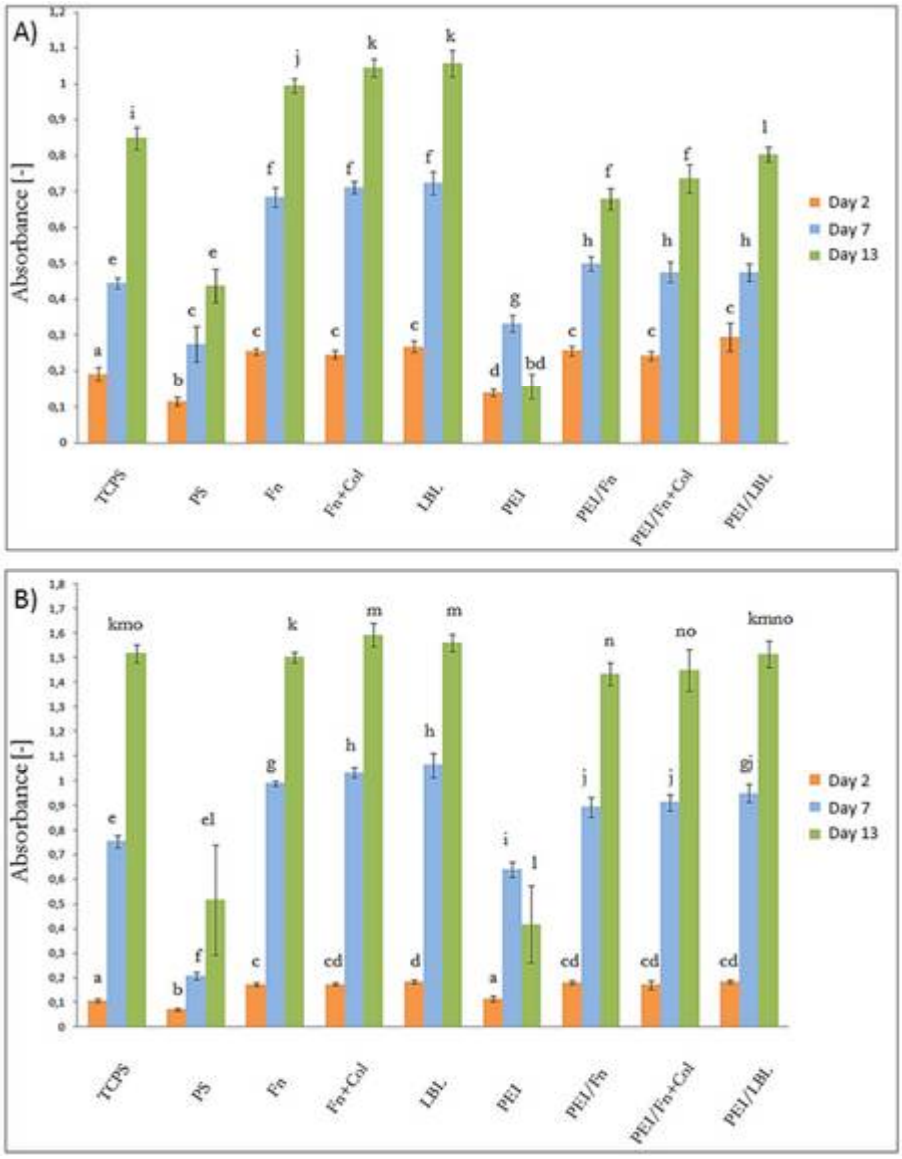

Figure IV. 2. 2: Proliferation of DPSC measured by MTS assay. Cells are seeded at 10,000 cells/well. Statistical analysis performed is t-student test (α = 0.01). If two data have the same letter, they are not different statistically, if they do not share the same letter, they are different. Two repetitions were performed and shown in (A) and (B). They were not combined because they are significantly different due to high biological variability.

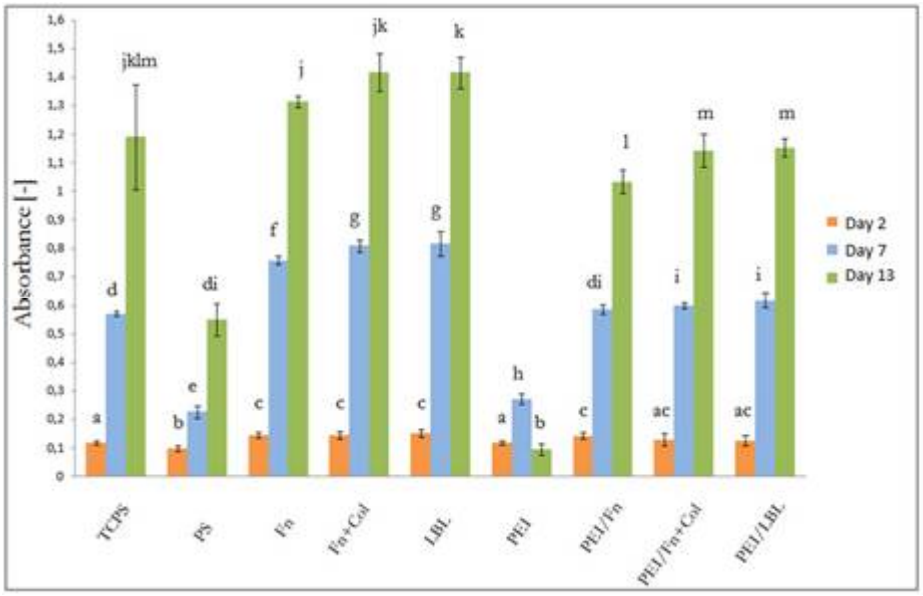

Figure IV. 2. 3: Proliferation of SCAP measured by MTS assay. Cells are seeded at 10,000 cells/well. Statistical analysis performed is t-student test (α = 0.01). If two data have the same letter, they are not different statistically, if they do not share the same letter, they are different.

The results of the differentiation study are presented in Fig. IV.2.4. Negative control consists in cells cultured on TCPS in classical proliferation medium, positive control consists in cells cultured on TCPS in osteogenic medium. A first observation coming from Cédric's results is that cells need to be submitted to differentiation medium to differentiate, even if the PS surface is modified with a protein film. In proliferation medium, cell layers are not colored in red after alizarin staining because they are not osteodifferentiated at all, whatever the nature of the protein film (results not shown). When cells are cultured in differentiation medium, cell matrix mineralization is observed by alizarin red staining (Fig. IV.2.4). Red coloration is observed in all the conditions, showing that differentiation happens in each kind of film. This differentiation is even better than on the positive control. However, some parts of the surface are darker and correspond to very mineralized extracellular matrix. These strongly mineralized parts are most present on films with an anchoring layer of PEI, what suggests that the PEI anchoring layer favor osteodifferentiation. Finally, a

last unexpected observation is that differentiation in osteogenic medium is better on pure PS ("-" ;"without PEI") than on TCPS (C+). Even if proliferation is very slow on pure PS, cell activity increases with time (Fig. IV.2.2), which is not the case in this thesis. Secretion of ECM molecules thus happens and these ACM molecules can adsorb on pure PS. Higher adsorption of secreted proteins on PS than on TCPS could explain the unexpected result of better differentiation on PS.

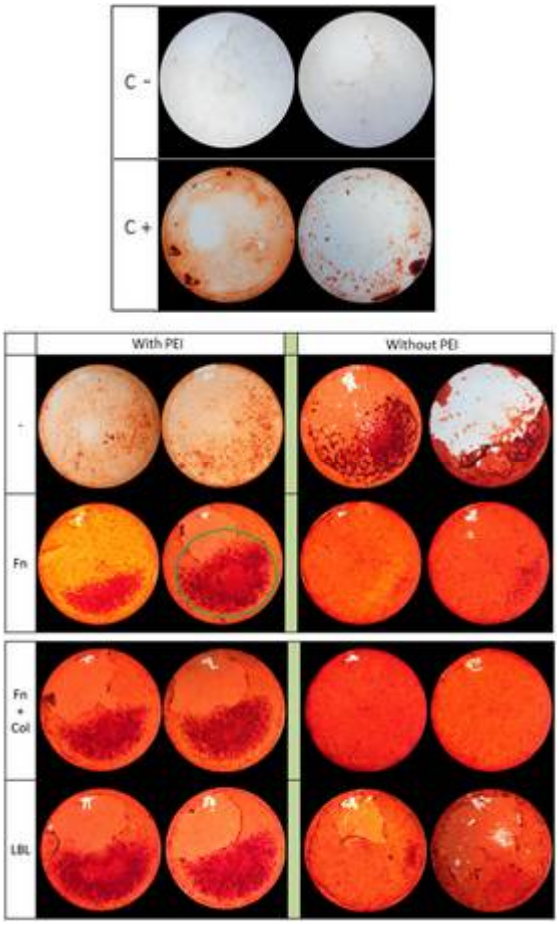

Figure IV.2. 4: Study of osteogenic differentiation of DPSC by Alizarin red staining. After 29 days, differentiation is induced by the addition of osteogenic differentiation medium, except for negative control. Positive (C+) and negative (C-) controls are TCPS with and without osteogenic induction. The films are built on pure PS.

4. Conclusion

The work of Cédric Vranckx, based on the same type of films than this thesis, shows interesting results regarding the organization of the biointerfaces and the behavior of DPSC and SCAP. First, it shows that physico-chemical characterization changes depending of the operator and /or the way to dry the samples. Very different results are observed for simultaneous adsorption between the two works. However, the PEI anchoring layer has the same impact on the films in the two studies.

Moreover, even if some differences are observed in the cell behavior, a main general conclusion can be drawn from both works. The PEI anchoring layer, that allows thicker protein films to be obtained, decreases the proliferation rate but improves differentiation.

1. Vranckx, C., *Développement de surfaces biomimétiques en vue de mieux comprendre et maîtriser le comportement de cellules souches dentaires*, Master thesis, 2016, Université catholique de Louvain: Louvain-la-Neuve.
2. Liu, J., et al., *Concise reviews: Characteristics and potential applications of human dental tissue-derived mesenchymal stem cells.* Stem Cells, 2015. **33**(3): p. 627-38.
3. Volponi, A.A. and P.T. Sharpe, *The tooth - a treasure chest of stem cells.* Br Dent J, 2013. **215**(7): p. 353-358.

Appendix 3: Preliminary results about demineralized bone matrix analysis

During this thesis, a few investigations on the use of demineralized bone matrix (DBM) were performed. The initial aim was to use DBM or DBM extracts to increase the complexity of the designed biointerfaces. Although this aim was not reached, the obtained preliminary results are reported in this appendix.

1. Introduction

DBM powder is obtained from bone pieces that are crushed, decellularized and demineralized. This powder shows interesting properties to be used as a scaffold for adipose-derived mesenchymal stem cells. For example, it was demonstrated by Schubert et al. that supplementation of osteogenic medium with DBM during AMSC differentiation allows a kind of paste to be obtained, that can be used to treat bone defects [1]. DBM powder has good properties to support cell osteogenic differentiation. It constitutes in fact the ECM of bone cells. It has thus probably the good morphology and composition to support this differentiation. Some studies show that DBM contains interesting factors for differentiation. DBM is mainly composed of type I Col and of different kinds of growth factors [2]. Wildemann et al. [3] measured the amount of different growth factors in DBM extracts by ELISA. They proved that there is bone morphogenetic protein (BMP-2), transforming growth factor (TGF-β1), insulin-like growth factor (IGF-I), fibroblast growth factor (FGFa), vascular endothelial growth factor (VEGF) and platelet-derived growth factor (PDGF) in the extracts, with an amount of extracted BMP-2 of 3.6 µg/g.

To improve the biointerfaces designed in this work, it could be interesting to add molecules that directly promote osteogenic differentiation in the created layers. Many factors, such as BMP-2, can be useful in this aim. However, they are expensive and it is not easy to identify the appropriate combination of factors to induce differentiation. The use of DBM can thus be interesting because it directly mimics the complexity of factors met *in vivo.* However, DMB particles cannot be included directly in the films because they are too large.

The use of DBM extracts can thus be interesting. Extraction procedures are already well known and allowed the different compounds present in DBM to be analyzed, as shown previously. However, these extraction methods use denaturing agents, such as guanidine, to extract the proteins. Proteins can thus be denatured during the process and lose their activity. In this work, the idea was to develop a soft method to extract relevant proteins from DBM powder.

This appendix will describe some characterization of the DBM powder. It will also give some details on the extraction procedure and on the characterization of the extracts.

2. Materials and methods

This section will briefly describe the protocols used in the characterization of DBM. Some experiments were performed on porcine DBM, others on human DBM and some on both. Indeed, in the beginning of the thesis, the idea was to work with porcine AMSC. But this changed in the course of the thesis because human AMSC were more used by the team of Pr. Dufrane, and porcine AMSC were outdated.

XPS analysis: The analyses were performed on a SSX 100/206 photoelectron spectrometer from Surface Science Instruments (USA) equipped with a monochromatized micro focused Al X-ray source (powered at 20 mA and 10 kV). The pressure in the analysis chamber was around 10^{-6} Pa. The analyzed area was approximately 1.4 mm^2 and the pass energy was set at 150 eV. The C-(C,H) component of the C 1s peak of carbon was fixed to 284.8 eV to set the binding energy scale. Data treatment was performed with the CasaXPS program (Casa Software Ltd, UK), some spectra were decomposed with the least squares fitting routine provided by the software with a Gaussian/Lorentzian (85/15) product function and after subtraction of a nonlinear baseline. Molar fractions were calculated using peak areas normalized on the basis of acquisition parameters and sensitivity factors provided by the manufacturer.

For the analysis of DBM powder, the powder samples were pressed in small stainless steel troughs of 4 mm diameter. For the analysis after deposition on a

Si or Au substrate, DBM extracts were adsorbed on these surfaces and were then rinsed with water and dried under nitrogen flow. Samples were then glued with adhesive tape on the carousel for analysis.

Scanning electron microscopy analysis (SEM): Images were acquired by Sylvie Derclaye on a SEM Leo 982 (Carl Zeiss).

Elementary analysis: Analysis was performed in Spectropole (Marseille, France).

Extraction protocol: DBM powder was suspended at 10 mg/ml in PBS. This suspension was put under agitation during 72 h at 4°C, room temperature or 37°C. After this agitation, suspensions were centrifuged and the supernatant was used as the DBM extract. For the extraction with pepsine, DBM powder was suspended in a solution of 1 mg/ml pepsine in 0.01 N HCl. In this case, almost all the DBM powder was dissolved after 72 h. It is for this reason that this extraction was performed. It allows to characterize samples in which all DBM is dissolved, even if proteins are probably denatured in these extracts. Centrifugation was also performed and the supernatant was used as the DBM extract.

Protein quantification: Protein amount was quantified by Bradford assay and by BCA assay. For Bradford assay, Bradford reagent (Brillant Blue G, Sigam-Aldrich) was used and absorbance was measured at 595 nm. Reaction was performed at room temperature. For BCA assay, reaction between protein solution and BCA reagent was performed during 30 min at 60°C. Absorbance was then read at 559 nm.

Gel electrophoresis and mass spectroscopy: 2D polyacrylamide gels were performed to separate proteins according to their mass. Migration of a standard was also performed to determine the mass of the detected band. Some parts of the gel were further recovered and analyzed by mass spectroscopy.

3. Results and discussion

3.1. Chemical and morphological analysis of DBM powder

Morphology: Morphological analysis of DBM powder was made on porcine DBM with SEM as illustrated in Fig. IV.3.1. The DBM particles have a size around 600 µm and are porous. Visual analysis of human DBM powder shows that particles are smaller.

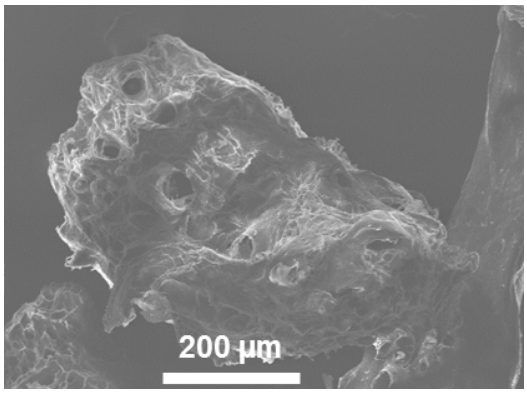

Figure IV. 3. 1: SEM picture of porcine demineralized bone matrix

XPS analysis: XPS analysis of the powder was made both on porcine and human DBM. It is important to keep in mind that XPS allows to analyze the first 10 nm of the powder particles. Results presented in Table IV.3.1 and IV.3.2 thus show the chemistry of the surface of the particles. Detection of Nitrogen shows that there are probably proteins at the surface in both cases. The excellent correlation between the atomic percentage of N and (**C**=O)-N confirms that Nitrogen comes mostly from proteins. However, N/C ratios are too low compared to the theoretical one for proteins (around 0.3). There are thus other kinds of molecules on the surface. Calcium detected on porcine DBM comes probably from the mineral phase of bone. Calcium was not detected on human DBM. This latter is probably better demineralized. Sodium, phosphorus and chlorine probably come from the buffers used during demineralization.

Porcine and human DBM do not have the same surface composition. In human DBM, Oxygen percentage is higher and Carbon percentage lower than in

porcine DBM. Moreover, variability is higher for porcine DBM than for human DBM.

Table IV. 3. 1: XPS analysis of porcine DBM powder. Position (Pos.) in eV gives the average binding energy of each component of carbon spectra. A, B, C: three different samples from the same DBM batch.

	C					O	N	Na	Cl	Ca	N/C	O/C
	(C=O)-O	(C=O)-N, C=O, O-C-O	C-O, C-N	C-(C,H)	tot							
Pos. (eV)	289	287,8	286,2	284,8								
A	2.4	11.5	15.5	39.4	68.7	18.9	11.5	0.53	0.14	0.23	0.17	0.27
B	3.4	10.5	16.9	39.0	69.8	18.5	11.0	0.61	0.06	-	0.16	0.27
C	2.9	8.0	12.6	52.9	76.4	15.2	7.7	0.27	0.12	0.34	0.10	0.20

Table IV. 3. 2: XPS analysis of human DBM powder. Position (Pos.) in eV gives the average binding energy of each component of carbon spectra. . A, B, C, D: four different samples from the same DBM batch.

	C					O	N	Na	P	N/C	O/C
	(C=O)-O, arom.	(C=O)-N, C=O, O-C-O	C-O, C-N	C-(C,H)	tot						
Pos. (eV)	289.1 289.6	287,8	286.1	284.8							
A	1,1	9,4	17,1	15,7	43,3	32,6	8,7	10,6	4,9	0,20	0,75
B	1,1	9,0	17,1	16,1	43,3	32,1	8,4	10,6	5,6	0,19	0,74
C	1,7	12,1	15,5	15,5	44,7	30,4	9,9	9,5	5,5	0,22	0,68
D	1,2	10,6	15,4	21,9	49,0	28,2	9,9	8,1	4,8	0,20	0,58

Elementary analysis: On the contrary to XPS analysis, elementary analysis gives the global composition of the powder. Moreover, each percentage is a mass percentage. These values are summarized in Table IV.3.3 and show that elementary composition of porcine and human DBM are very close. However, it was not the case for the composition determined by XPS. Even if they are globally composed of the same elements, the exposed molecules at the surfaces are not the same for porcine and human DBM powder.

Unfortunately, the percentages determined in the results of elementary analysis (Table IV.3.3) represent only 88 – 90 % of the total mass. It is surprising because all the expected elements were analyzed by elementary determination. We thus suspect an underestimation of one or many of the elements.

To compare the result obtained by elementary analysis to the XPS results, computation of molar N/C and O/C from mass ratio of the elementary analysis is needed. These ratios are presented in Table IV.3.4. They are not similar to the one measured by XPS analysis. It confirms that the molecules exposed on the surface are not the same than in the bulk of the powder.

Table IV. 3. 3: Elementary analysis of DBM powder (porcine and human). Percentages of each elements are indicated in the table. Mass ratio are also summarized in the table.

	Percent in mass (%)	
	Porcine DBM	Human DBM
C	42,3	44,4
H	7,1	6,7
N	15,4	16,1
S	0,2	0,2
O	22,5	21,9
Ca	0,0074	0,0201
P	0,5	0,2
total	**88,0**	**89,5**
	Atomic mass ratio	
	Porcine DBM	Human DBM
N/C	0,36	0,36
O/C	0,53	0,49

Table IV. 3. 4: Computed molar ratio from mass ratio determined by elementary analysis

	Atomic molar ratio	
	Porcine DBM	Human DBM
N/C	0,31	0,31
O/C	0,40	0,37

3.2. Chemical analysis of DBM extract

Protein concentration: Protein concentration in the extracts was determined for extraction from porcine DBM. Two different methods are used for this determination. Results are presented in Table IV.3.5. Protein concentration in the extracts increases with the extraction temperature. If pepsine is used, all the DBM particles are dissolved, the concentration is thus the highest. We can conclude that proteins constitute a large part of DBM content. However, we have prepared a solution of 10 mg/ml of DBM. Even with pepsine, the highest concentration reached is 5 mg/ml. It thus proves that there is not only proteins in DBM.

The two assays do not give the same protein amount. Calibration curves are made in both cases with BSA. It is always difficult to determine if the proteins of the unknown react in the same way than the proteins used for calibration. Here, we do not know the multiplicative factor between the signal of the proteins in the unknown and the signal of BSA. This factor is probably different depending on the assay. It is probably the explanation of the differences observed between values measured for the two tests.

Table IV. 3. 5: Protein concentration in the DBM extracts obtained at different temperature and with pepsine digestion.

	Bradford assay [µg/ml]	BCA assay [µg/ml]
PBS - 4°C	30	120
PBS - 20°C	60	310
PBS - 37°C	550	2000
PBS + pepsine - 20°C	1200	4000-5000

Chemical analysis of the extract after adsorption: XPS analysis of the different extracts adsorbed on a silicon surface is presented in Table IV.3.6. For all the extracts, a good correlation is observed between N and (**C**=O)-N atomic percentage confirming that nitrogen comes almost totally from proteins. Extractions without pepsin give a high percentage of nitrogen and high N/C ratio. Proteins are thus an important fraction of the molecules in the extract

and adsorb readily. The atomic percentage of oxygen is high because the surface coverage is not complete. Oxygen from the SiO_2 layer present on the top of silicon surfaces is thus detected. This surface coverage increases with the extraction temperature (Si atomic percentage decrease) probably because the concentration in the extract increases. When pepsin is added for the extraction, the surface coverage is almost complete but the nitrogen percentage is very low. Moreover, the amount of detected carbon is quite important compared to the amount of oxygen and nitrogen. It is also traduced by a very high atomic percentage for the C-(C,H) function. This information shows that molecules with a high content in carbon and a low content of oxygen are detected that could be fatty acids. It seems to be confirmed by the higher amount of (C=O)-O function compared to the other samples. For this extract, all the powder is digested. These molecules could be present in the bulk of DBM particles and could adsorb preferentially.

Table IV. 3. 6: XPS analysis of DBM extract adsorbed on Si. First line, Si, gives the XPS analysis of the substrate. The other lines give XPS analysis after adsorption of extracts (Ex.) obtained at different temperatures and conditions on the Si substrate.

	C					O	N	Ca	P	Si	N/C	Si/C
	(C=O)-O	(C=O)-N, C=O, O-C-O	C-O, C-N	C-(C,H)	tot							
Si	1,1	1,1	5,0	15,6	22,9	40,7	-	0,78	-	35,7	-	1,56
Ex. 4°C	1,2	5,4	9,4	15,2	31,3	30,4	6,6	-	-	31,7	0,21	1,02
Ex. 20°C	0,6	6,6	10,4	15,7	33,3	29,4	6,8	-	-	30,5	0,20	0,92
Ex. 37°C	1,0	10,5	15,6	19,5	46,6	25,0	11,1	-	-	17,3	0,24	0,37
Ex. 20°C /Pepsin	3,8	3,2	8,7	70,2	85,9	11,0	2,0	-	0,51	0,56	0,02	0,01

The same experiment was performed on gold surfaces and the results are presented in Table IV.3.7. The same conclusions can be drawn than from adsorption on silicon. However, adsorbed amount on gold is higher than on silicon because percentage of detected gold is lower. Oxygen comes here always from adsorbed molecules and not from the substrate. The N/C ratios are quite close to the one measured on silicon for each condition. Even if the adsorbed amount is different, the proportion of protein in the adsorbed layer is almost the same.

Table IV. 3. 7: XPS analysis of DBM extract adsorbed on Gold. First line, Au, gives the XPS analysis of the substrate. The other lines give XPS analysis after adsorption of extracts (Ex.) obtained at different temperatures and conditions on the gold substrate.

	C					O	N	Au	N/C	Au/C
	(C=O)-O	(C=O)-N, C=O, O-C-O	C-O, C-N	C-(C,H)	tot					
Au	2,3	2,1	6,6	28,5	39,6	25,7	-	34,7	-	0,88
Ex. 4°C	1,1	12,4	17,5	22,4	53,3	21,1	11,7	13,9	0,22	0,26
Ex. 20°C	1,1	12,3	16,5	20,7	50,5	19,8	12,0	17,7	0,24	0,35
Ex. 37°C	1,1	13,8	19,2	22,0	56,2	20,7	14,1	9,1	0,25	0,16
Ex. 20°C/pepsine	3,8	4,3	9,7	66,2	83,9	13,2	2,7	0,22	0,03	0,003

3.3. Detection of specific proteins in the extract

Gel electrophoresis: Gel electrophoresis was performed on porcine DBM extracts and result is presented in Fig. IV.3.2. Extracts with pepsine are not presented here because pepsine cut the proteins into small pieces and there is thus no more interest to determine their mass. Three bands at 60, 45 and 35 kDa were found after extraction at 4°C and 20°C but smearing was observed after extraction at 37°C. Smearing can traduce problems of migration, the presence of proteins of all masses in the sample or too high concentration in the extract. Identification of the protein bands will be done by mass spectrometry.

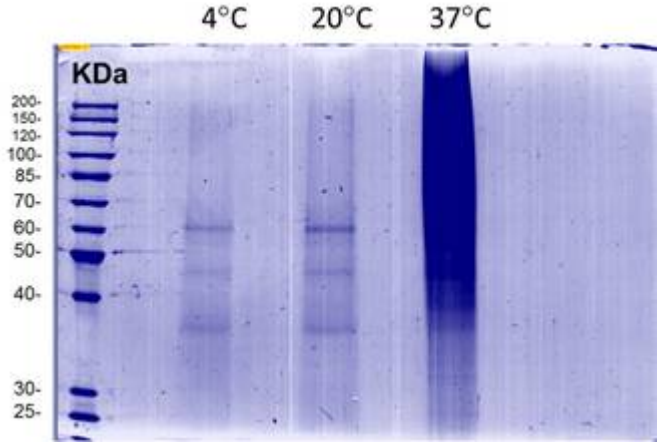

Figure IV. 3. 2: Gel electrophoresis of DBM extracts obtained at different temperatures.

Fig. IV.3.3 shows which bands were analyzed by masse spectrometry and Table IV.3.8 shows the results of the identification. Unfortunetly, bands 1, 2 and 3, which are the three bands that appear during separation, were not identified as specific proteins. It is thus very difficult to draw conclusions from this identification. Moreover, all the bands cut in the 37° extract are identified as Col type I. The extraction thus probably allows the recovery of the most abundant protein in DBM, type I Col. This method does not allow to determine if interesting growth factors are present in the extracts. ELISA will be performed to be more specific and detect smaller amount.

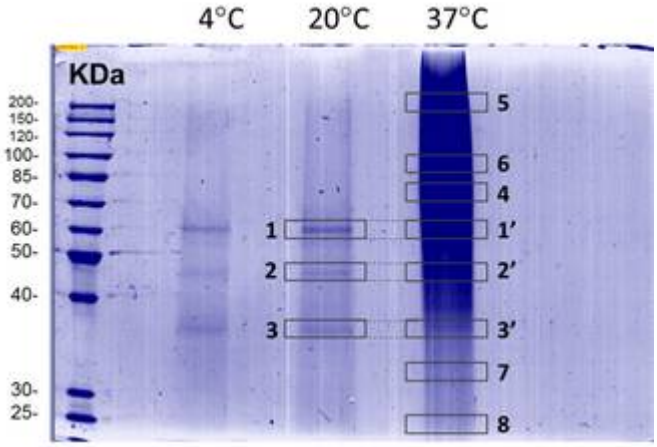

Figure IV. 3. 3: Gel electrophoresis of DBM extracts obtained at different temperature. Bands from 20° and 37° extracts were analyzed by mass spectroscopy. Each analyzed spot is determined by a rectangle and by a number.

Table IV. 3. 8: Results of the mass spectrometry analysis of the different bands determined in Fig. IV.3.3.

1	Alpha-2-HS-glycoprotein	Wild pig
2	Alpha-2-HS-glycoprotein	Wild pig
3	secreted protein, acidic, cysteine-rich Alpha-2-HS-glycoprotein	Wild pig Wild pig
4	collagen alpha-1(I)chain preproprotein	Human
5	collagen alpha-1(I)chain preproprotein	Human
6	x	x
7	PREDICTED: collagen alpha-1(I)	Wild pig
8	PREDICTED: keratin	Chinchilla
1'	collagen alpha-1(I)chain preproprotein	Human
2'	PREDICTED: collagen alpha-1(I) chain-like isoform X1	Chinchilla
3'	collagen alpha-1(I) chain-like	Wild pig

ELISA for the detection of VEGF and BMP-2: More specific detection of two interesting proteins, VEGF and BMP-2, was performed by ELISA. These tests were performed on extracts of human DBM because they do not exist for porcine proteins. Obtained results are presented in Table IV.3.9 and they are converted in protein amount per g of DBM. Wildemann et al. [3] reported extraction of around 3800 ng/g and 2 ng/g for BMP-2 and VEGF, respectively. The data obtained in this study are thus far from the literature for BMP-2 but in good agreement for VEGF.

Table IV. 3. 9: Concentration in VEGF and BMP-2 measured by ELISA test on the extract of human DBM

	Concentration (pg/ml)		Concentration (ng/g DBM)	
	20°C	37°C	20°C	37°C
VEGF	9.7 – 12.5	22.6 – 28.0	0.97 – 1.25	2.26 – 2.8
BMP-2	26.2 – 45.4	9.7 – 23.7	2.62 – 4.54	0.97 – 2.37

4. Conclusions

With all these experiments, we have partly characterized the composition of DBM powder. We have also shown that it is possible to recover proteins from DBM with a mild extraction procedure and without denaturing agent. Even if we do not have recovered a high amount of BMP-2, it could be enough to induce a cell response and there are probably other growth factors present in small amount in the extracts. It could thus be interesting to test if these extracts help to induce differentiation. Moreover, the extracted proteins could be added in the future to the interfaces designed in this work.

1. Schubert, T., et al., *Critical size bone defect reconstruction by an autologous 3D osteogenic-like tissue derived from differentiated adipose MSCs.* Biomaterials, 2013. **34**(18): p. 4428-4438.
2. Holt, D.J. and D.W. Grainger, *Demineralized bone matrix as a vehicle for delivering endogenous and exogenous therapeutics in bone repair.* Advanced Drug Delivery Reviews, 2012. **64**(12): p. 1123-1128.
3. Wildemann, B., et al., *Quantification of various growth factors in different demineralized bone matrix preparations.* Journal of Biomedical Materials Research - Part A, 2007. **81**(2): p. 437-442.